AD-A149 809 3-D DOME/ROTMAN LENS ANTENNA BREADBOARD DEMONSTRATION 1/2
(U) RAYTHEON CO GOLETA CA ELECTROMAGNETIC SYSTEMS DIV
D T THOMAS ET AL. JAN 85 ONR-252-008-3 N00014-80-C-0143
UNCLASSIFIED F/G 9/5 NL

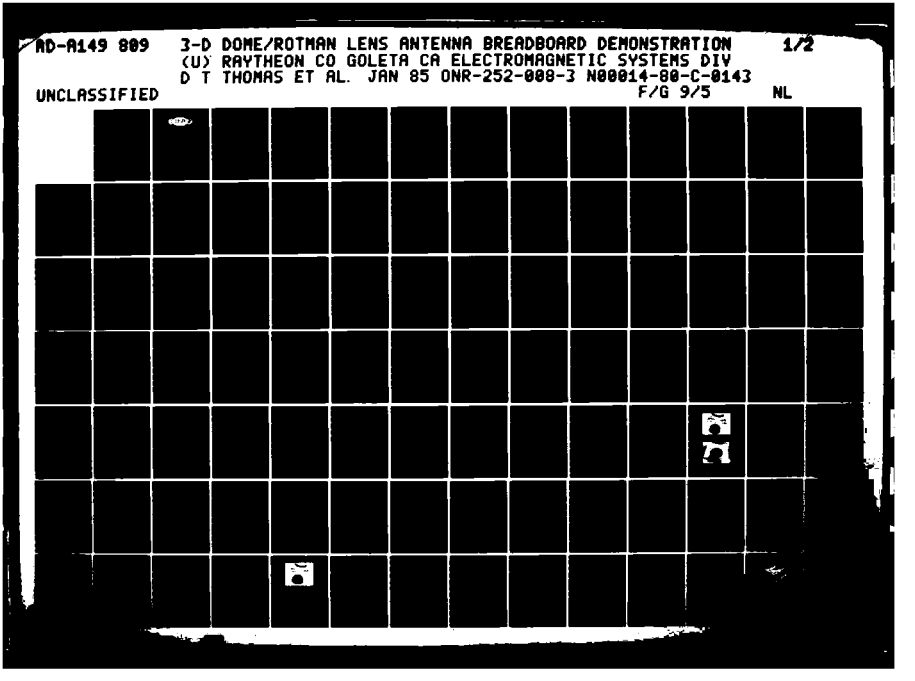

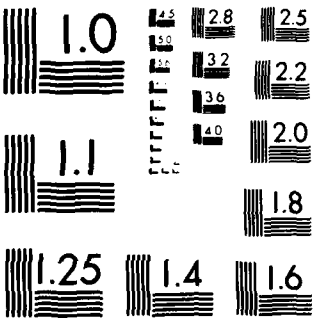

Report ONR 252-008-3

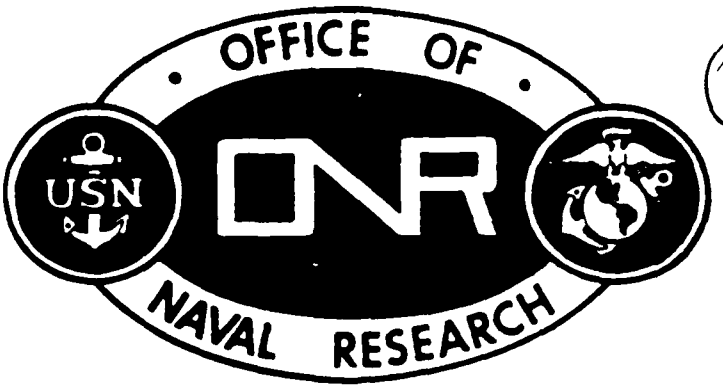

3-D DOME/ROTMAN LENS ANTENNA BREADBOARD DEMONSTRATION – PHASE I

DR. DAVID T. THOMAS
DR. DENNIS HOLST

JANUARY 1985

FINAL TECHNICAL REPORT FOR PERIOD OF
NOVEMBER 1979-JANUARY 1982

APPROVED FOR PUBLIC RELEASE, DISTRIBUTION UNLIMITED

PREPARED FOR THE

OFFICE OF NAVAL RESEARCH • 800 N. QUINCY STREET • ARLINGTON, VA • 22217

RAYTHEON COMPANY
ELECTROMAGNETIC SYSTEMS DIVISION
6380 HOLLISTER AVENUE
GOLETA, CALIFORNIA 93117

Raytheon

NOTICES

Change of Address

Organizations receiving reports on the initial distribution list should confirm correct address. This list is located at the end of the report. Any change of address or distribution should be conveyed to the Office of Naval Research, Arlington, VA 22217, Attn: Code 221.

Disposition

When this report is no longer needed, it may be transmitted to other authorized organizations. Do not return it to the originator or the monitoring office.

Disclaimer

The findings in this report are not to be construed as an official Department of Defense or Military Department position unless so designated by other official documents.

Reproduction

REPORT DOCUMENTATION PAGE

1a. REPORT SECURITY CLASSIFICATION UNCLASSIFIED	1b. RESTRICTIVE MARKINGS
2a. SECURITY CLASSIFICATION AUTHORITY -	3. DISTRIBUTION/AVAILABILITY OF REPORT Approved for public release; distribution unlimited
2b. DECLASSIFICATION/DOWNGRADING SCHEDULE -	
4. PERFORMING ORGANIZATION REPORT NUMBER(S)	5. MONITORING ORGANIZATION REPORT NUMBER(S) ONR 252-008-3
6a. NAME OF PERFORMING ORGANIZATION Raytheon Company Electromagnetic Systems Division 6b. OFFICE SYMBOL (If applicable)	7a. NAME OF MONITORING ORGANIZATION Department of the Navy Office of Naval Research
6c. ADDRESS (City, State and ZIP Code) 6380 Hollister Avenue Goleta, CA 93117	7b. ADDRESS (City, State and ZIP Code) Arlington, VA 22217
8a. NAME OF FUNDING/SPONSORING ORGANIZATION 8b. OFFICE SYMBOL (If applicable)	9. PROCUREMENT INSTRUMENT IDENTIFICATION NUMBER N00014-80-C-0143
8c. ADDRESS (City, State and ZIP Code)	10. SOURCE OF FUNDING NOS. PROGRAM ELEMENT NO.: ONR TASK 256-008-3 PROJECT NO.: TASK NO.: WORK UNIT NO.:
11. TITLE (Include Security Classification) 3-D Dome/Rotman Lens Antenna-Breadboard Demonstration - Phase I (U)	
12. PERSONAL AUTHOR(S) Dr. David T. Thomas, Dr. Dennis Holst	
13a. TYPE OF REPORT Final Report 13b. TIME COVERED FROM 1-79 TO 1-82	14. DATE OF REPORT (Yr., Mo., Day) January 1985 15. PAGE COUNT 140
16. SUPPLEMENTARY NOTATION	
17. COSATI CODES FIELD / GROUP / SUB. GR.	18. SUBJECT TERMS (Continue on reverse if necessary and identify by block number)

19. ABSTRACT (Continue on reverse if necessary and identify by block number)

This report describes a 3-D Dome/Rotman Lens Antenna preliminary system design, and also a demonstration of the critical hardware is given. It offers the capability for (1) greater than hemisphere scan coverage from a single feed array, (2) greater than octave bandwidth, and (3) multiple simultaneous beams. The history and selected results of related programs are included.

20. DISTRIBUTION/AVAILABILITY OF ABSTRACT UNCLASSIFIED/UNLIMITED ☒ SAME AS RPT ☐ OTIC USERS ☐	21. ABSTRACT SECURITY CLASSIFICATION UNCLASSIFIED
22a. NAME OF RESPONSIBLE INDIVIDUAL Dr. D. Thomas	22b. TELEPHONE NUMBER (Include Area Code) (805) 967-5511 - 2420 22c. OFFICE SYMBOL

1002

3-D DOME/ROTMAN LENS ANTENNA

BREADBOARD DEMONSTRATION - PHASE I

FINAL TECHNICAL REPORT FOR PERIOD

NOV 1979 - JAN 1982

Dr. David T. Thomas

Dr. Dennis Holst

RAYTHEON COMPANY
Electromagnetic Systems Division
6380 Hollister Avenue
Goleta, CA 93117

Contract N00014-80-C-0143

OFFICE OF NAVAL RESEARCH

Prepared for the
OFFICE OF NAVAL RESEARCH
800 N. Quincy Street
Arlington, VA 22217

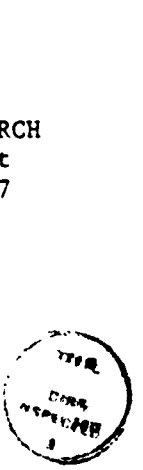

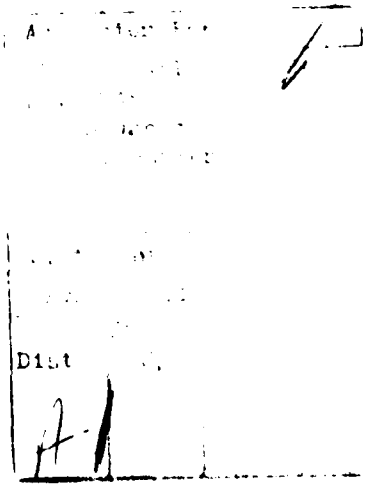

ACKNOWLEDGEMENTS

In addition to Dr. David Thomas, Program Manager, and Dr. Dennis Holst, Project Engineer, the following people contributed to the effort described in this report:

S. Douglas Bixler
Kim McInturff
Steve Owens
Emil Schnitzke
Michael D. Miller

TABLE OF CONTENTS

LIST OF ILLUSTRATIONS

LIST OF ILLUSTRATIONS (CONCL)

LIST OF TABLES

LIST OF REFERENCES

1 Stangel, J.J. and Valentino, P.A., "Phased Array Fed Lens," U.S. Patent No. 3755815.

2 Archer, D.H., "Lens Fed Multibeam Arrays," Electronic Progress (Raytheon Co.), Vol. XVI, No. 4, pp. 24-32, Winter 1974.

3 Rotman, W. and Turner, R.F., "Wide Angle Lens for Line Source Applications," IEEE Trans., Vol. AP-11, pp. 623-632 (1963).

4 Dome Antenna/Rotman Lens Study - Phase II Final Report, ONR-N00014-76-C-0651, 1979.

5 "Design Studies of Wide Angle Array Fed Lens"

6 "Hardware Demonstration of 2-Dimensional Wide Angle Array Fed Lens," Presented to 1979 IEEE/AP-S International Symposium, June 20, 1979, Seattle, WA.

7 Feed Lens Portion of 3-D Dome Antenna Study, Report ONR 252-008-1 (AD A076298), October 1979.

8 Thomas, D.T., et al, "Agile Polarization Feed Array for 3-D Dome Antenna," Report ONR 252-008-2, Raytheon Co. Electromagnetic Systems Division, Goleta, CA 93117 (November 1980).

9 Ludwig, A.C., Miller, M.D., Wideman, G.A., "Design of a Meanderline Polarizer Integrated with a Radome," IEEE International Symposium on Antennas and Propagation, June 20, 1977, Stanford, CA.

10 Hessel, A. and Shapira, J., "Mutual Coupling Coefficients in Collector Arrays on Circular Cylindrical Concave Surfaces," IEEE Trans. Ant. and Prop., Vol. AP-25, No. 6, November 1977, pp. 741-747.

11 Feed Lens Portion of 3-D Dome Antenna Study, Report ONR 252-008-1 (AD A076298), October 1979.

12 Dome Antenna/Rotman Lens Study - Phase II Final Report, ONR-N00014-76-C-0651, 1979.

13 Schwartzmann, L. and Stangel, J., "The Dome Antenna." Microwave Journal, pp. 31-34, October 1975.

14 Archer, pp. 24-32.

15 Thomas, D., Design Studies of a Wide Angle Array Fed Lens, Paper presented to 1979 IEEE AP-S International Symposium.

16 Rotman and Turner, pp. 623-632.

I. INTRODUCTION AND SUMMARY

This is the final report of Contract N00014-80-C-0143 entitled 3-D Dome/Rotman Lens Antenna. The two end items of this contract were:

(1) Preliminary System Design for a 3-D Dome/Rotman Lens Antenna, a concept of which is shown in Figure 1, and
(2) Demonstration of critical hardware including one central slice lens array, and a concave curved subarray (7x7 elements).

A brief history of related prior programs is also included.

1. RESULTS OF PRESENT CONTRACT

The operational scenario shows a gain tailored dome with highest gain on the horizon to be preferable for shipboard applications. The selected concept and preliminary tradeoff studies of the 3-D Dome/Rotman Lens Antenna are described, based on a Raytheon Baseline Dome design derived from GFE data provided by ONR and Sperry, Inc. for a dielectric dome designed and built by Sperry. The baseline dome was necessary to permit use of curved feed arrays which improve the feed lens shape and performance, and in addition reduce the phase variations along the feed array.

Tradeoff results for various feed lens and array configurations for the central slice are presented. An optimized design with very good performance for the central slice was selected for the critical hardware phase of the program.

Several pieces of hardware were built and tested including (1) a beam-forming lens (BFL) and array cables, (2) an integrated BFL with printed transmission lines, (3) a central slice array of 17 elements, and (4) a 7x7 concave curved subarray of notch elements. Performance of all critical components was as expected, and the very good results prove the feasibility of the 3-D Dome/Rotman Lens Antenna concept as described herein.

A two-stack lens concept was selected, based on proven technology on several programs. Error contributors in the two-stack feed lens are listed and described. Several candidate designs are investigated, including a novel "minor axis" lens design and an optimized feed array which successfully reduce phase errors in the principal scan axis planes. Substantial co-phase errors occur for diagonal scan (45°), and are inherent in the two-stack lens approach to the 3-D Dome/Rotman Lens Antenna.

The recommended design offers good performance for transmit applications but would have limited performance in receive applications due to high peak side lobes of around 17 dB for diagonal scan. Details of this design are presented herein.

From prior work, the best application of the Dome/Lens technology is for transmit applications of semicircular arrays scanning 180° or more in one plane.

2. HISTORY OF 3-D DOME/ROTMAN LENS ANTENNA RELATED PROGRAMS

In 1975, the first of a series of programs was initiated to investigate a new antenna system concept which combines the 3-D dome antenna technology with Rotman lens-fed array technology.

The dome antenna[1] incorporates a new concept in electronic-scan antenna design which affords cost-effective applicability to a wide range of current and future systems. The dome antenna uses a passive conformal lens to extend the scan range of a conventional planar array to hemispheric (or greater) coverage. This represents a new capability heretofore unknown in antenna technology. The result is a substantially less complex antenna with fewer electronic control devices meaning lower cost than alternate configurations.

---

[1] Stangel, J.J. and Valentino, P.A., "Phased Array Fed Lens," U.S. Patent No. 3755815.

Conceived and initially studied under Sperry's internal research and development activity, the continuing development of the dome antenna technique has been receiving support from a number of Government agencies, including the U.S. Army Missile Command (MICOM), U.S. Air Force Rome Air Development Center (RADC), and the Office of Naval Research (ONR).

The Rotman lens-fed array Technology[2,3] is capable of generating multiple scanned beams from a single array aperture, and doing so over extreme bandwidths (3 to 1 or more). This technology has had extensive development at Raytheon ESD over the past twelve years. Over $10 million in Raytheon internal development funds and over $100 million in Government contract funds have been expended on research, development, and production of systems employing lens-fed multibeam arrays. Appendix B describes the operation of the Rotman lens.

The first joint program, Octave Bandwidth Wide Angle Antenna Study (ONR Contract N00014-76-C-0652) studied a two-dimensional dome slice and designed the required feed lens. Results of that study indicated that large phase errors and poor lens shape would result from feeding a dome antenna with its flat feed array.

Subsequent to this first contract, new investigations were carried out on Raytheon internal research funds. A new concept was discovered which offers substantial improvements in performance. This effort was continued on Raytheon internal funds to design, fabricate, and test a two-dimensional breadboard model. (This invention was patented in September 1982.)

---

[2] Archer, D.H., "Lens Fed Multibeam Arrays," Electronic Progress (Raytheon Co.), Vol. XVI, No. 4, pp. 24-32, Winter 1974.

[3] Rotman, W. and Turner, R.F., "Wide Angle Lens for Line Source Applications," IEEE Trans., Vol. AP-11, pp. 623-632 (1963).

The next program, Feed Lens Portion of 3-D Dome Antenna Study (ONR Contract N00014-77-C-0760) was a 15-month study program to design and predict performance of the feed lens portion of a 3-D dome antenna. The ultimate goals are the development of wideband, multibeam 3-D dome antenna systems.

Analyses performed using a hemispherical dome with constant scan amplification, K = 1.5, demonstrated peak phase errors of 15° for scanning in the principal axis scan planes. The two-stack feed lens approach was used.

Contract N00014-78-C-0690 entitled Agile Polarization Feed Array for a 3-D Dome Antenna investigated polarization agility for octave-bandwidth feed arrays in a 3-D Dome Antenna system. Both studies and experimental investigations were performed on this program.

The studies included analyses of the polarization needs of 3-D Dome Antenna systems, especially the feed array portion, and investigation of techniques for implementation, including octave-bandwidth, dual-polarization array elements and circuits for agile polarization.

The experimental investigations consisted of design, fabrication and test of two small arrays of orthogonal notch elements and of a similar, linear notch array. Both dual-polarization elements exhibited wide azimuth scan capability over at least an octave bandwidth. Beamwidths of the coincident-center notch elements remain uniformly broad over the octave band.

II. SYSTEM CONCEPT DEFINITION

The selected concept and preliminary tradeoff studies of the 3-D Dome/Rotman Lens will now be described. The operational scenario will be discussed together with the features of the 3-D Dome/Rotman Lens antenna systems and their impact on the system operation. A summary of the system goals is included.

A Baseline Dome configuration is presented which is derived from data provided by Sperry, Inc.[4] for a dielectric Dome designed and built by Sperry. The Baseline Dome was necessary to permit use of curved feed arrays which improve the feed lens shape and performance, in addition to reducing the phase variations along the feed array. Agreement between the Sperry Dome data and Raytheon's Baseline Dome data is quite good.

Tradeoff results for various feed array configurations (curvature and "drop") are presented. An optimized concept selected for the critical hardware phase of the program is described. The various computer programs used in modeling are also described.

1. OPERATIONAL SCENARIOS

The 3-D Dome/Rotman Lens Antenna System offers several advantages:

a. Hemisphere or greater scan coverage for a single electronically scanned phased array,
b. Ultra wide bandwidths of 3 to 1 or more in a single electronically scanned system, and
c. Multiple simultaneous beams from a single array aperture.

Operationally, this permits great flexibility which in a single system can perform a wide variety of functions. The baseline systems described here were developed specifically for selected Naval applications.

---

[4] Dome Antenna/Rotman Lens Study - Phase II Final Report, ONR-N00014-76-C-0651, 1979.

The primary application is EW based on integrated multipurpose system (IMPS) parameters, such as point defense of a ship. The system is configured to provide maximum effective radiated power (ERP) on target, with the gain tailored to shipboard applications. Peak gain will occur on the horizon, with high gain coverage above and below the horizon to account for ship's roll, and reduced gain coverage at higher elevation angles where distance to target is reduced.

Both passive and active EW functions can be accommodated in the 3-D Dome/ Rotman Lens Antenna System, and in addition radar functions. The latter requires low sidelobe capabilities, which in turn require very low phase errors in the array. This explains the concern which will be shown throughout for the phase or path-length errors generated by the feed lens. The IMPS made possible by the 3-D Dome/Rotman Lens Antenna offers substantial cost reduction potential over use of multiple conventional systems.

A typical scenario is shown in Figure 2. The multibeam capability of the 3-D Dome/Rotman Lens Antenna permits beams pointed in several directions to handle the many threats encountered in point defense applications. The wide bandwidth made possible by the Rotman lens technology covers a wide range of threats in a single system, and permits multifunction use.

One additional advantage of such a system is the coverage of the entire hemisphere. This eliminates handoff problems between sectors, a common problem in conventional systems. Also the EW, ESM, and radar functions will be coordinated in a single beam with no directional error or handoff error. This is also possible because of the frequency independent nature of the Rotman lens feed.

2. RAYTHEON BASELINE DOME CONFIGURATION

a. Sperry data for a dielectric dome. As an input to the current contract, ONR and Sperry were to provide GFE design data for a dielectric dome which was designed by Sperry. The details of the design appear in ONR Report ONR-N00014-76-C-0651, entitled Dome Antenna/Rotman Lens Study-Phase II Final Report (September 1979).

The Sperry Dome design incorporates an integrated dielectric dome lens which is gain tailored for optimum coverage. Maximum gain is realized near the horizon, with reduced gain at higher elevations. The dome configuration and parameters are shown in Figure 3. The relative gain contour is shown in Figure 4. As Figure 3 shows, the Sperry Dome is of approximately elliptical shape.

b. Curved feed arrays. Earlier Raytheon studies and hardware demonstration [5,6] show that concave curved feed arrays are necessary to (1) reduce phase errors to a minimum, (2) allow smaller, more efficient shaped Rotman lenses used to feed the feed array, and (3) reduce amplitude distortion which contributes to loss of gain and higher side lobes. A summary of this work appears in Appendix A.

Use of curved feed arrays (Figure 5) would require translating the Sperry data from the flat array in the dome plane, to the concave curved feed array which is dropped below the dome for better performance of the final 3-D Dome/Rotman Lens Antenna System. Since the analysis for translating the data did not exist, and the resulting data on the curved feed array would be incomplete (the "shadow" of the flat feed array does not fully cover the curved feed array), it was decided to design a baseline dome which would be "equivalent" to the Sperry Dielectric Dome.

---

5 "Design Studies of Wide Angle Array Fed Lens"

6 "Hardware Demonstration of 2-Dimensional Wide Angle Array Fed Lens," Presented to 1979 IEEE/AP-S International Symposium, June 20, 1979, Seattle, WA

c. 3-D Dome computer programs. As a result of previous programs related to the current 3-D Dome/Rotman Lens Antenna program, computer programs for the design of conventional hemispherical Dome antennas and feed lens exist[7]. These computer programs were revised to allow (1) use of dielectric domes and (2) use of elliptical cross section, i.e., spheroidal dome shapes. Examination of the Sperry design concept drawing (Figure 3) indicated that elliptical cross sections should be quite close to the actual gain tailored designs, and are readily soluable for ray path geometries.

The main computer programs available for use in designing 3-D Dome/Rotman Lens Antenna Systems are:

TRANS3D - calculates phase and amplitude distributions from feed array through the dome to planar wavefront at any angle for hemispherical and spheroidal dome shapes. Dielectric domes can be accommodated.

ROLED3D - designs Rotman lens for two-stack feed lens from TRANS3D input data; outputs amplitude and phase data at array.

CHECKLE - compares TRANS3D phase path length data with ROLED3D design data to generate phase path length errors.

WAA2DBP - generates far-field beam patterns from a single port feed of a Rotman lens through a central slice of the solid dielectric dome.

It is the TRANS3D computer programs which were modified to accommodate spheroidal dome shapes and dielectric domes. Documentation for the computer programs appears in Appendix C. Complete program listings and sample runs are available upon request.

---

[7] Feed Lens Portion of 3-D Dome Antenna Study, Report ONR 252-008-1 (AD A076298), October 1979.

d. Raytheon Baseline Dome. In order to permit use of curved feed arrays which were found to improve performance, a Raytheon Baseline Dome was derived which best fits the data provided by Sperry. The TRANS3D computer program was exercised for various elliptical cross-section dielectric domes until an acceptable design was obtained whose data closely agreed with the GFE/ Sperry Dome data for the flat feed array. Figures 6 and 7 compare the path length distributions (in inches) of the two dome designs at selected points in the feed array.

Additional confirmation of the design is available from the beam shape and pointing angle of the resulting beams in the two cases as shown in Figure 7. For the 90° scan case (horizon), the beam formed by the Raytheon baseline dome peaks at 94° but is otherwise well-formed and in fact has lower sidelobes and deeper nulls than the beam formed using the Sperry data. This indicates that the amplitude distribution of the Raytheon Baseline Dome is more uniform.

The Raytheon Baseline Dome was used in all designs and design tradeoffs described in the remainder of this report.

3. PRELIMINARY SYSTEM CONCEPT TRADEOFFS (CENTRAL SLICE)

Once the Raytheon Baseline Dome configuration was established, preliminary lens design and feed array design tradeoffs were performed to establish the configuration to be used for the critical hardware phase of the program.

The goal of the tradeoffs was to arrive at a feed array shape and location which optimized the following three features:

a. Feed array is as flat as possible to minimize element-to-element mutual coupling effects

b. Good lens shape such that all beamports point toward the array ports and a significant portion of signal to all array ports

c. Comparison of the far field radiation patterns through the Dome generated from the lens feed array design track the far field pattern generated from the phase and amplitude data submitted by Sperry for a planar feed array.

The first lens was designed using Sperry's amplitude and phase distribution data and a planar feed array. Figure 8 is the resulting lens shape, which is unacceptable due to size and poor shape.

Several redesigns with a flat array at different heights with respect to the dome were done. It was apparent that the feed array must be curved to improve the lens shape. However, curving the feed array obscures the meaning of direct phase and amplitude distribution comparisons. To check the agreement between Sperry's data and the data generated from a lens designed for a curved feed array, far-field patterns through the dome were compared. Figure 8 compares these patterns generated by the flat array without lens. A lens was designed from data derived from the ray path calculations from planar wavefronts at 0° and 90° (outside the dome). The beam formed from this lens was pointed at 90° (Figure 9). Thus, the Raytheon baseline approximation causes 4° of beam pointing error at degrees, but otherwise closely follows Sperry data. Figure 10 shows the three cases, for 0°. In both Figures 9 and 10 the dotted curves (derived from the lens designed for a flat feed) and the ray path model are used as templates to evaluate the far-field patterns of various lens/array feed configurations for optimization. The optimization consists of raising and lowering the feed and evaluating lens shape and far-field patterns. Once the feed height is optimized, the feed array curvature was evaluated in the same way. The process was repeated until no further improvement was observed. Table 1 tabulates the parameters of the various test cases run during this optimization.

Figure 11 is the ray path illustration of a feed array radius of curvature of 10.77 inches, taken at 0° and 90° scan angles. Figure 12 illustrates that the lens corresponding to this feed curvature is too deep for acceptable performance. Figures 13 and 14 are the ray path illustrations for a feed array radius of curvature of 10.77 inches but with a drop of 2 inches with respect to the dome. Figure 15 is the lens resulting from the feed array drop. Although Figure 15 is a significant improvement over Figure 12, Figure 14 shows some of the ray paths missing the dome surface position on their way from the feed array to the exterior plane wave.

Figures 16 and 17 are the ray path illustrations for a radius of curvature of 9.90 inches instead of the flatter 10.77 inch radius of curvature. Figure 18 shows the better shaped lens resulting from curved array. Figures 19 and 20 show fairly good far-field pattern agreement between the template and that generated by the model of Figures 16 and 17. This iteration process continued until the best curvature and drop of the feed array was determined. The list of candidates considered appears in Table 1.

4. SELECTED DESIGN CONCEPT

The preliminary concept selected has a concave curved array feed surface with radius of curvature 6.9 inches and zero "drop". Mutual coupling between array elements for this curvature is estimated to be less than -24 dB based on theoretical considerations. Although this is an increase from the flat array case, coupling is still an acceptably low level.

Figures 21 and 22 illustrate ray paths of the selected dome-feed array configuration for 0° and 90° scan. Lens shape (Figure 23) is quite acceptable and all beamports will easily communicate with all array ports. Far-field patterns (Figures 24 and 25) compare favorably with those generated from the Sperry data.

III. CRITICAL HARDWARE DEMONSTRATION

Several pieces of test hardware were designed, fabricated, and tested to provide the data necessary to support a follow-on program. This hardware also lends confidence to the lens feed concept by substantiating computed performance for the present and former progams. Several pieces of hardware were tested including (1) a beamforming lens (BFL) with separate cables, (2) a BFL with integrated cables, (3) central array slice (1 x 17 elements) with concave geometry, and (4) a 7 x 7 concave subarray of notch elements. Various performance parameters were measured for the separate pieces as well as for a lens/array combination for the central feed array slice.

1. ROTMAN LENS

a. Design Procedure. The lens parameters G, α, η, determined in the previous trade study, establish lens size and the shape of the array and feed arcs. It remains to establish array ports and beamports along these arcs. On the array side of the lens, the ports are placed with uniform spacing along the array arc consistent with the array element spacing of 0.5 inch. A single dummy port was placed on each end of the array port arc to minimize reflections in the region of intersection of the array and feed arcs. The dummy ports are terminated for normal lens operation.

The beamports are initially positioned along the feed arc in a manner consistent with the beam pointing directions in sine-space. For this arrangement the beam port center-to-center separation increases from the lens center outward, hence, outer beamports are physically larger than control beamports. Following this initial procedure, the beamports are further adjusted to provide minimum phase error and optimize adjacent beam crossovers. This is accomplished employing an iterative process in which the focal distance and focal angle H_i and α_i, are adjusted individually for each port. The means for evaluating the effects of these adjustments was to compute

and compare exterior dome radiation patterns. Based on these comparisons, a final set of beamport positions was determined. The result of the above procedure is to slightly distort the feed arc so that it becomes a compound curve rather than a true arc. However, the deviation from the original arc is not large. Again, a single dummy port is located at each end of the feed arc. These ports are terminated during normal lens operation. A plot of the dome elevation beams following the above process is shown in Figure 26. Beam positions, crossover angles, and crossover levels are evident.

The final lens configuration is shown in Figure 27 for the central slice, i.e., for the array elements falling along a diameter of the dome feed array. The transmission lines terminating array and beam ports are selected to be 50 ohms in the medium in which the lens is to be fabricated. In addition to the lens contours shown in Figure 27, a set of differential cable lengths are prescribed which constitute a part of the lens design. The cables connect the array ports to the individual elements of the feed array. These differential phase lengths may be built into individual cables or incorporated into the lens structure. Both approaches are demonstrated in the hardware phase of this program. The differential cable lengths employed for the central slice lens are listed in Table 2.

b. Theoretical Performance. Theoretical amplitude and phase performance was computed for the central slice lens as functions of both scan angle and frequency. Some typical plots of the theoretical data are presented in Figures 28 to 30. These plots show both amplitude and phase at each array port position across the lens. Each figure presents this data for a fixed exterior dome scan angle, Z_o, and for three frequencies across the band.

An appreciation for theoretical lens performance is best obtained from Figure 28 for the $\xi = 0°$ (zenith) beam. This beam is symmetrical with respect to both the dome and the lens. The amplitude and phase distributions at 8, 12, and 16 GHz are presented in Figure 28. At 8 GHz the amplitude distribution is seen to be symmetrical and relatively flat, displaying about

1.5 dB of rolloff at the edge ports relative to the center port. The amplitude distribution remains symmetrical across the frequency band with the edge rolloff slowly increasing to a maximum of 4.5 dB at 16 GHz.

The phase distribution is also seen to be symmetrical across the frequency band. The phase shown in these figures includes both the beamforming lens and the specific phase deltas provided by the cables of Table 2. This is the phase present at the elements of the concave feed array. As shown in the Figure 28 this phase is plotted modulo 360 to remain within the -180 to +180 degrees range of the plot.

For scanned beams the amplitude and phase distributions are no longer symmetrical as evidenced by Figures 29 and 30. These figures present data for beams scanned to ξ = 59 degrees and 90 degrees. The corresponding feed array pointing angles (dome interior) are 21 degrees and 44 degrees. The amplitude still becomes increasingly tapered with frequency, but it is also inclined in the direction of beam scan. Hence for beams scanned to the right a beamport on the left side of the lens is excited. The phase distributions are also strongly inclined providing a planar wavefront which corresponds to the interior dome pointing angles (21 and 44 degrees). Again the phase is modulo 360 to remain within the range of the graph.

c. Measured Performance. To confirm the predicted performance for the beamforming lens (BFL), two versions were fabricated and extensively tested. The first breadboard lens was fabricated using techniques standard at Raytheon. This includes the use of separate cables to provide the connections between the lens array ports and the feed array elements. However, for the dome application these cables must be integrated into the lens stacks for simplicity. To confirm that this integration is easily accomplished a second BFL was fabricated. This second BFL was identical to the first except that printed transmission lines were substituted for the cables. The stripline transmission lines were fabricated on the same dielectric substrate as the lens to provide a single integrated assembly.

The two lenses are shown in Figures 31 and 32. They shall be referred to as the standard lens and the integrated lens respectively. In Figure 31 the standard lens is seen attached to a central slice feed array using 0.141 inch semi-rigid coaxial cable assemblies. These cables must be phase matched to provide the specific phase deltas prescribed in Table 2. The equivalent structure is shown in Figure 32 for the integrated lens using strip transmission lines. The meandering configuration for the transmission lines is necessary to provide the phase deltas equivalent to the cables of the standard lens. The two lines which run to the sides are terminated ports. In the final configuration they might be terminated internally using "pill" terminations, depending on operating power levels. The following sections will describe measured performance for both the standard and integrated lens.

(1) Standard Lens Results. Data for the standard lens is presented in Figures 33 to 35. The format employed is the same as used for the theoretical data of Section III-1-b. As for the theoretical case, data is presented at three frequencies across the band, and for three exterior scan angles, ξ = 0° (zenith), 59, and 90°.

Only amplitude data is presented for the standard lens. This data may be compared directly with the theoretical amplitude data presented previously. For the standard lens phase data was measured directly at the lens array ports without the cable assemblies, hence, the phase cannot be directly compared with theoretical results, which include cable phase. In the next section we shall provide a direct comparison for the integrated lens.

The standard lens amplitude data shows generally good comparison with the theoretical plots. For the ξ = 0° case, the delta is highly symmetrical. Rolloff is slight at 8 GHz . A ±1.5 dB amplitude ripple is seen on the mean performance. The amplitude becomes more tapered with higher frequency, until it reaches about 5 to 6 dB rolloff at 16 GHz. This compares favorably with the computer value of 4.5 dB shown previously.

For scanned beamports, the measured amplitude data displays a tilted characteristic with the nominal amplitude inclined from one side of the lens to the other. The measured data corresponds to scan angles of -59° and -90° while the computed data was for scan angles of +59° and +90°. In general the comparison is favorable, with the measured performance showing somewhat more rolloff, particularly at the edge array ports.

(2) Integrated Lens Results. The integrated lens is identical to the standard lens except for the addition of the integrated stripline transmission lines to provide the phase deltas of Table 2. The measurement of amplitude and phase for this lens results in data which is directly comparable to the theoretical data. The amplitude data may also be compared with that provided for the standard lens. Figures 36 to 38 provide plots of the amplitude data corresponding to exterior dome scan angles of ξ = 0°, 59°, and 90°, respectively. These plots are seen to be very similar to those provided for the standard lens, except that somewhat less rolloff is exhibited for the edge array ports.

Phase performance is depicted for the integrated lens in Figures 39 to 41.

c. Concave Feed Array. To obtain an understanding of concave feed array performance, a 7 x 7 subarray was fabricated and tested. Prior to this, however, a single row of the concave array was also fabricated and tested in considerable detail. The reasons for this were several:

(1) A single row (referred to hereafter as slice) would contain a full complement of elements along a complete arc length,
(2) The complete slice could be mated to the breadboard lens for radiation patterns and active VSWR tests, and
(3) Mutual coupling tests would include the effects of elements on the opposite side of the feed arc.

The single slice selected for fabrication was that along the feed array diameter and is therefore referred to as the central slice.

A 7 x 7 concave subarray was fabricated and tested following evaluation of the central slice. This subarray represented the central 49 elements of the complete feed array.

d. Central Slice Array. A nominal element spacing of 0.5 inch was employed for all test array hardware. Sperry data was provided on a 0.5 inch by 0.5 inch grid on the dome base plane at the single midband frequency of 12.0 GHz. An element spacing of 0.5 inches allows grating lobes to occur at the high end of the band. However, the ability to compare test data directly with the Sperry data was judged a very useful outcome. For a final array design, the array element spacing would be reduced to 0.37 inches so that it does not exceed one-half wavelength at 16 GHz. This closer element spacing will eliminate grating lobes and their detrimental effect on active VSWR.

(1) Array Geometry. The tapered notch was selected as the element for the concave feed array. This choice was predicated on previous work with this element[8] and on the ease of achieving concave geometries using the printed circuit construction. The printed notch employs both radial and parallel orientations to accommodate the concave feed surface. Both orientations are shown in Figure 26. The surface is cut into a specific number of slices. Each slice consists of a concave printed circuit containing the appropriate number of notch elements. The number of elements varies from slice to slice to conform to the circular array outline. The radial element

---

8 Thomas, D.T., et al, "Agile Polarization Feed Array for 3-D Dome Antenna," Report ONR 252-008-2, Raytheon Co. Electromagnetic Systems Division, Goleta, CA 93117. (November 1980)

orientation for a single slice is shown in Figure 42. The multiple slices are joined together in a parallel orientation as shown in Figure 42. The parallel arrangement offers more direct interface connections with the feed system below. Also, the element radiation pattern is identically oriented for all elements. One potential difficulty was the "steps" between adjacent array elements, particularly near the array edges. These steps are created when the individual slices are displaced by different amounts to conform to the curved aperture surface. The effect of these steps on overall array performance was found not to be significant.

Element polarization is linear and therefore polarization outside the dome changes orientation with changing azimuth scan angle. All major objectives of this program can be achieved with linear polarization, however, so no effort was expended to provide a polarization diversity capability. If required, such a capability may be provided at a later time. Circular polarization, if required, can be provided by adding a meanderline transmission polarizer[9] to the feed array.

The notch element has generally been employed in linear arrays where knowledge of the precise element phase center is not critical. It is known that the element phase center lies on the axis, but its exact position from the notch aperture is not known. It was necessary to measure the phase center for the notch element embedded in a concave array since this geometry might influence the phase center position. However, in order to fabricate the array, it was necessary to initially estimate the position of the phase center. Therefore the phase center was initially assumed to reside at the

---

[9] Ludwig, A.C., Miller, M.D., Wideman, G.A., "Design of a Meanderline Polarizer Integrated with a Radome," IEEE International Symposium on Antennas and Propagation, June 20, 1977, Stanford, CA.

intersection of the notch and element feed probe, as indicated in Figure 43. Proceeding with this assumption, a concave central slice array was designed containing 17 elements arrayed in the E-place with 0.5 inch spacing along the arc connecting the assumed phase centers. The radius of curvature to the phase center arc is 6.923 inches as determined in the trade studies described previously. For the element geometry of Figure 43 this results in a radius of curvature of 6.46 inches at the notch physical aperture. These dimensions are depicted in Figure 44 showing a pictorial of the central slice array.

The central slice array described above was fabricated and numerous measurements were conducted to characterize its performance. The first measurements were concerned with establishing the element phase center. The technique employed consisted of measuring radiation patterns for element pairs fed in phase. This was performed for a number of different pairs and then noting the beamwidth-to-first-nulls for the various pairs across the frequency band. With this information and the array physical dimensions, the element phase centers may be determined using simple geometry. The results are presented in Figure 45, which shows the radius of curvature to the element phase center arc as a function of frequency. The vertical bars indicate the error tolerance on the measurements. The actual radius of curvature was found to be 6.573 inches, a reduction of 0.35 inches compared to the desired 6.923 inches. Figure 43 indicates the position of the notch phase center located 0.35 inch away from the feed point and approximately midway between the feed point and notch aperture. The indicated location represents the mean value for all measurements at all frequencies.

With the shift in element phase center toward the center of curvature, the effective element spacing decreases. The actual element spacing for the central slice is 0.475 inch, compared with the desired 0.5 inch spacing. This change is small and will not result in any significant changes to measured array performance. Array testing was continued with

high confidence in the results. Design of the final dome feed array can proceed with complete confidence once the location of the element phase center has been determined.

(2) Element Patterns. Following measurement of the element phase center, several measurements of single element performance were conducted. Radiation patterns and gain were measured throughout the octave frequency band. Typical radiation patterns for the center embedded element are presented in Figure 46 for the E-plane (array plane) and in Figure 47 for the H-plane. All other array elements were terminated in their characteristics impedance during these measurements. The patterns are seen to be generally broad and well-behaved for all frequencies in both planes. At 16 GHz the H-plane pattern displays some lobing, but sufficient coverage is still provided by the main beam. The partial lobe seen in all E-plane patterns at broadside is the standard gain horn reference pattern employed for gain measurements.

Summaries of element gain and beamwidths are presented in Figures 48 and 49 respectively. The element gain varies between 2 and 8 dB across the octave band. The dashed line indicates nominal values and the circled dots indicate measured values. In Figure 49 both E-plane (solid curve) and H-plane (dashed curve) plots are presented. Minimum -3 dB beamwidths are approximately 70 to 80 degrees. This is sufficient to accommodate the maximum feed array scan angle of approximately 40 degrees.

(3) Active and Passive VSWR. Both active and passive VSWRs were measured for the central slice array. The passive VSWR was measured for the notch element using swept frequency techniques across the 8 to 16 GHz band. The 17 elements were measured singly, with all remaining elements terminated in their characteristic impedance. The data is presented in terms of return loss (in dB) versus frequency in Figure 50, for several elements. Corresponding VSWRs are indicated at several points on the plot. A return loss

of -10 dB is equivalent to a VSWR of 1.92:1. Note that the several plots track very closely. This was found to be true for all 17 array elements, indicating the high reproducibility of the notch element due to its printed circuit nature. A maximum passive VSWR of 4.4:1 is seen to occur near the low end of the band. The nominal VSWR is about 2.0:1.

The active VSWR is a function of scan angle, frequency, and element position in the array. Measurement of the active VSWR requires that all elements be excited with the appropriate amplitude and phase for producing beam scan. The non-integrated beamforming lens with cables described previously was employed to properly excite the central slice array. Array and BFL were connected using phase matched 0.141 inch semi-rigid cable. The complete central slice antenna is shown in Figure 51.

Measurements for the center and a near edge element are presented in Figures 52 and 53, respectively. Again, the active VSWR is provided in terms of the element return loss versus frequency for three scan angles. The indicated angles are for the exterior dome pointing angles of 0 degrees (zenith), 59, and 90 degrees (horizon).

A nominal return of loss of about -8 dB is found for both element positions and all scan angles. This corresponds to an overall active VSWR of 2.3:1. However, in all cases very narrow band spikes are seen to occur in different parts of the band. These spikes correspond to very high VSWRs representing almost total power reflection at the elements. The occurrance of VSWR spikes is strongly related to the array geometry and element spacing, which, as pointed out previously, is greater than desired for the usual feed array. No attempt was made to match this active VSWR since the single slice is not entirely representative of the full feed array.

The central slice, in the form tested, is representative of a two-dimensional cylindrical geometry rather than the three-dimensional spherical geometry of the actual feed array. It has been previously noted in the

literature[10] that the spherical geometry will experience considerably reduced coupling compared to the cylindrical case. Active matching of the feed array aperture should be reserved for the actual array geometry. It is expected that the magnitude of the effects indicated in the figures will be reduced for the actual feed array and conventional matching techniques may be employed to produce a comfortable active match. The central slice measurements provide at least a qualitative measure of the effects to be expected.

(4) Array Measurements. A final series of measurements using the complete central slice antenna consisted of sets of radiation patterns for three beam scan angles in the dome interior. These measurements were conducted with the assembly pictured in Figure 51 at frequency intervals of 1 GHz across the band. Selected scan angles were 0°, 71°, and 90° for the dome exterior, corresponding to feed array (dome interior) pointing angles of 0°, 28°, and 44°, respectively. Other relations between interior and exterior scan angles are listed in Table 3 for reference.

Typical radiation patterns measured with the central slice antenna are provided in Figures 54 to 57. These figures show patterns for 0° (zenith) and 90° (horizon) scan at both ends of the frequency bands, 8 and 16 GHz. Also shown for comparison in each figure is a computed radiation pattern using theoretical BFL amplitude and phase data. Note that the relative peak gains shown on measured and computed patterns have no significance. These peaks were simply set at convenient levels for test and computation purposes and do not indicate a loss for the measured case.

---

10 Hessel, A. and J. Shapira, "Mutual Coupling Coefficients in Collector Arrays on Circular Cylindrical Concave Surfaces," IEEE Trans. Ant. and Prop., Vol. AP-25, No. 6, November 1977, pp. 741-747.

Comparisons for the measured and computed patterns are presented in Table 4 which lists the -3 dB beamwidth, the -10 dB beamwidth, and the scan angle. The various pattern characteristics are seen to compare favorably. Reasonable comparison is also seen from a simple visual comparison of each pair of patterns. The feed array is required to generate particular amplitude and phase patterns in the dome interior. It is therefore not focused at infinity as is the usual case for an array. This results in the shoulder lobes and dips in the center of the beam as seen in 8 and 16 GHz patterns for the 0 degree beam. Also, the computed patterns are ideal since they do not include any mutual coupling effects. The fine grain structure for the measured and computed patterns therefore do not agree in detail.

The patterns of Figures 56 and 57 are for maximum scan at 8 and 16 GHz, respectively. Again, general beam characteristics are similar with differences in the fine structure. At 8 GHz the pattern was measured for the symmetrical port on the opposite side of zenith, but pattern comparisons are still valid. Due to the large element spacing (0.5 inch) described previously, a grating lobe is confirmed by measurement of the central slice array. It is the appearance of this grating lobe which contributes to some of the high VSWR spikes in the active VSWR as discussed earlier. Reduction of the array element spacing to one-half wavelength at 16 GHz (0.370 inch) should eliminate both the grating lobe and VSWR spikes.

b. Concave Subarray. The final hardware fabricated for evaluation was a 7 x 7 subarray from the center portion of the concave feed array. The finished hardware is shown in Figure 58. The notch element is employed with a nominal element spacing of 0.5 inch in both the E- and H-planes. Note that a radial element orientation is employed in the E-plane (plane of the notch) while a parallel orientation is employed in the H-plane. The array is fabricated as separate (E-plane) arcs which are then joined together in a stepped manner to approximate the concave geometry in the H-plane. Mounting holes are drilled through each arc so that two close-tolerance bolts through all arcs will correctly align the arrays.

As discussed earlier, the array element spacing was chosen for ease of data comparison and is too large for operation to 16 GHz. The selected spacing of 0.5 inch equals $\lambda/2$ at 12 GHz so this is the proper high band edge for the subarray. Therefore, to demonstrate octave bandwidth performance, element patterns were measured from 6 to 12 GHz. Pattern measurements were then continued to 16 GHz to demonstrate the influence of grating lobes on pattern performance.

Element radiation patterns are presented in Figures 59 and 60 for the E-plane and H-plane respectively. Four patterns are shown in each figure, at 6, 8, 12, and 16 GHz. The first three frequencies cover the octave band of interest, while the influence of excessive spacing (grating lobe) is seen at 16 GHz.

Coverage performance for the notch element is summarized in Figure 61, which presents beamwidths for both the E- and H-planes. The nominal element beamwidth is seen to be in the range of 90° to 100°. In the E-plane, a coupling effect produces a ripple on the element pattern. At 6 GHz the E-plane pattern shows a central lobe with a 28° halfpower beamwidth. The overall coverage is relatively broad (at about the -5 dB level). This behavior is an inherent characteristic of the 7 x 7 subarray. As the number of E-plane elements increased, the number of pattern ripples will increase and their amplitude will decrease. It is expected that the notch element will provide sufficient coverage for the dome feed array.

IV. FEED LENS DESIGN

In prior reports, various concepts for 3-D Dome Feed Lens were studied and the two-stack lens concept was selected, and is described in this section. Error contributors of the two-stack feed lens are listed and described. The two-stack feed lens is a proven technology in use on several programs.

Design tradeoffs of feed lens and array with performance of each candidate are given. Candidates include single lens design for all lenses, three different lens designs, a novel "minor-axis" lens design and optimized feed arrays (curvature and drop). Of primary interest are phase errors, which can be held to an acceptable 10° RMS or less in the principal plane, but increase to 40° RMS, and ±100° peak to peak for 45° scan. The errors at 45° scan are due to co-phase errors inherent from the dome phase variations, and cannot be eliminated in the two-stack feed lens design.

1. TWO-STACK FEED LENS CONCEPT

a. Lens Design in Three Dimensions. The extension from two to three dimensions adds another dimension to the feed lens design. There are basically two approaches to the three dimensional lens:

(1) Three Dimensional Bootlace (or other type) lens

(2) Two-stacks of Rotman lenses as demonstrated on MUSTRAC, EATS and GPS programs. (See Appendix B)

Three Dimensional Bootlace lenses were considered in an earlier report [11]. Although compact and efficient, the phase errors resulting in the 3-D Bootlace lens are excessive by comparison with the Two-Stack Feed Lens approach and would limit the size and usefulness of the 3-D Dome/Lens Antenna.

---

[11] Feed Lens Portion of 3-D Dome Antenna Study, Report ONR 252-008-1 (AD 076298), October 1979.

An alternative, proposed by Sperry [12] is an integrated Bootlace lens approach which allows additional degrees of freedom in the design to improve performance. This integrated Dome/Bootlace lens would selectively be designed for good performance near the horizon at the expense of zenith performance. In their report, Sperry showed an Integrated Dome/Lens design with good performance over 50° scan to 120° scan (horizon is 90° scan). RMS phase errors at 12 GH_z were 36°, with peak errors up to 150° over 50 to 120° of scan. These phase errors are comparable to the two-stack Feed lens errors of a comparable size system (which will be demonstrated in paragraph IV-2). The simpler approach makes the Integrated Dome/lens attractive where near-horizon coverage is the sole concern.

b. The Two-Stack Feed Lens Approach. The two-stack lens configuration is illustrated in Figure 62. Included are cable connections between selected lens sets expressly for the purpose of illustrating orientation. The correspondence between excitation of a particular beamport and pointing of a beam in a particular direction is shown in Figure 62. It shows an example in which an outer beamport of the third lens from one end is excited. Note that only the array ports of that third lens of the lower stack are excited to produce a phase ramp across the row of ports. This row of array ports is connected to the third beamport from the edge of all lenses on the upper stack of lenses. Each lens on the upper stack then produces a "ramped" phase distribution on its array port surface to excite the entire upper stack array port surface. Note that the phase ramp contributed by the single lens on the lower stack is imposed on the array port distributions of the upper stack, orthogonal to the phase ramps produced by the lenses of the upper stack. Thus, the normal to the phase distribution surface is pointed somewhat toward the diagonal of the upper stack. The phase distribution is transmitted

---

[12] Dome Antenna/Rotman Lens Study - Phase II Final Report, ONR-N00014-76-C-0651, September 1979.

through cabling directly to the dome array feed surface. Once at the array feed surface, the phase front is refracted by the dome into a planar wavefront of a beam within the hemisphere scan coverage.

The two-stack feed lens configuration is equivalent to row/column steering in phase shifted array feeds. The array ports in each lens in the top stack feeds a column of array elements, and each lens in the bottom stack feeds provides the phase variation for a row of points on the upper stack. Each beam port on the bottom corresponds to a specific pencil beam in space, whose direction is independent of RF frequency. Multiple beams are simply accomplished by feeding multiple beam ports, with no loss in aperture gain for each beam port fed. Only adjacent beamports fed simultaneously at the same frequency suffer loss and produce an intermediate beam.

The coordinates used in this report are standard spherical coordinates as shown in Figure 63. Zenith angle is 0°, and horizon angles are 90°. The two lens stacks are aligned with the X-axis ($\phi = 0$) and the Y-axis ($\phi = 90°$). Principal scan planes are the X-axis and the Y-axis ($\phi = 0$ or $\phi = 90°$). The main problem area in the two-stack feed lens approach will be for $\phi = \pm 45°$ scan planes, where greatest phase errors will occur.

As described in Appendix B, the two-stack feed lens approach is a proven technology which to date has been used on three major programs, EATS, GPS and MUSTRAC, and is planned for use on other major programs in the near future.

C. Error Contributors. Five sources of phase errors have been identified in the two-stack feed lens approach:

(1) Conduit error. Associated with path length variations arising from different lens designs for each lens in the upper lens stack.

(2) Lens implementation error. The lenses are designed for correct phase focus at only three scan angles; phase errors exist at all other angles.

(3) Single lens design error. When using the phase distribution correct for only one row of elements on the feed array to suffice for all rows, the difference between desired and required phase distributions from row-to-row is the error addressed here.

(4) Co-phase error. Multiple phase distribution requirements on a single minor axis row of elements to fit varying scan angles along a major axis.

(5) Minor axis lens error. Difference in phase distribution required by the dome along a minor axis corresponding to a particular scan angle (ξ), and the phase distribution provided by the lens feeding that minor axis row, corresponding to the slant of the scan plane used.

Identification of the error type plays an important role in error reduction since different corrective measures and design improvements are required for each type. These measures will now be described.

Conduit errors occur whenever all lenses of one stack are not of identical design. Reduction of conduit error thus requires identical or nearly identical lens designs for each stack. Since the errors introduced by using a single lens design are not large by comparison with other sources of error, conduit error is a minimal problem in most designs.

Lens implementation errors for lens atennas with beamwidths greater than 2° are not a problem. Maximum errors are less than random lens errors of ±20° which are commonly seen. Random lens errors are due to internal lens reflections and mutual coupling between lens ports.

Single lens design error can be corrected by using multiple lens designs for each stack. This however introduces conduit error so that a compromise position is needed. However, for our designs this error is less than other error types and not a problem. A single lens design will be used for simplicity.

The final two error types, co-phase error and minor axis lens error, are related in a way. Both are the result of phase variations with scan angles in two dimensional scanning. And both error types are the worst contributors to the overall error problem. There are several ways to minimize these error types, but eliminating them is impossible.

Minor Axis Lens error is caused by the fact that near the horizon the phase variations orthogonal to the plane of scan are different than phase variations for $\xi = 0°$ (zenith). Minor Axis Lens error can be corrected in two ways:

(1) Use the minor axis phase variation for horizon scan instead of $\xi = 0°$ scan phase variation in the lens design. This of course will introduce errors at or near zenith - but these can probably be tolerated.

(2) Reduce the differences between zenith scan data and minor axis phase data by lowering the feed array and/or adjusting its curvature for minimum variations.

Co-phase error, which is greatest for $\phi = \pm 45°$ azimuth scan planes (midway between the two lens stacks), results from different phase variations required of the lens for $\phi = 0°$ or 90° azimuth scan. Co-phase error is also the most difficult to reduce, and in fact as Section IV-2.b. shows, there is a limit below which co-phase errors cannot be reduced. This limit is created by different Dome phase variations in the X-axis and Y-axis for $\phi = 45°$ azimuth scan. This limit for the recommended Feed lens design of Section IV.3 is about 28° RMS error or ±80° peak error. This level of error while acceptable for transmit applications, limits achievable peak sidelobe levels to about 17 dB, a value which is unacceptable for most receive applications.

2. FEED LENS AND ARRAY TRADEOFFS

a. Tradeoff Candidates. Four candidate approaches to feed lens design were investigated:

(1) Single Lens. Where one lens design was used throughout both stacks. Feed array shape was that of the preliminary design concept.

(2) Three Lens. Where three different lens designs were used (center, midway, and outer lenses) in an effort to reduce "single lens" errors (see paragraph II). Feed array shape was still that of the preliminary design concept.

(3) "Minor Axis". Where the minor axis phase data for ξ = 81.3° scan replaced the zenith (ξ = 0) scan data in the Rotman lens design. This appraoch significantly reduced "minor axis" errors (see paragraph IV c) for near horizon scan (ξ = 70° to 90°), while increasing zenith scan errors. Feed array shape was still that of the preliminary concept. Errors for ϕ = 45° scan angle were examined in this case.

(4) Optimized Feed Array. Where feed array curvature was reduced (flattened). This approach reduced overall errors. Errors for ϕ = 45° scan angles were examined for this case. A minor axis lens design was also used in this case.

Table 5 gives the 3-D Dome design parameters of the four candidates. Design parameters are illustrated in Figure 64.

Table 6 presents a summary of the RMS phase errors and peak-to-peak phase errors for each of the candidates, both for principal plane scan angles (ϕ = 0 and 90°) and for ϕ =45° scan where available. Details of phase error distributions appear later in the discussion of each candidate.

Phase error distributions will be presented in the form of 2-dimensional plots of the feed array projected on the X-Y plane. Large phase errors appear as dark in these plots. Also in all cases, symmetry about the scan axis is present, so data for only half the feed array is shown.

Figures 65 and 66 show the 12 GHz phase errors for the Single Lens design model, for $\xi = 90.2°$ (horizon) in the principal scan planes; with $\phi = 0°$ and $\phi = 90°$, respectively. Phase error distributions for zenith scan ($\xi = 0°$) are not shown, since the sheet would be blank - all phase errors are less than 20°. Phase errors below 20° peak continue for scan angles of $\xi = 42°$ or less.

The Single Lens design model phase errors for $\xi = 90.2°$ increase quadratically in bands away from the scan axis (Y = 0 for $\phi = 0°$ scan) At the edges of the feed array, peak errors of 100° are present. RMS errors are 25.05° which is excessive for low sidelobe applications, and also restricts the useable size of 3-D Dome/Rotman Lens Antenna since errors will be proportional to size.

Phase errors and distributions for the model are Three Lens design model shown in Figure 66 again for horizon scan, $\xi = 90.2°$, in the principal scan plane. Phase errors here are not much different than the Single Lens model case, and show the same banded error pattern away from the scan axis.

The banded pattern of phase errors and lack of improvement with three lens designs points to minor-axis lens error as the dominant error contributor. If so, improvement is possible - at least for preferred horizon scan angles - by use of a novel approach to Rotman Lens design for 3-D Domes, the Minor Axis Lens design.

b. Minor Axis Lens Design. As Appendix B indicates, the Rotman Lens design uses data for three focal points or scan angles, ξ = -90° and +90° in our cases. This produced the excessive minor axis errors seen above. Replacing the ξ = 0° phase data by the "minor axis" phase data for ξ = 81.3° would, in theory, eliminate this error along the minor axis orthogonal to the scan axis. Scan axis and minor axis are illustrated in Figures 67 and 68. The price to be paid will be increased errors for near zenith angles. Also, the lens shape and size for such a design need to be examined.

The Minor Axis Lens design was implemented with very encouraging results. Phase error distributions for ξ = 71.2° and 90.2° in the principal scan plane show about 60% improvement (Figures 69 and 70). RMS errors are now 9.5° and 11°, respectively, with peak errors of 29° and 44°. These errors would produce very good sidelobes for those beams. Errors at zenith have increased to 20.5° RMS and 67° peak (Figure 71) which was expected.

For shipboard applications of the 3-D dome, with preferred horizon coverage, the degradation at zenith angles should not present a problem. Nonetheless, as section IV-c will show, an optimized feed array can be designed which will reduce zenith errors to acceptable limits and improve horizon coverage at the same time.

Diagonal scan (ϕ = 45°) cuts were taken for the first time with this minor axis lens design case. Results were not good, with 38.8° RMS errors and 123° peak errors for ξ = 87° scan at ϕ = 45°. This excessive level of error is attributed to co-phase error caused by great differences in phase variation between the X and Y principal plane data for diagonal scan. A discussion of co-phase error, and limitations on error performance appears in Section IV-d.

c. Optimized Feed Array. The second design change which should improve error performance is to reduce curvature (flatten) the feed array. While this goes against the preliminary design concept selected on the basis of 2-D central slice data, a flatter array will reduce the differences between minor-axis and scan-axis phase data.

The reduced curvature array was obtained by increasing the center of curvature, R_4, to 7.0 inches. (See Table 5 and Figure 65). Other design dimensions remain the same.

Principal scan plane performance with the optimized feed array is much improved. As Table 6 shows, RMS errors are below 10° except for 10.2° at $\xi = 0°$ (zenith), and peak errors are all below 36°.

Figures 72 through 83 show the phase error distributions. This design reduces principal scan plane errors to low acceptable limits, and sidelobe levels of 23 to 25 dB should be achievable in the principal scan plane.

Unfortunately, diagonal scan plane data ($\phi = 45°$) does not improve for the optimized feed array - in fact it gets a little worse. RMS errors reach 40.4° for $\xi = 87°$ and $\phi = 45°$, with peak errors of 123°. This will severely limit sidelobe performance for diagonal scan.

The above results led to consideration of the factors involved in co-phase errors for diagonal plane scan.

d. Limits On Co-Phase Error Reduction. As indicated before, co-phase errors in 3-D Domes using Two-Stack Feed lenses occur because of differing phase variations along principal X and Y axis for diagonal scan ($\phi = 45°$).

Referring to Figure 84, the two-orthogonal planes highlighted must, by symmetry, use the identical lens design. The 3-D Dome data for these two rows is summarized in Table 7 for $\xi = 87°$, and $\phi = 45°$. This data, taken from computer runs, gives the path length variations (in inches) which each lens provides if perfect focusing were to be achieved (only the path length differences matter - constant path lengths can be added or subtracted).

If the "ideal" lens was designed from a minimum co-phase error point of view (Table 6), phase errors at 12 GHz of + 65° to - 68° would still exist, which would produce errors of about 28°. RMS at $\xi = 87°$. While this is a 30% reduction over actual errors, it is still much too high for critical designs.

Limited further reduction in phase errors might be possible with changes in feed array configuration. However, any reductions will be small for practical configurations of feed array.

3. RECOMMENDED FEED LENS DESIGN

The final design (Section IV c.) with an optimized feed array and minor axis lens design is recommended. This design will have maximum phase errors somewhat higher than the integrated Dome/Lens design of Sperry (40° RMS versus 23° RMS) for horizon scan, but will not require special Dome designs which degrade significantly for high angles toward zenith. Also, RMS errors could be reduced to 28°. RMS by use of the "ideal" lens design of Table 7.

a. Mechanical Design. A preliminary estimate of system physical characteristics is given in Table 8. The system packaging concept and drawing tree are shown in Figures 85 and 86 respectively. This configuration consists of two primary subassemblies: Antenna array/elevation lens, and azimuth lens.

The antenna/elevation lens subassembly consists of 23 stripline circuits etched from copper clad duroid 5880, with each circuit assembly containing an integrated 23-port antenna array and lens. The duroid dielectric is banded with a thin film adhesive for strength and dimensional stability. The circuits are supported and spaced with aluminum plates which also serve as connector mounts for the lenses' beam ports. One lens design is used in all cases, with 23 array and 13 beam ports.

The azimuth lens subassembly is similar in construction to the array/elevation lens assembly except that it consists only of 13 identical lens circuits, with connectors at both beam and array ports. This set of lenses is oriented 90° with respect to the elevation lenses. Cable input/output to the system is done by the 169, (13 X 13,) beam port connectors.

Interface between the two subassemblies is accomplished by a panel matrix of floating "blind-mate", or quick-disconnect connectors. The array/lens panel containing guide pins and quick-disconnect jacks, and is supported by two brackets from the primary structure. The lens panel contains quick disconnect plugs, and is supported by standoffs. Semirigid cable (.085 in. diameter) is used between lens ports and quick-disconnects. The subassemblies are joined by two mounting brackets, which also serve as overall system mounts.

V. CONCLUSIONS

The preliminary design of a 3-D Dome/Rotman Lens Antenna has been presented which offers good performance except for diagonal scan (45°), performance which is comparable to the Sperry Integrated Dome/Lens Antenna.

Co-phase errors, which limit performance in the selected two-stack lens approach, are shown to be due to phase variations of principal scan plane and the orthogonal minor axis plane for diagonal scan. In the recommended design, errors due primarily to co-phase errors are 40° RMS.

Other phase errors have been reduced to minimal acceptable levels by a novel lens design and optimizing the feed array configuration.

Critical hardware was built and tested, and clearly demonstrated the feasibility of the 3-D Dome/Rotman Lens Antenna concept.

The best potential application of the Dome/Lens technology is the 2-D Wide Angle Array Fed Lens as demonstrated on an earlier Raytheon program. This concept offers 180° (or more) of scan from a single semicircular array, with multiple beams and ultra wide bandwidth. As a transmitter it could replace two quadrant transmitters with a single 180° transmitter, and thus reduce cost and handoff complications.

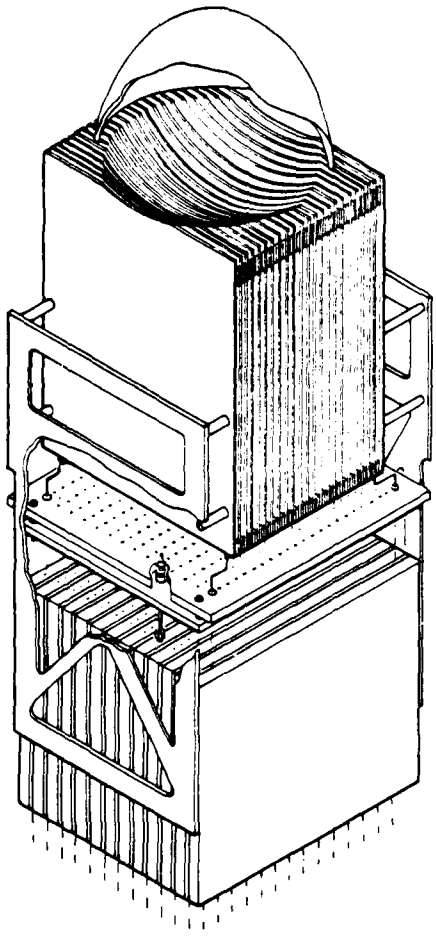

Figure 1. 3-D Dome/Rotman lens antenna.

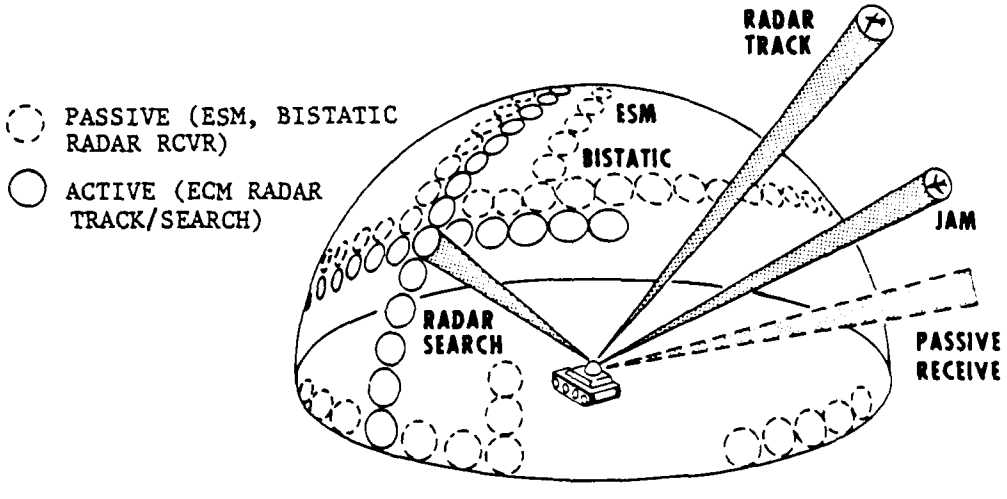

Figure 2. Scenario of 3-D Dome/Rotman lens antenna operation.

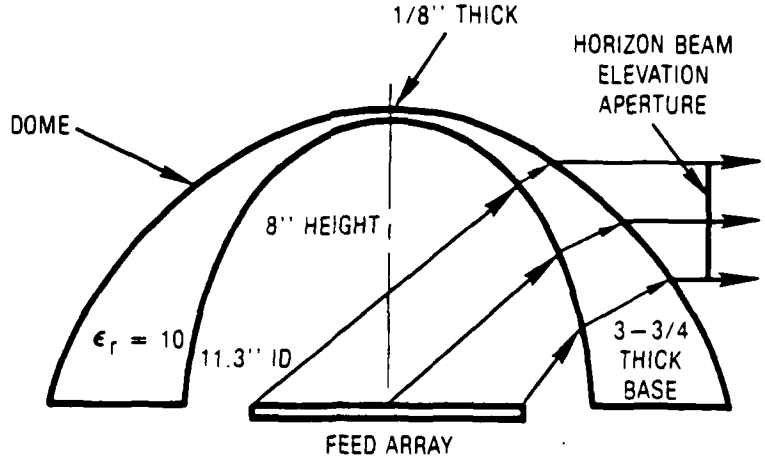

Figure 3. Gain tailored dome.

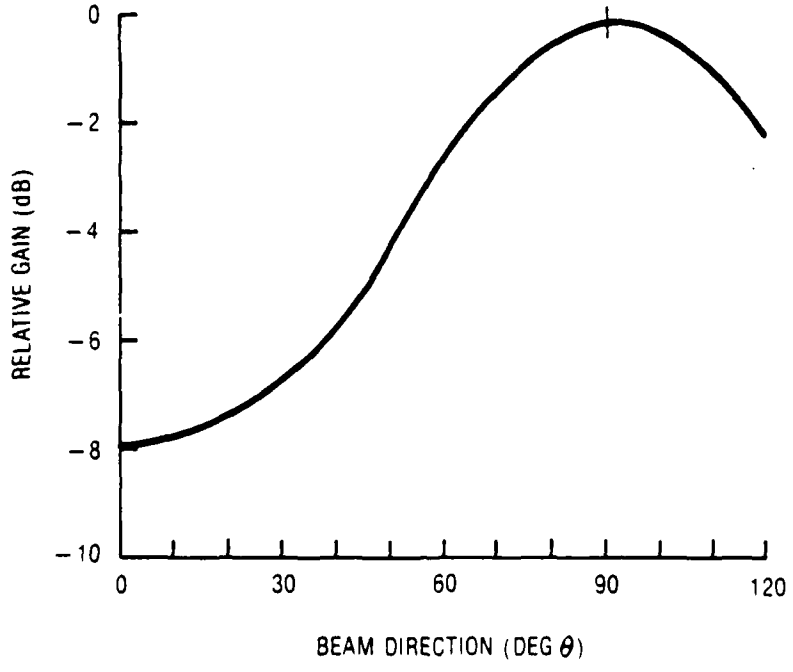

Figure 4. Relative gain of gain tailored dome.

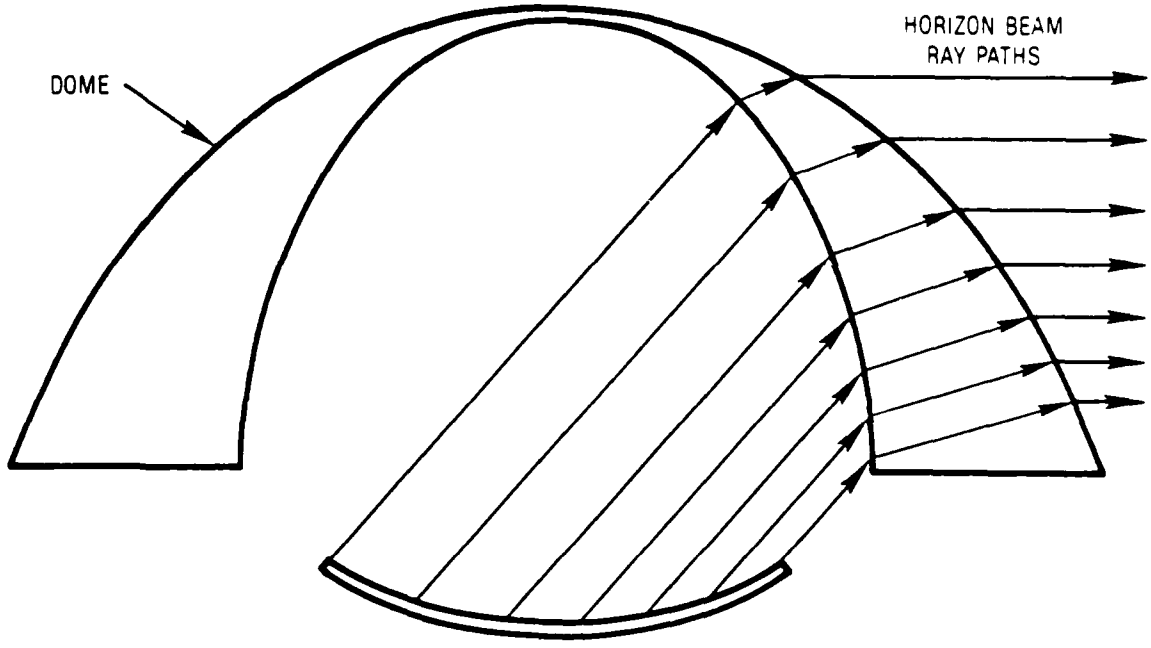

Figure 5. Dome with curved feed array.

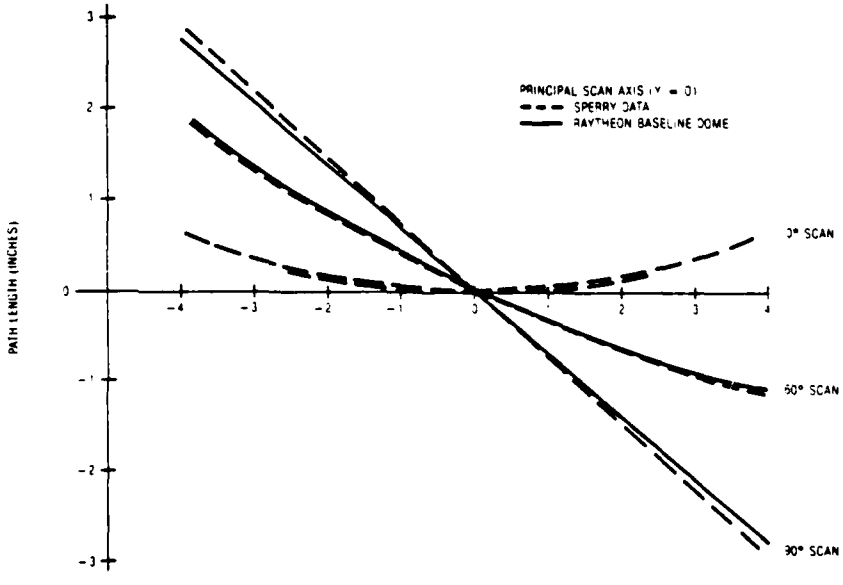

Figure 6. Comparison of dome path length variations, principal scan axis (flat array).

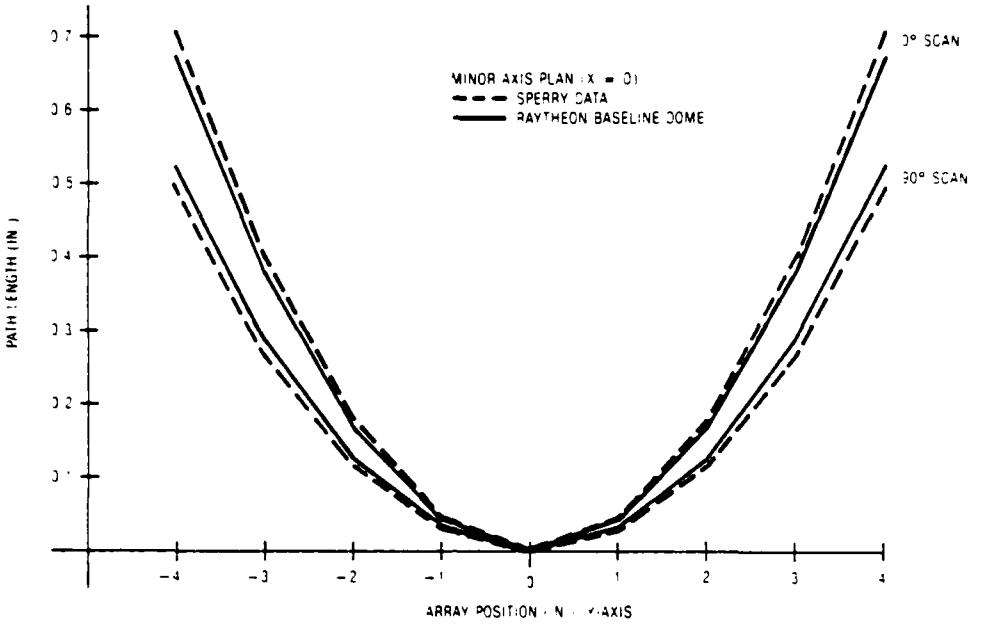

Figure 7. Comparison of dome path length variations, minor axis plane (flat array).

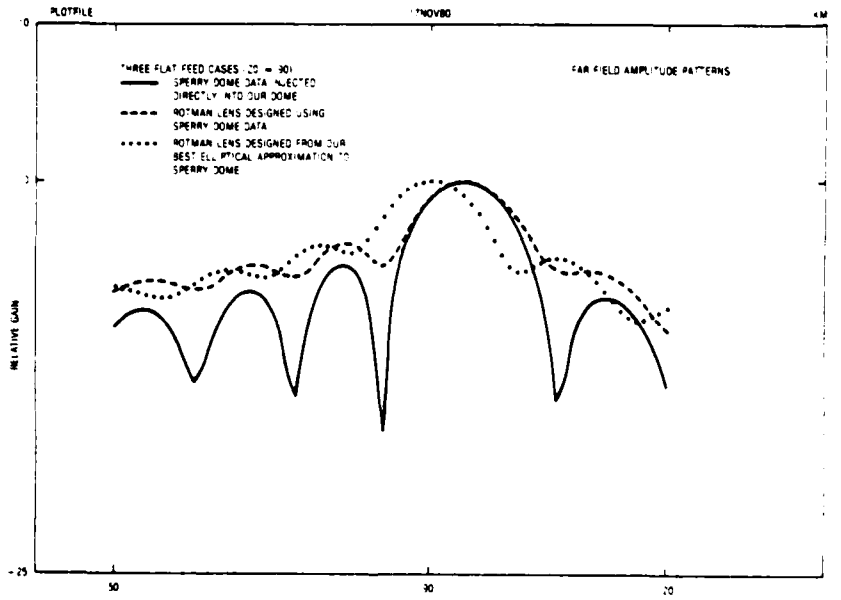

Figure 8. Comparison of dome radiated patterns (ξ_0 = 90°).

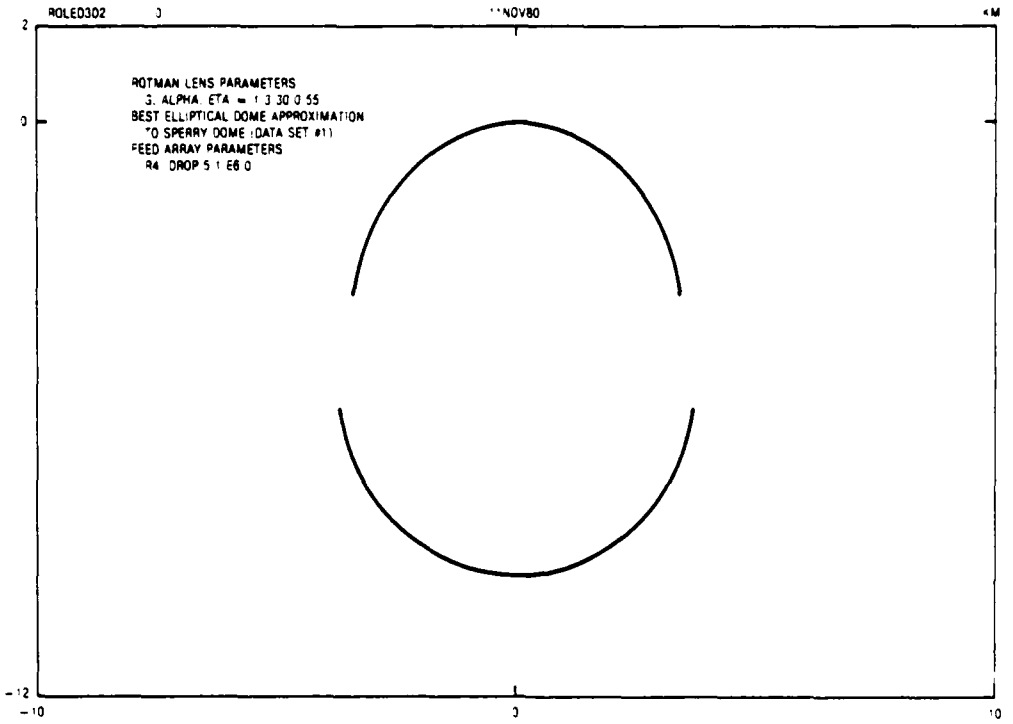

Figure 9. Lens design for flat array.

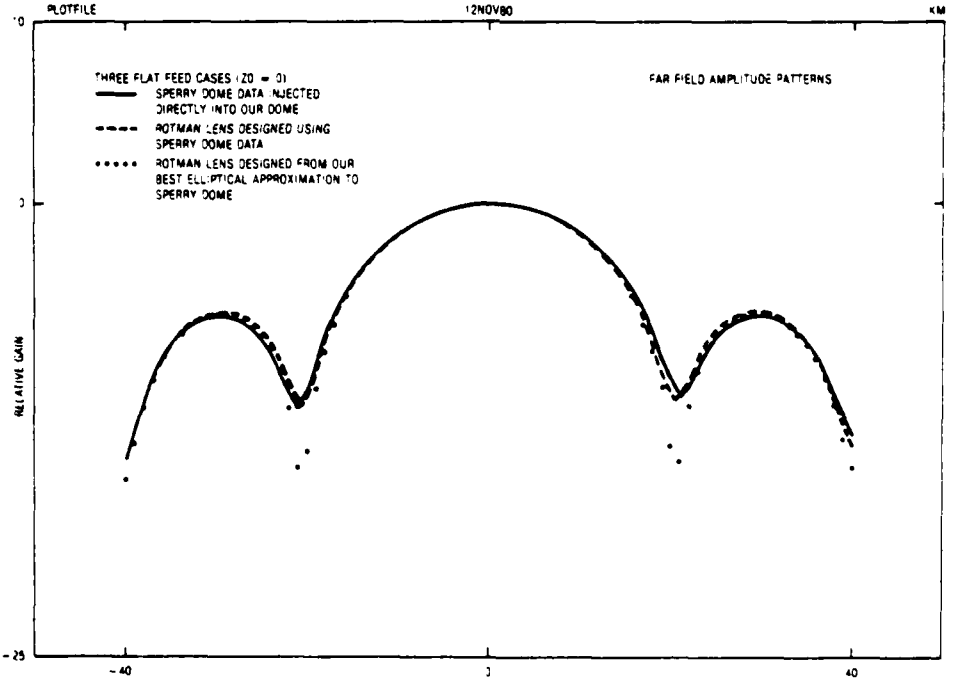

Figure 10. Comparison of dome radiated patterns ($\xi_o = 0°$).

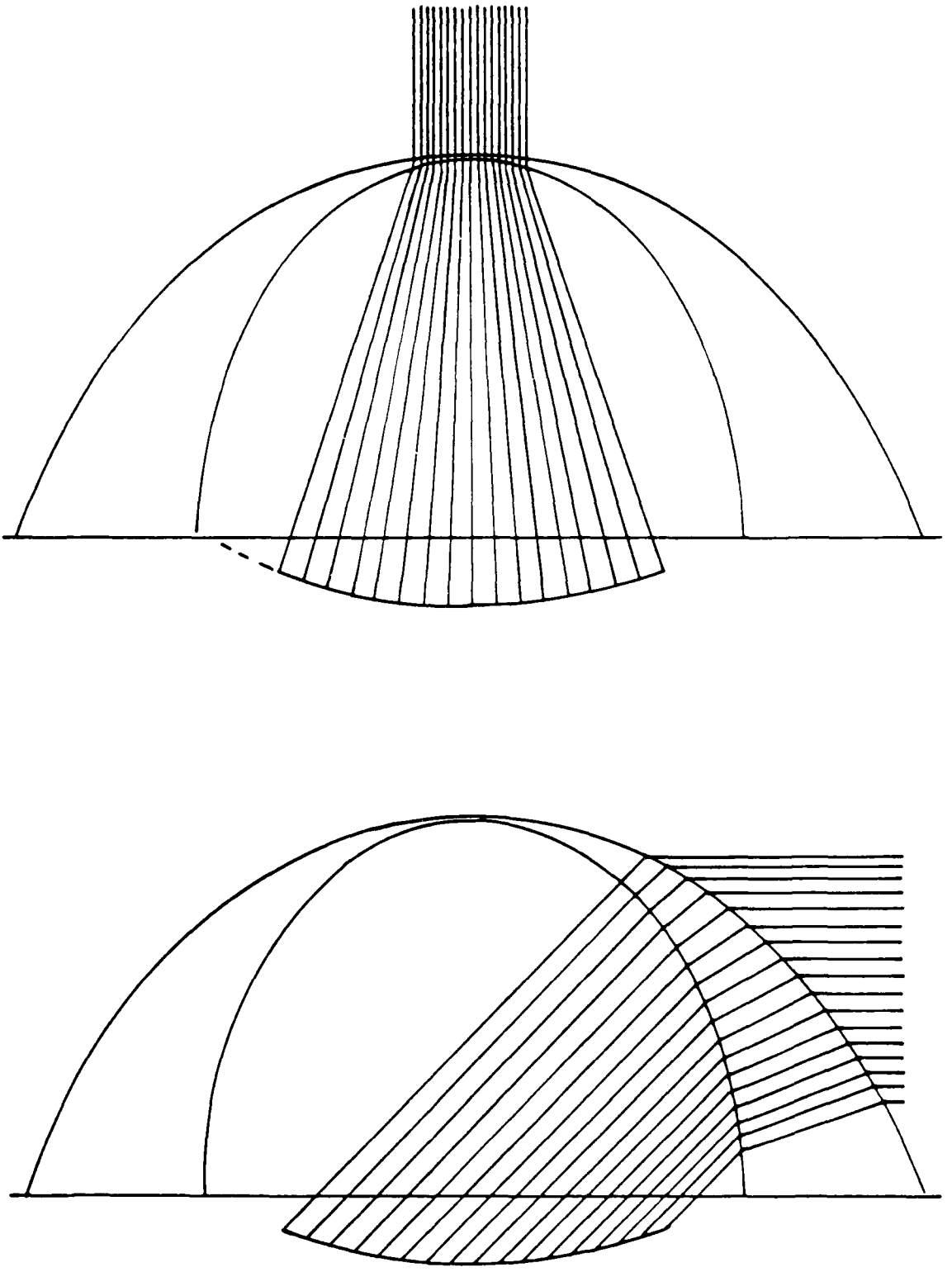

Figure 11. Ray paths of dome with curved array feed (radius of curvature 10.77 inches).

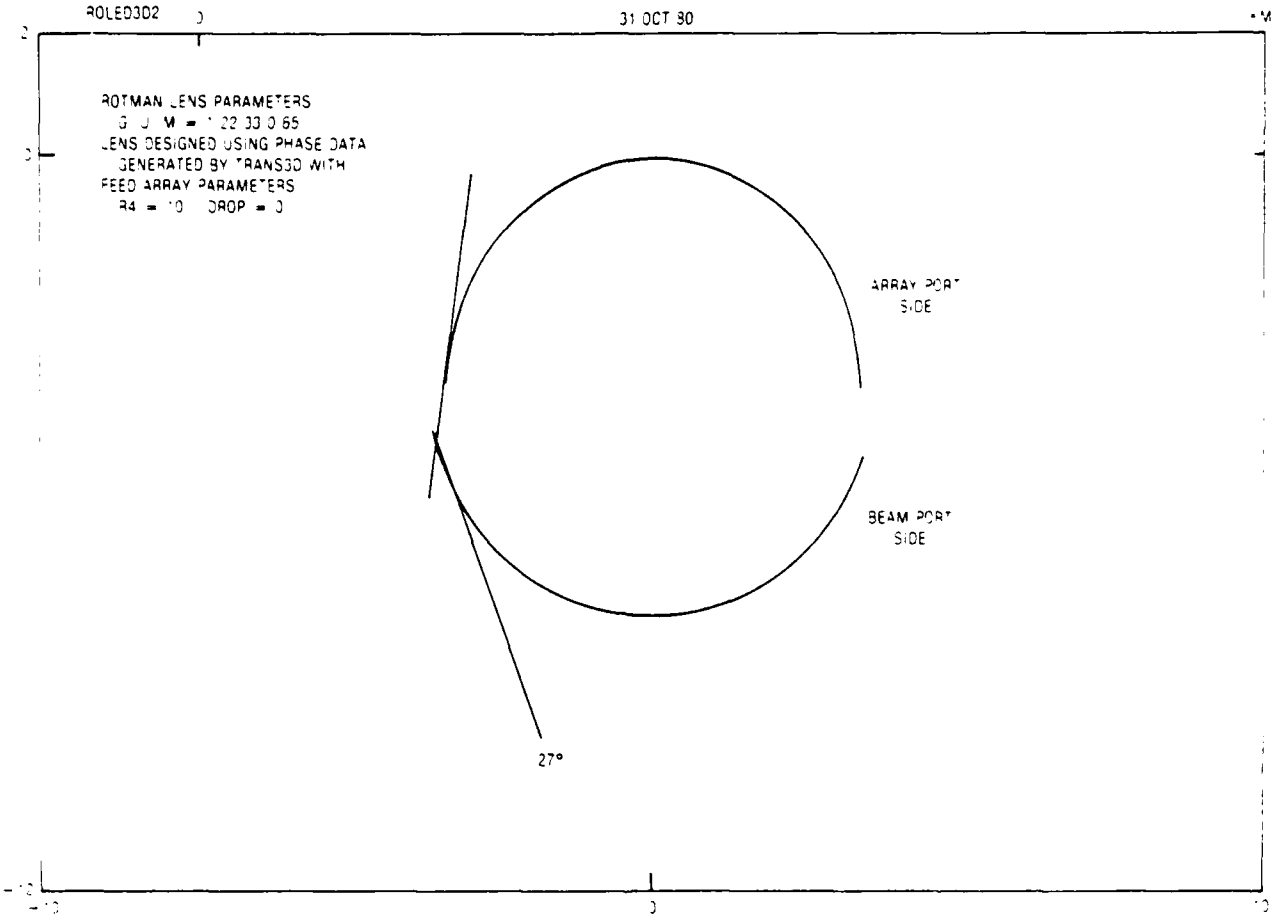

Figure 12. Lens design for Figure 11 dome (R4 = 10 inches).

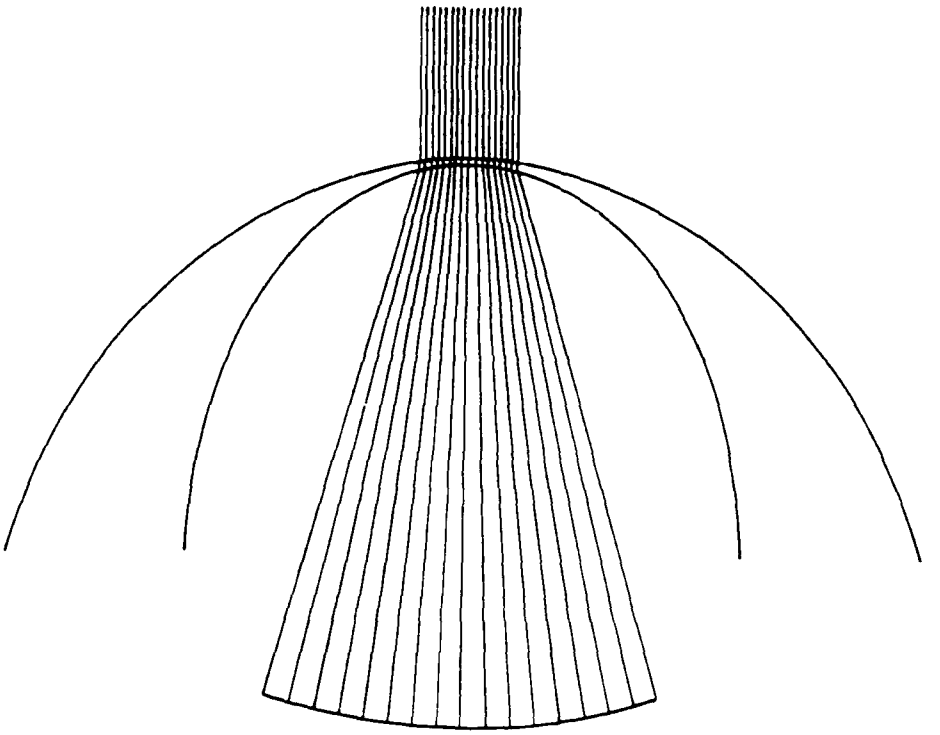

Figure 13. Ray paths of dome with dropped curved array (R4 = 10 inches) (ξ_o = 0°).

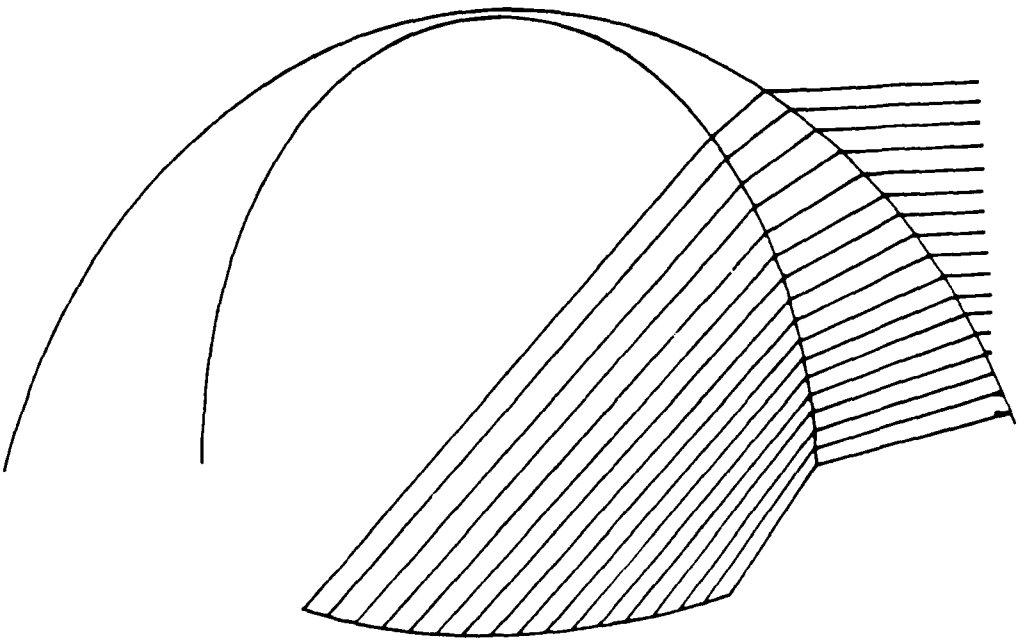

Figure 14. Ray paths of dome with dropped curved array (R4 = 10 inches) (ξ_o = 90°).

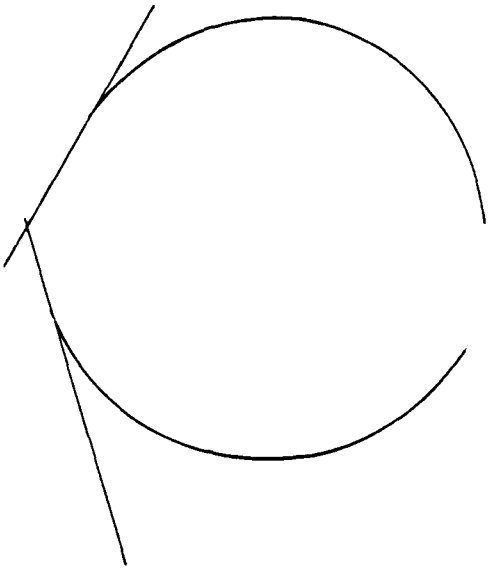

Figure 15. Lens shape for Figure 14 dome.

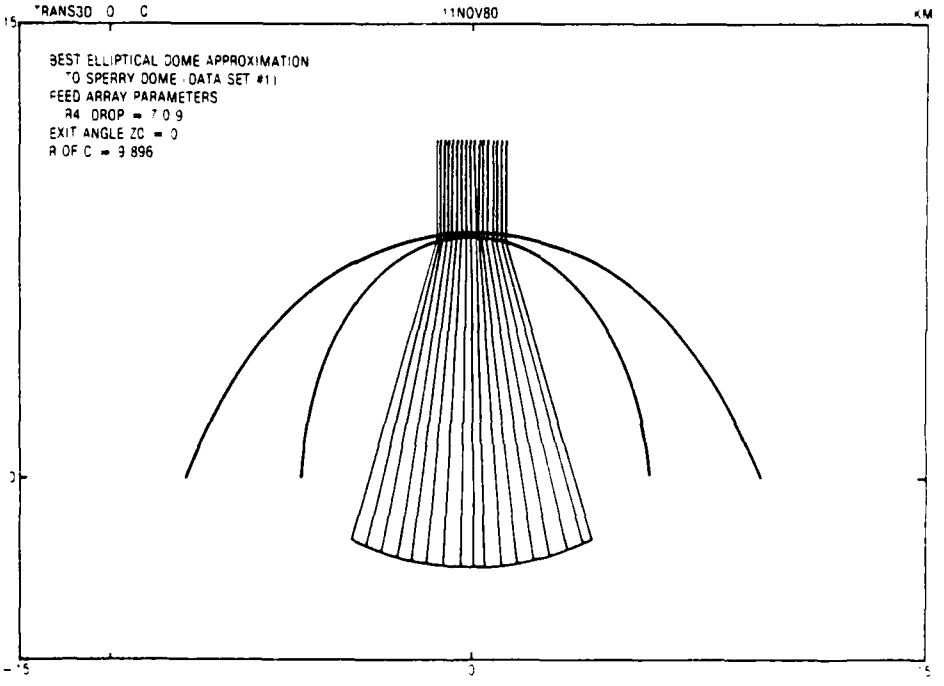

Figure 16. Ray paths for dome with curved array (R4 = 7 inches) ($\xi_o = 0°$).

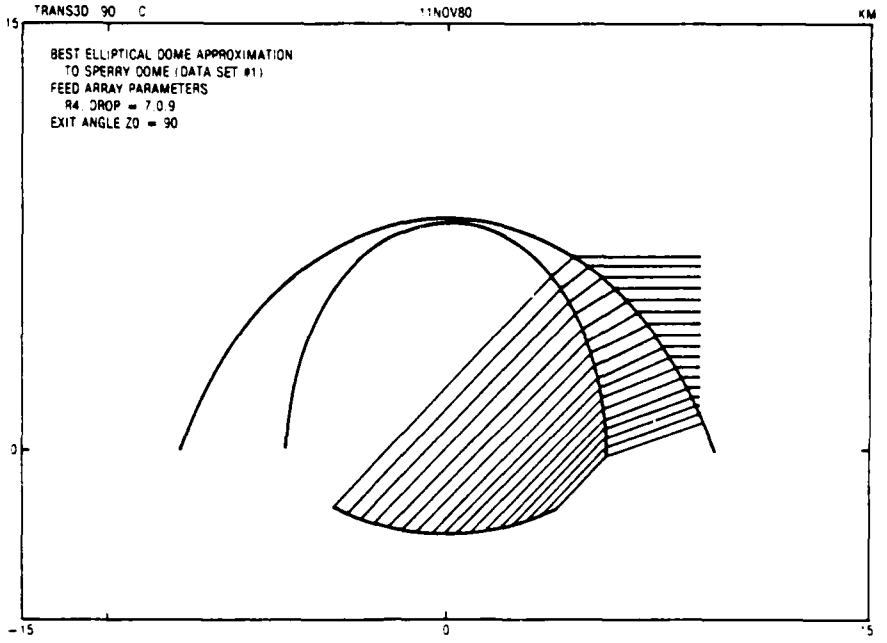

Figure 17. Ray paths for dome with curved array (R4 = 7 inches) (ξ_o = 90°).

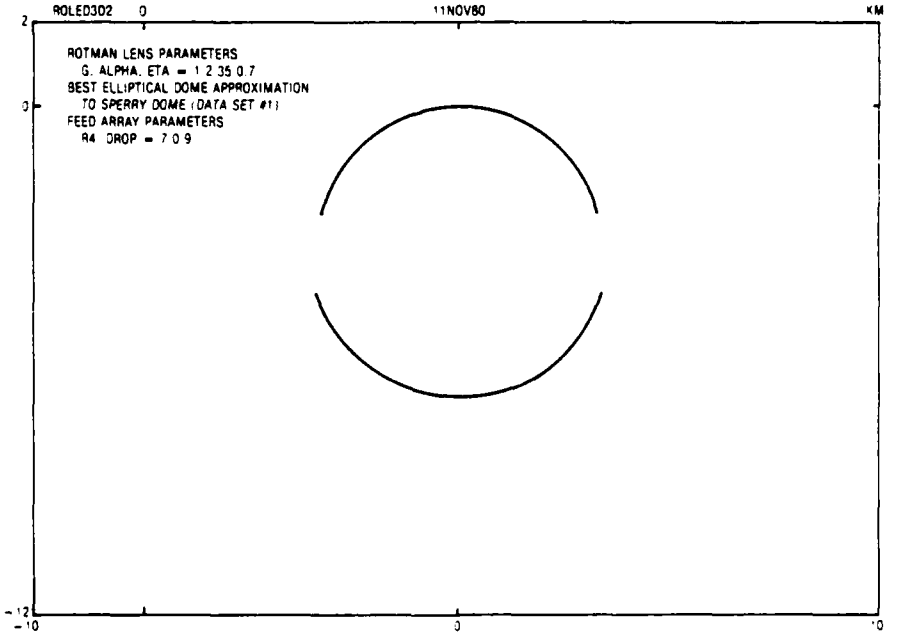

Figure 18. Lens design for Figure 17 dome.

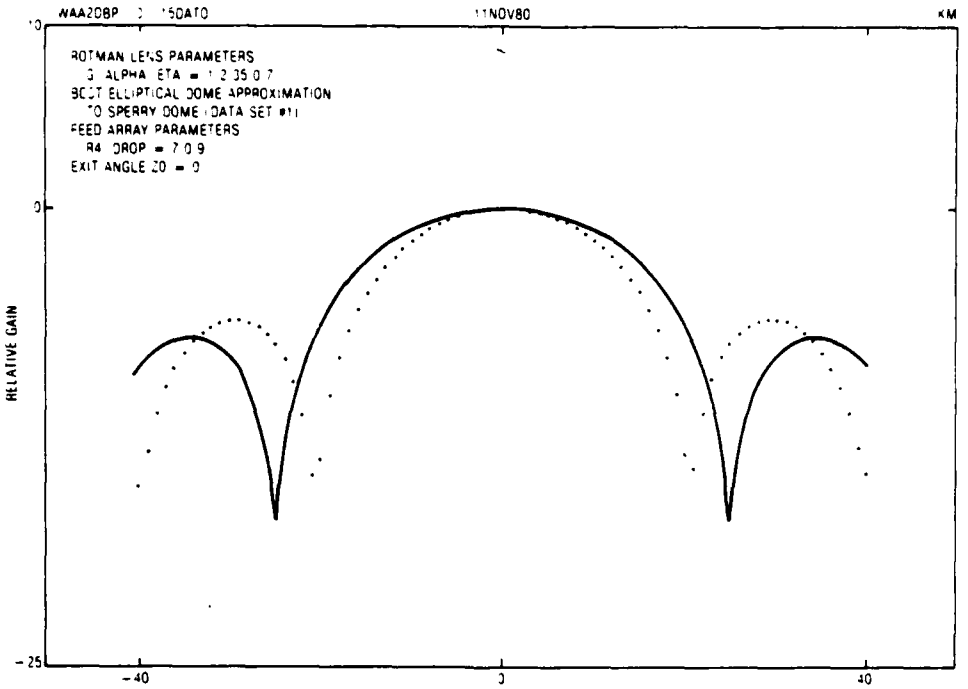

Figure 19. Radiation patterns (R4 = 7 inches) (ξ_o = 0°).

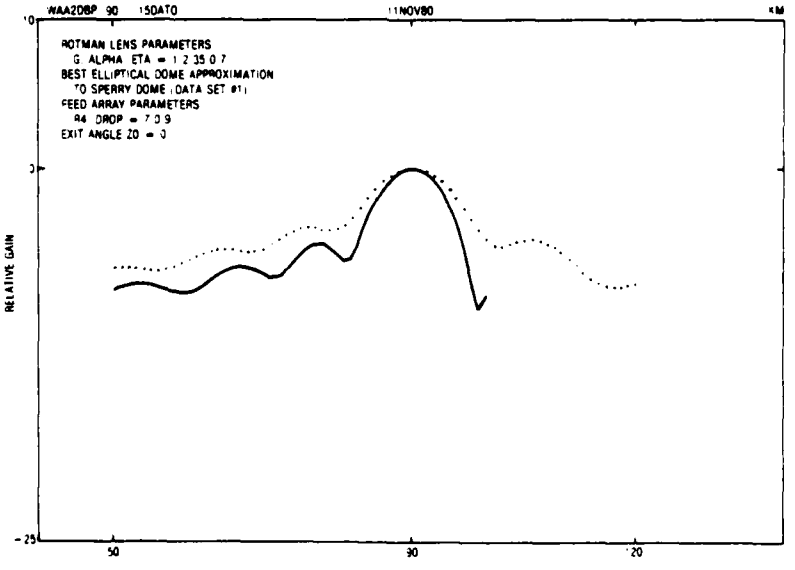

Figure 20. Radiation patterns (R4 = 7 inches) (ξ_o = 90°).

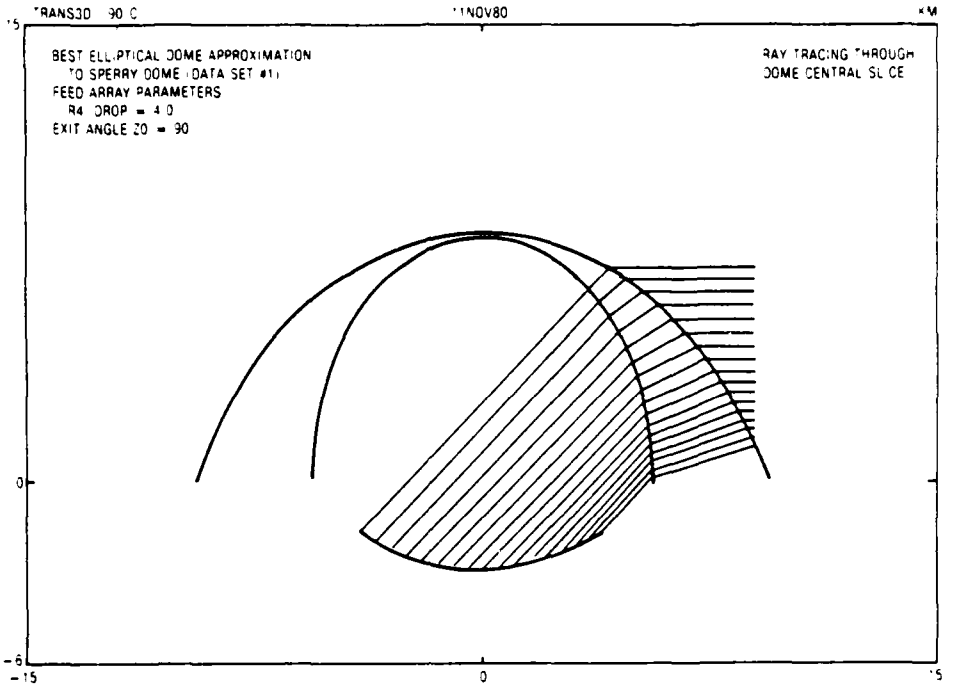

Figure 21. Ray paths of dome with curved array (R4 = 4 inches) ($\xi_o = 90^o$).

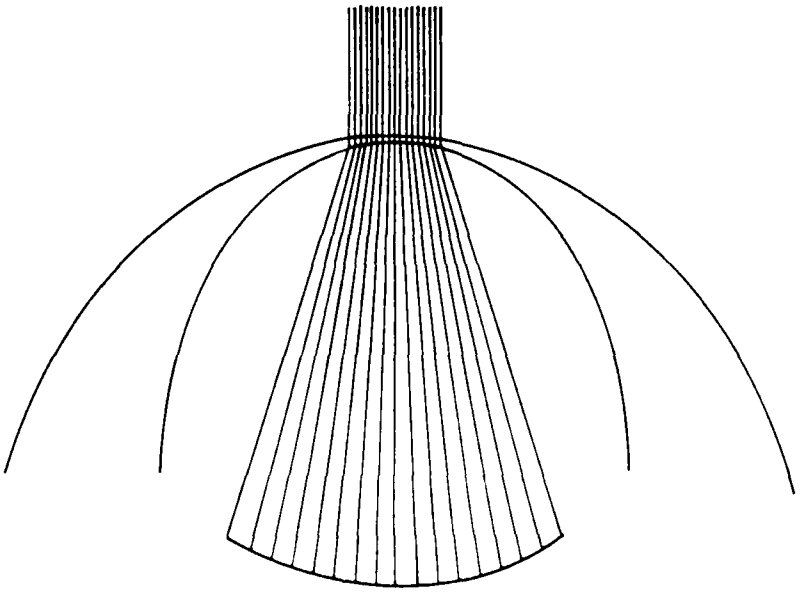

Figure 22. Ray paths of dome with curved array (R4 = 4 inches) ($\xi_o = 0^o$).

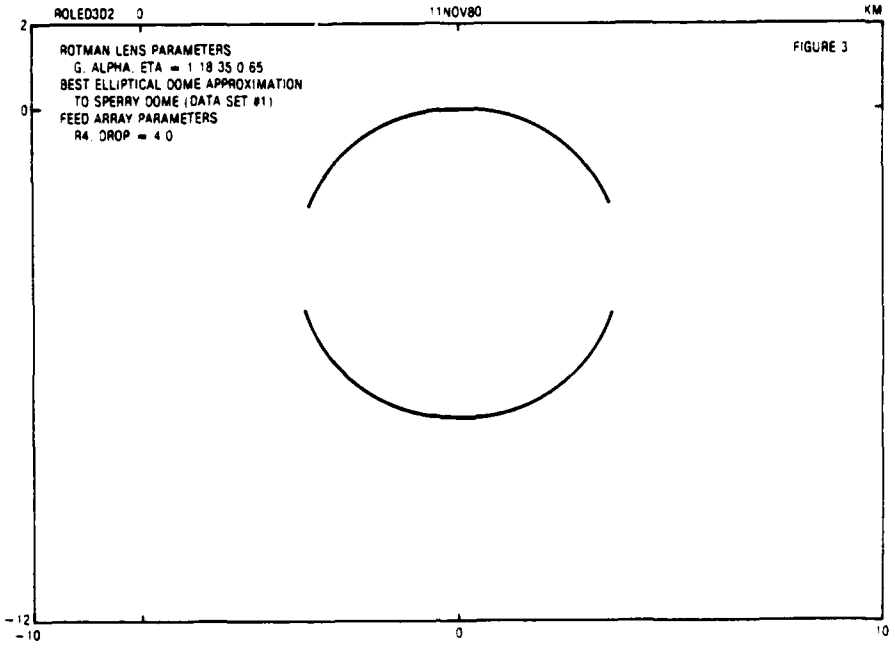

Figure 23. Lens shape of Figure 22 dome.

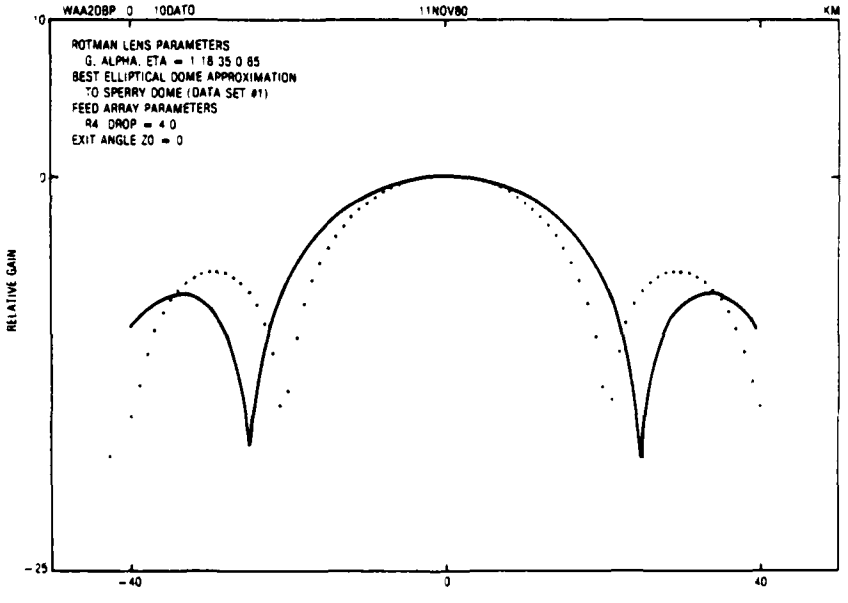

Figure 24. Radiated patterns (R4 = 4 inches) ($\xi_o = 0°$).

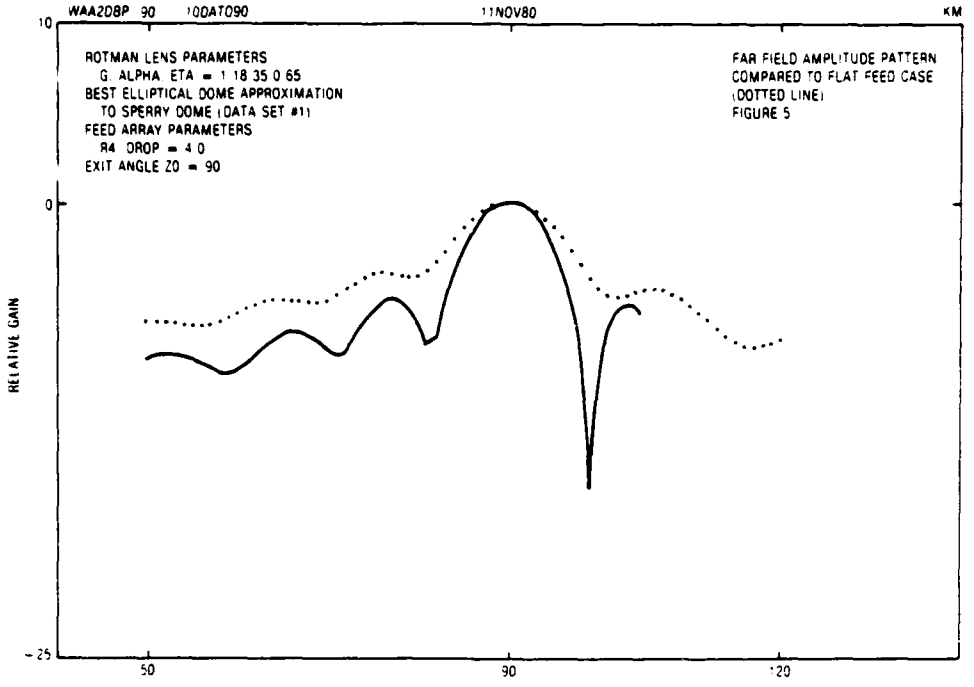

Figure 25. Radiated patterns (R4 = 4 inches) (ξ_o = 90°).

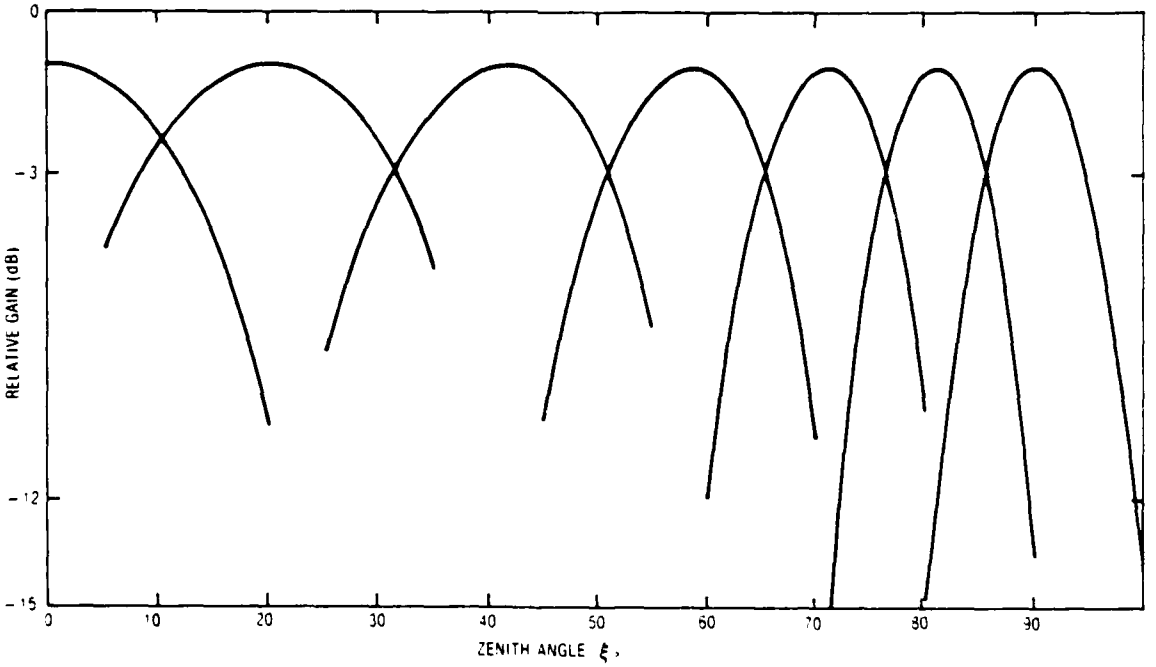

Figure 26. Exterior elevation beam patterns.

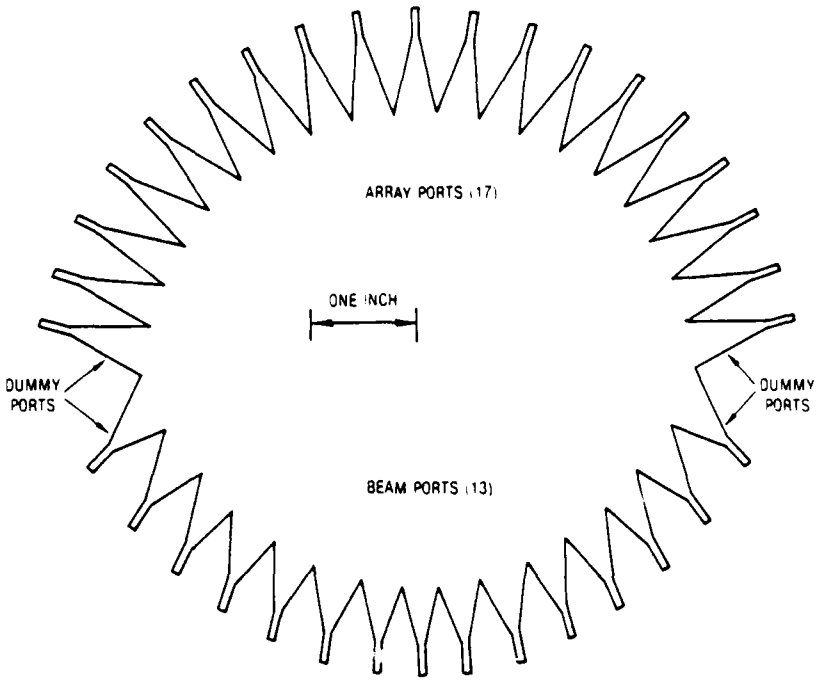

Figure 27. Central slice lens for dome feed array.

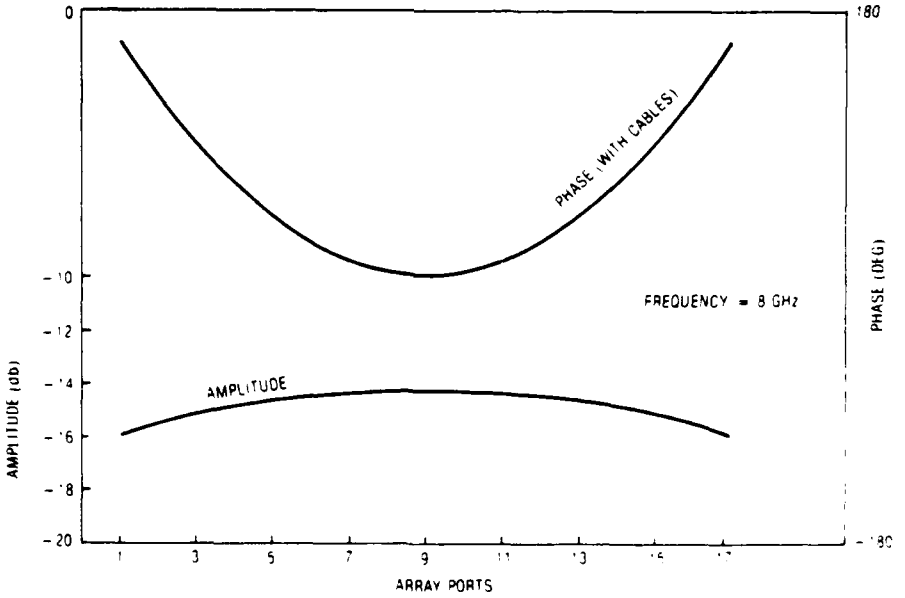

Figure 28A. Theoretical amplitude and phase for central lens, Z ϕ = 0°.

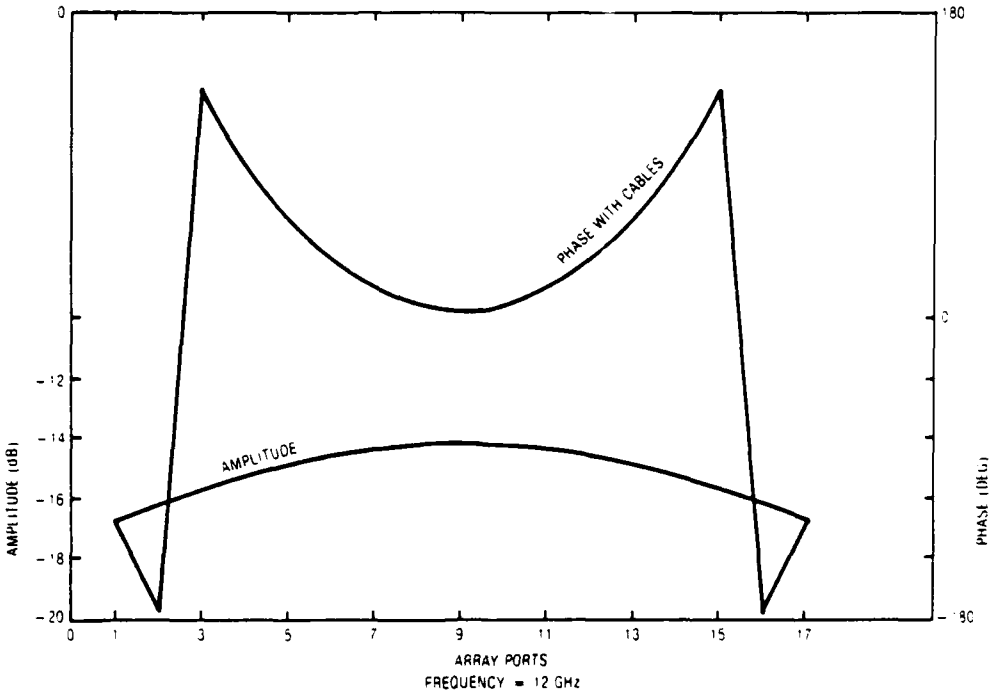

Figure 28B. Theoretical amplitude and phase for central slice lens, Z ϕ = 0°.

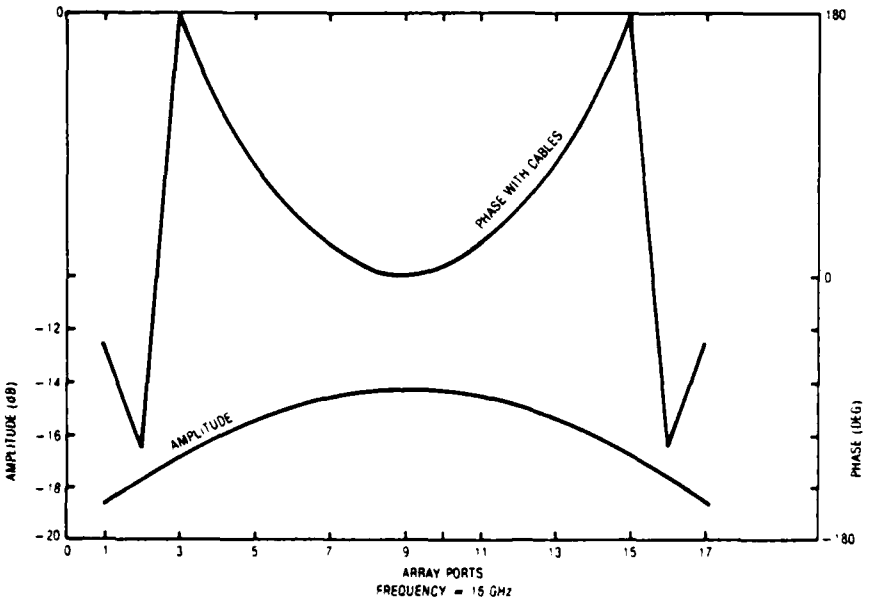

Figure 28C. Theoretical amplitude and phase for central slice lens, Z ϕ = 0°.

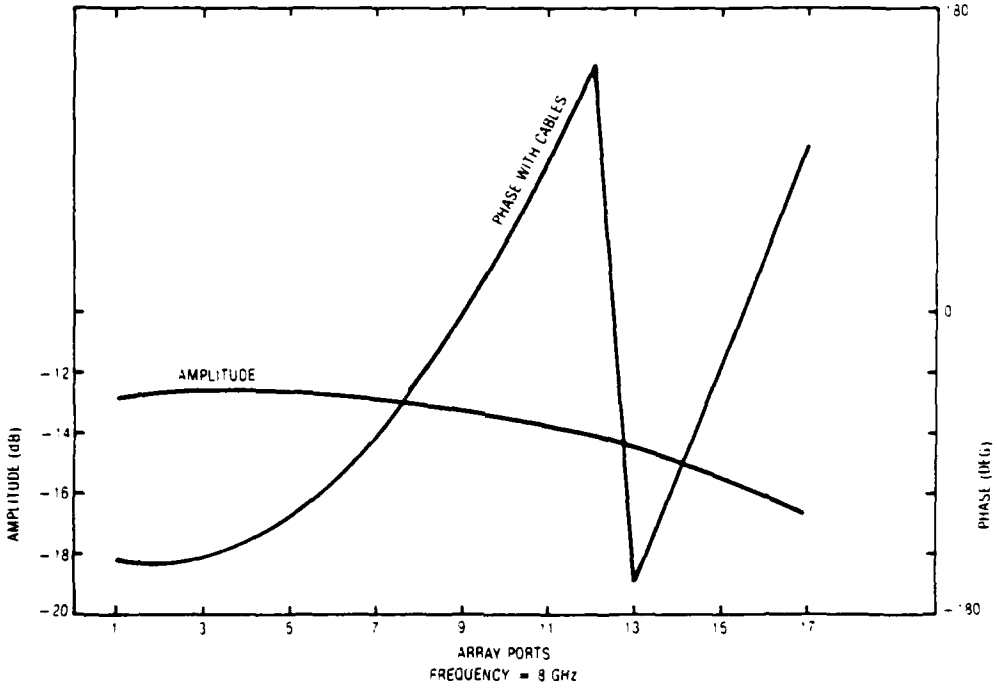

Figure 29A. Theoretical amplitude and phase for central slice lens, Z ϕ = 59°.

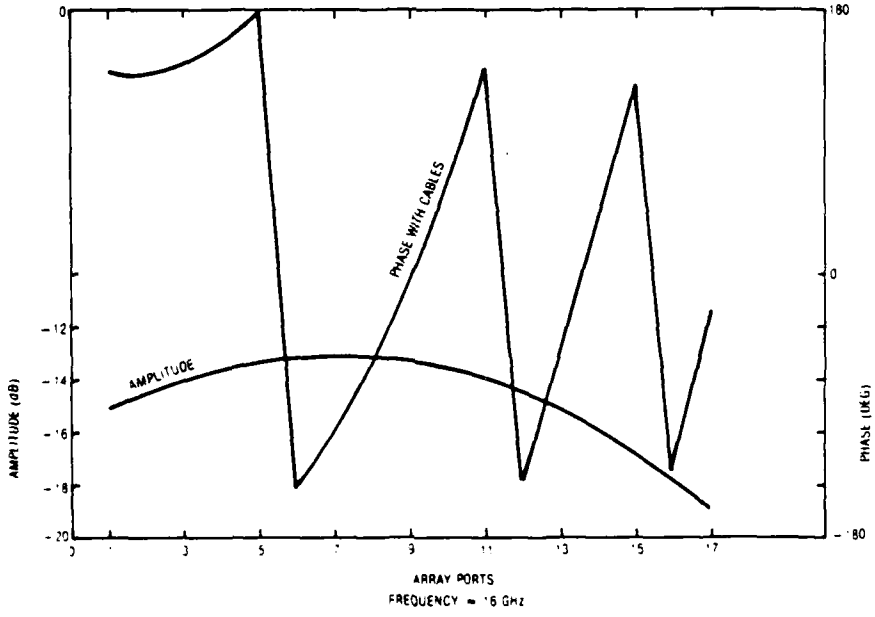

Figure 29B. Theoretical amplitude and phase for central slice lens, Z ϕ = 59°.

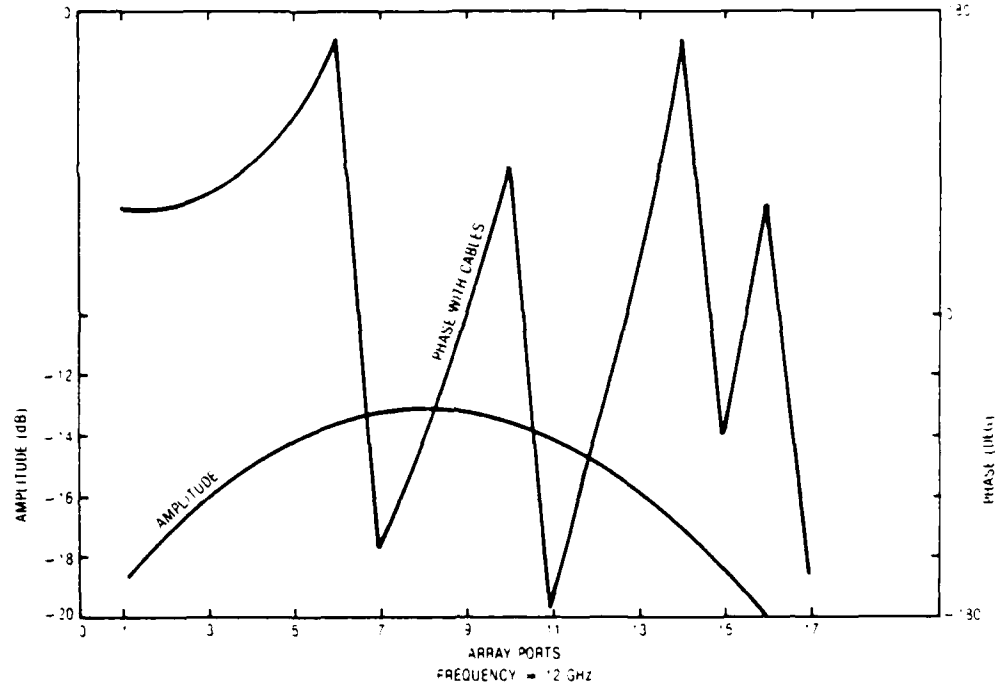

Figure 29C. Theoretical amplitude and phase for central slice lens, $Z\xi = 59$.

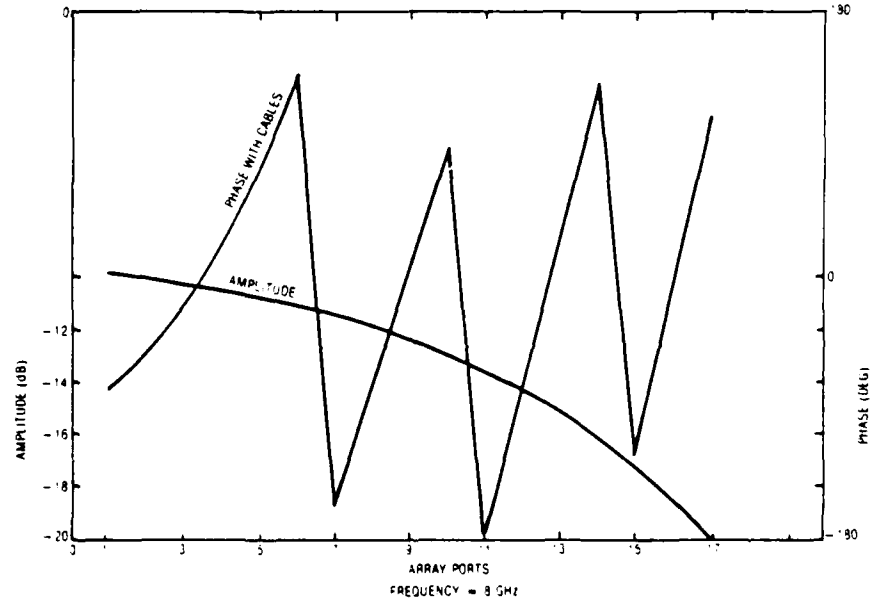

Figure 30A. Theoretical amplitude and phase for central slice lens, $Z\phi = 90°$.

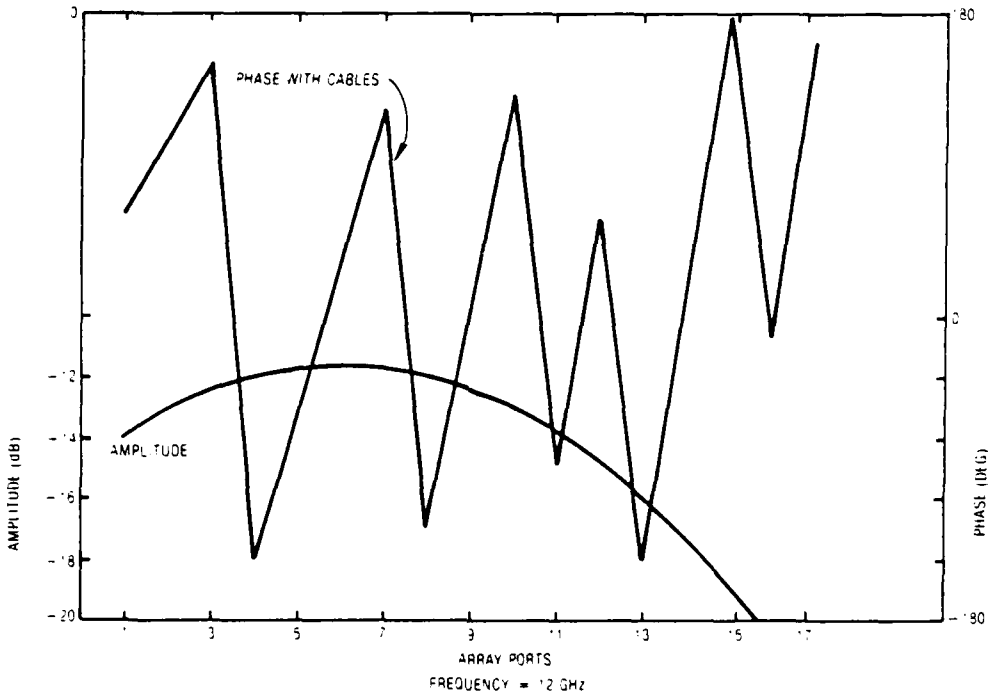

Figure 30B. Theoretical amplitude and phase for central slice lens, $Z\phi = 90°$.

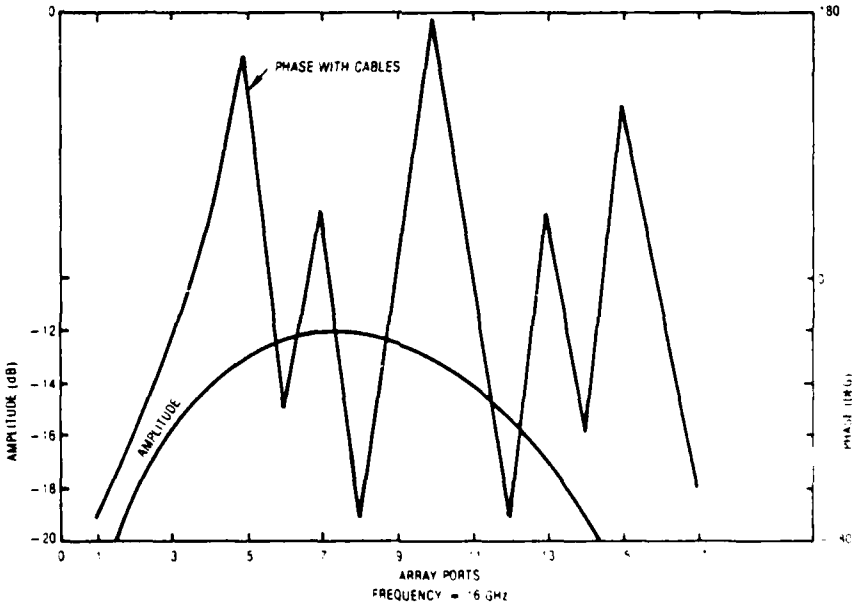

Figure 30C. Theoretical amplitude and phase for central slice lens, $Z\phi = 90°$.

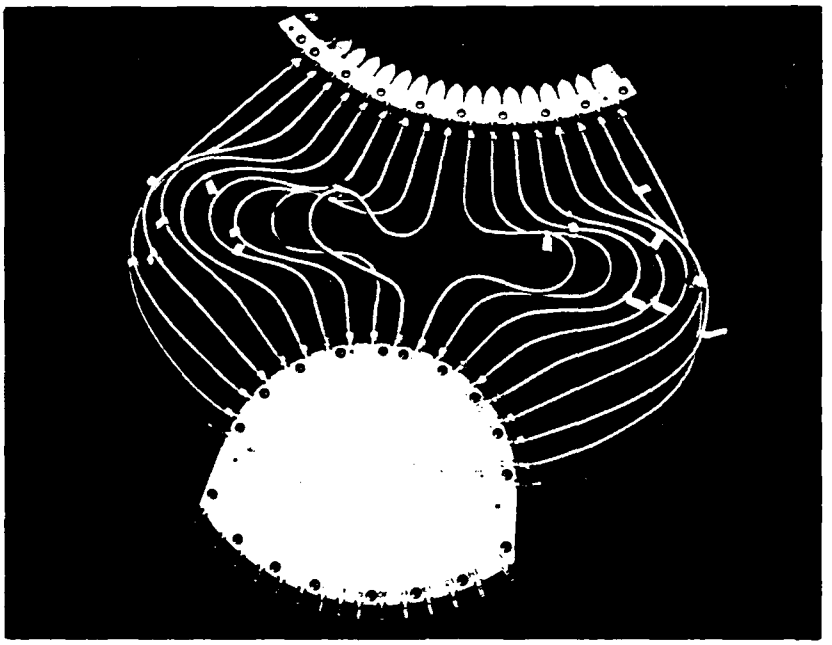

Figure 31. Standard beamforming lens.

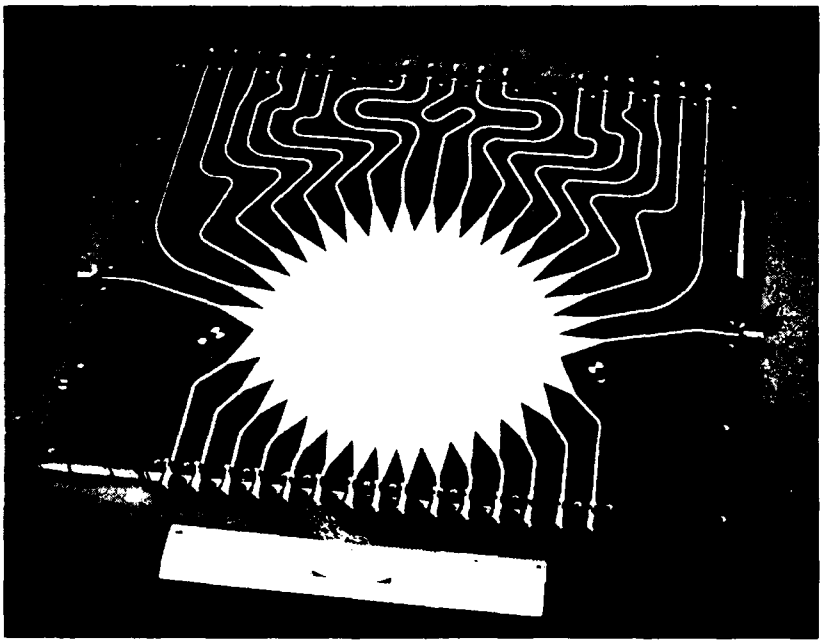

Figure 32. Integrated beamforming lens.

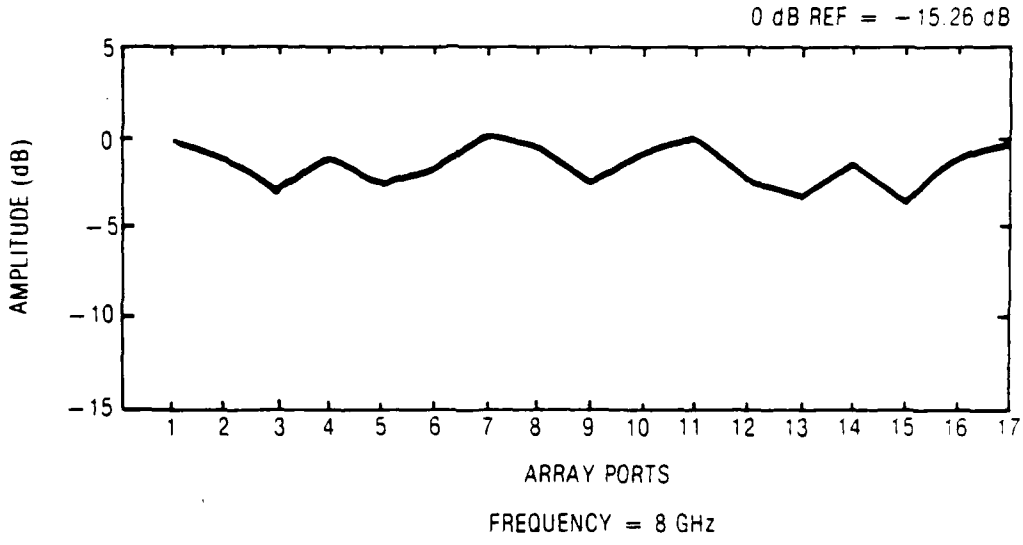

Figure 33A. Measured amplitude for standard lens, Zϕ = 0°.

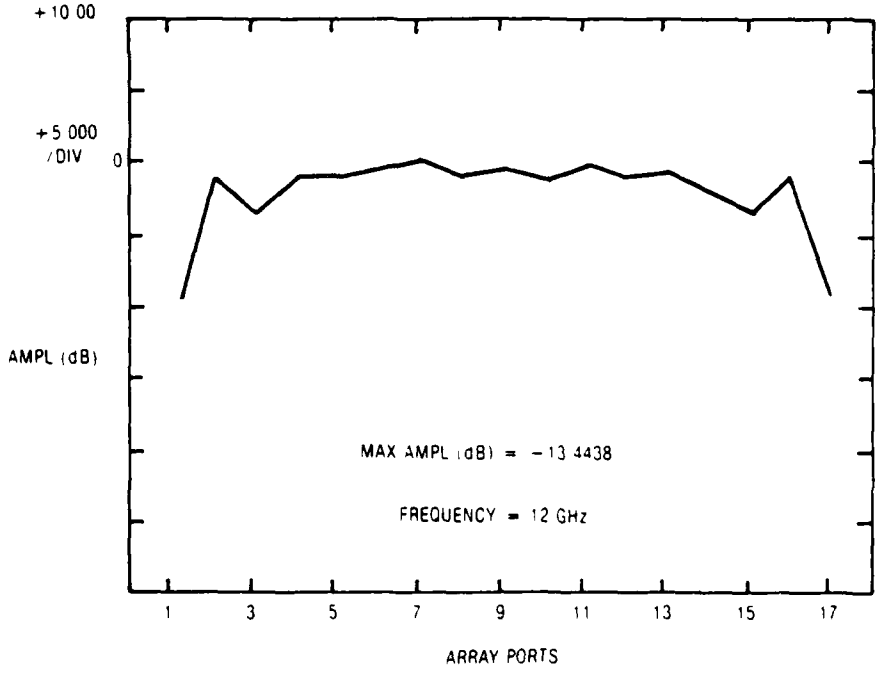

Figure 33B. Measured amplitude for standard lens, Zϕ = 0°.

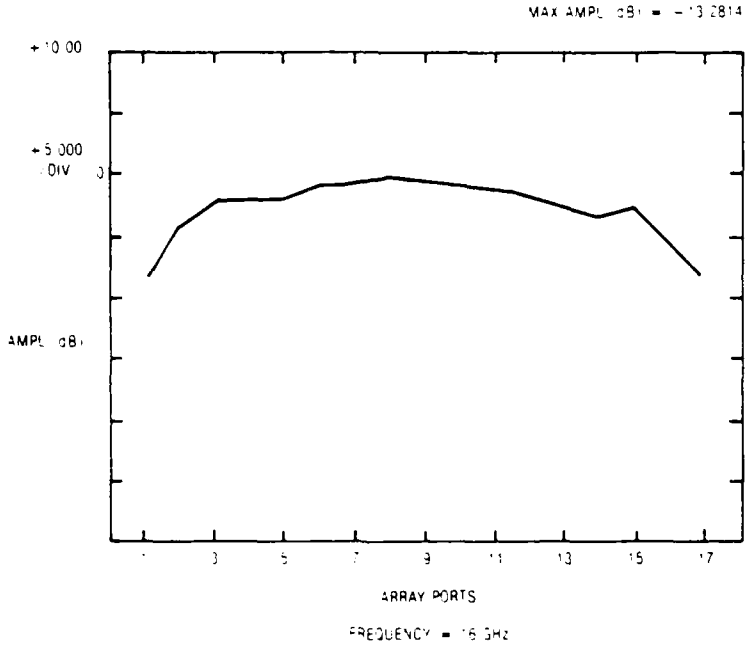

Figure 33C. Measured amplitude for standard lens, Zφ = 0°.

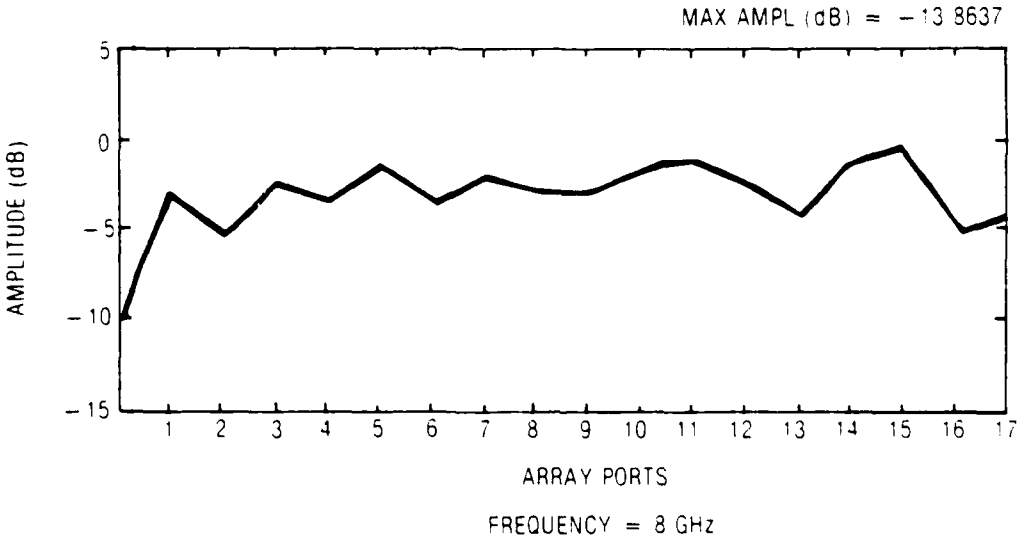

Figure 34A. Measured amplitude for standard lens, Zφ = 59°.

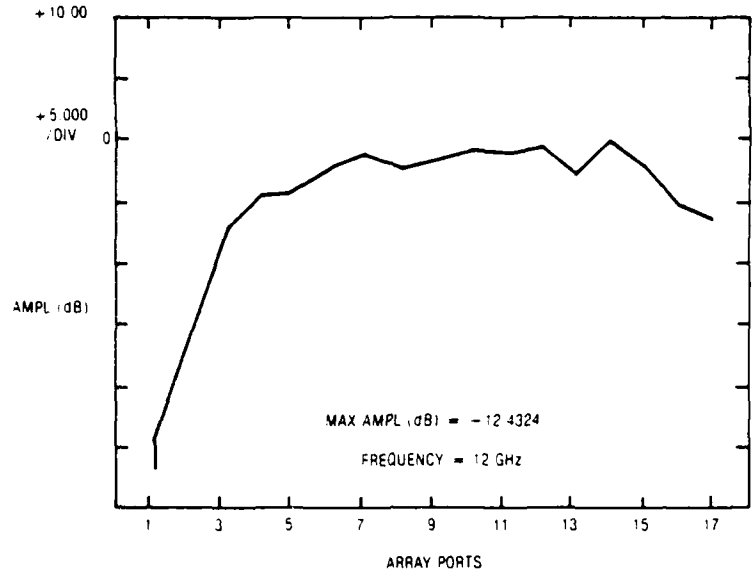

Figure 34B. Measured amplitude for standard lens, Zϕ = 59°.

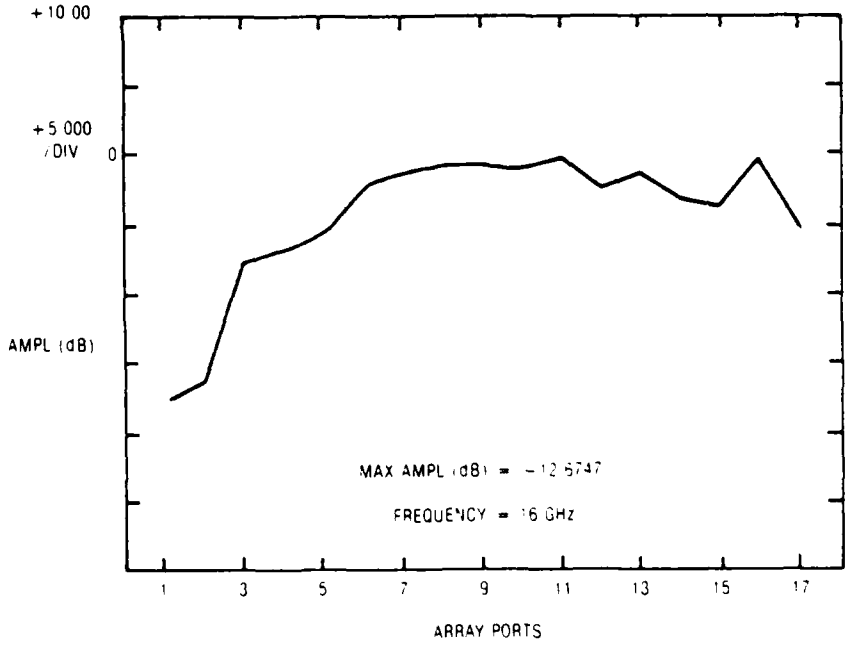

Figure 34C. Measured amplitude for standard lens, Zϕ = 59°.

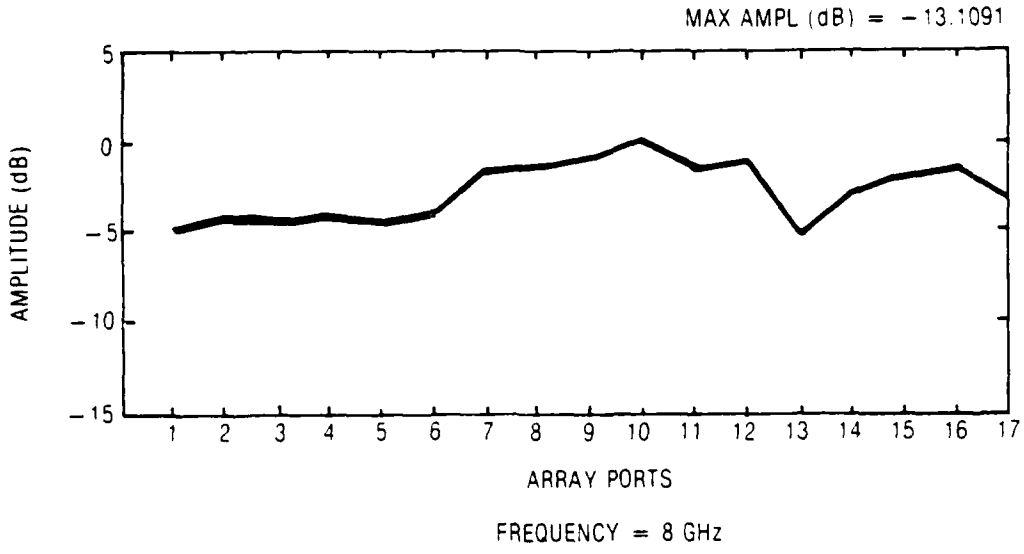

Figure 35A. Measured amplitude for standard lens, Zϕ = 90°.

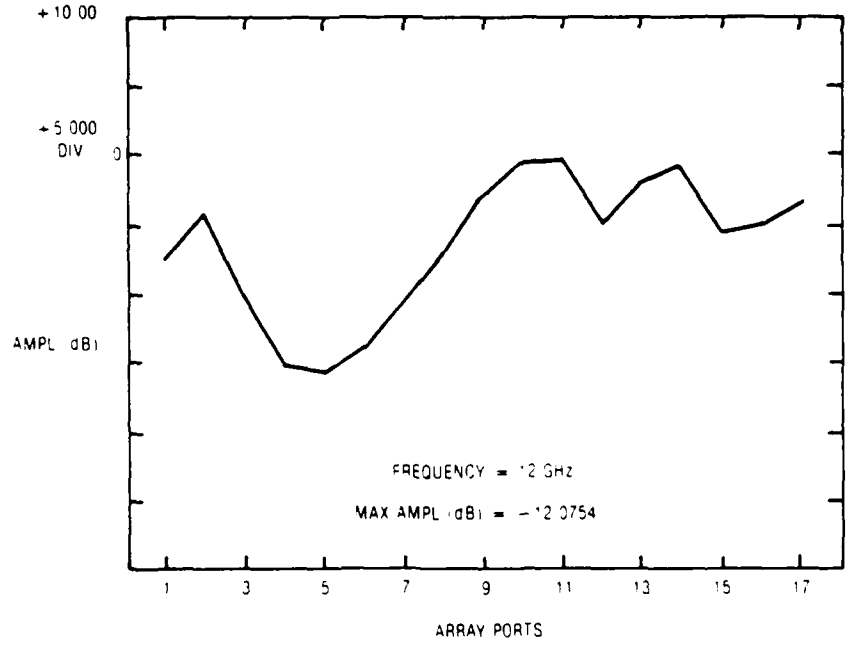

Figure 35B. Measured amplitude for standard lens, Zϕ = 90°.

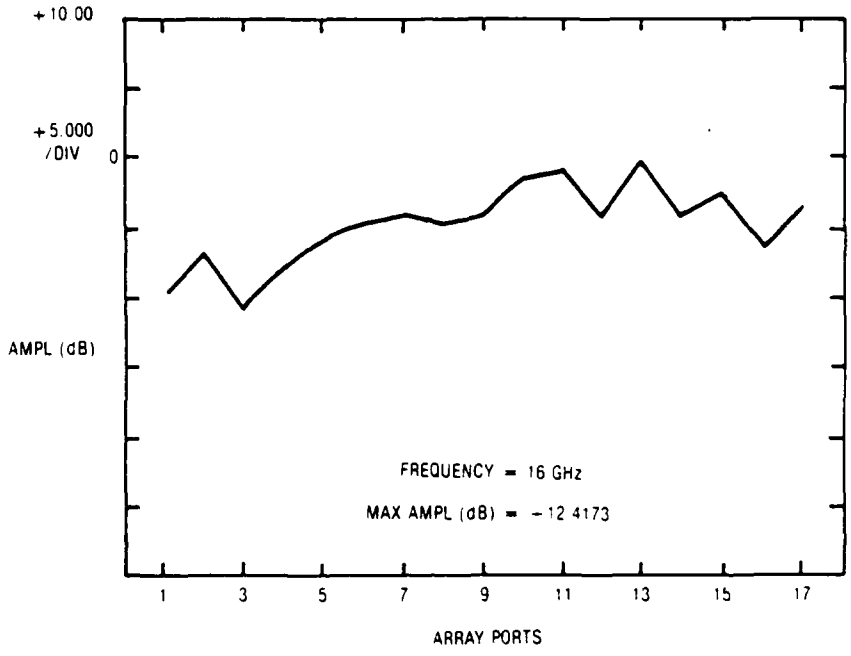

Figure 35C. Measured amplitude for standard lens, Zϕ = 90°.

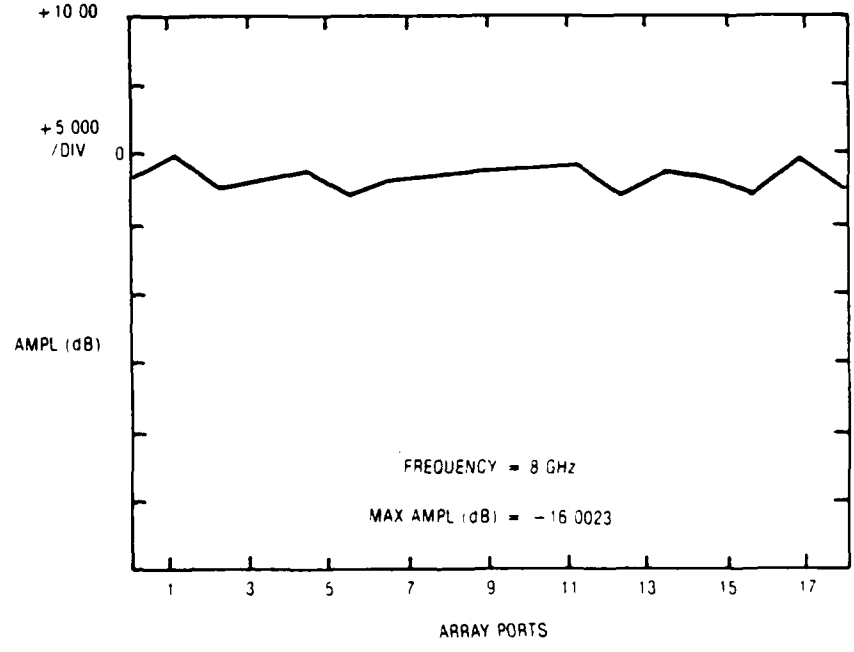

Figure 36A. Measured amplitude for integrated lens, Zϕ = 0°.

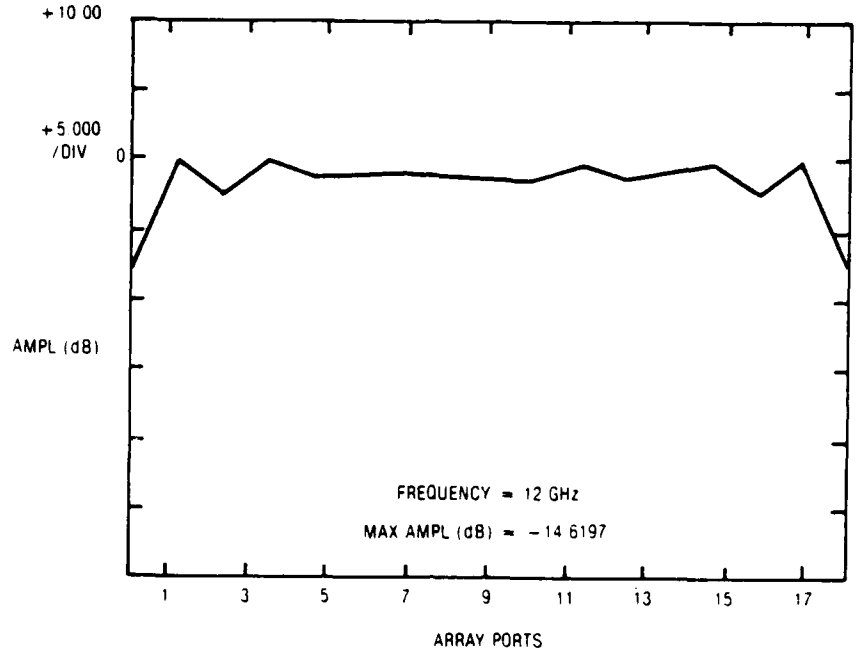

Figure 36B. Measured amplitude for integrated lens, Zϕ = 0°.

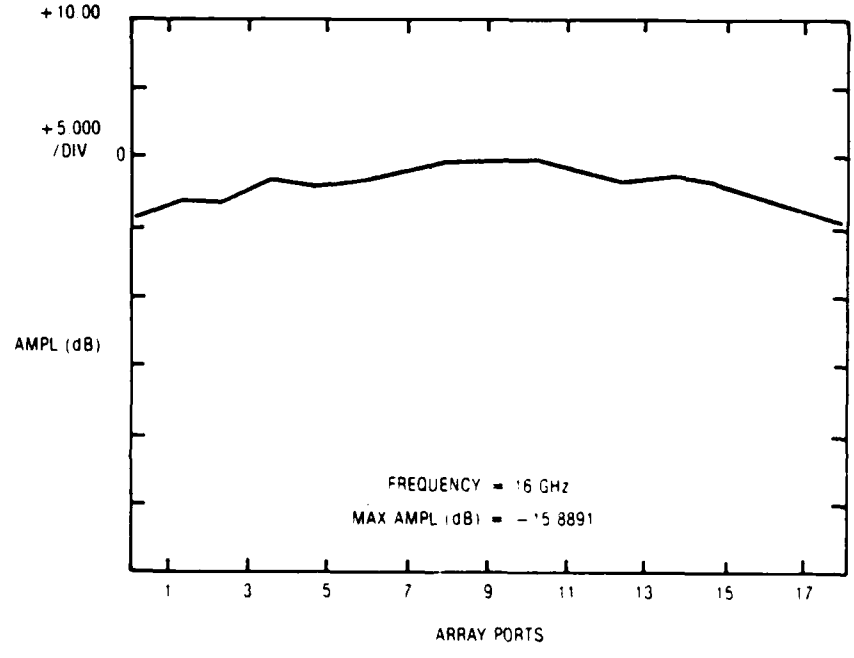

Figure 36C. Measured amplitude for integrated lens, Zϕ = 0°.

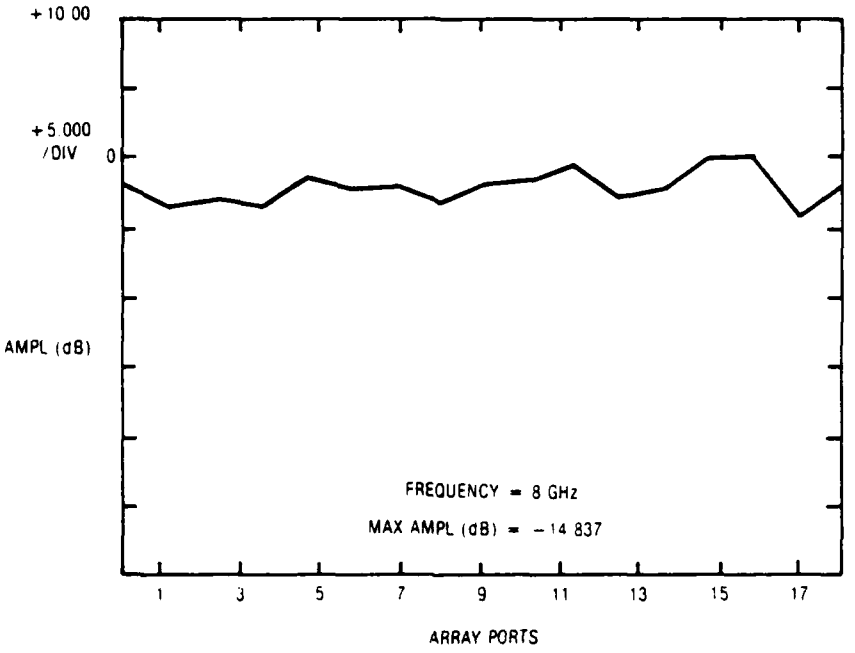

Figure 37A. Measured amplitude for integrated lens, Zϕ = 59°.

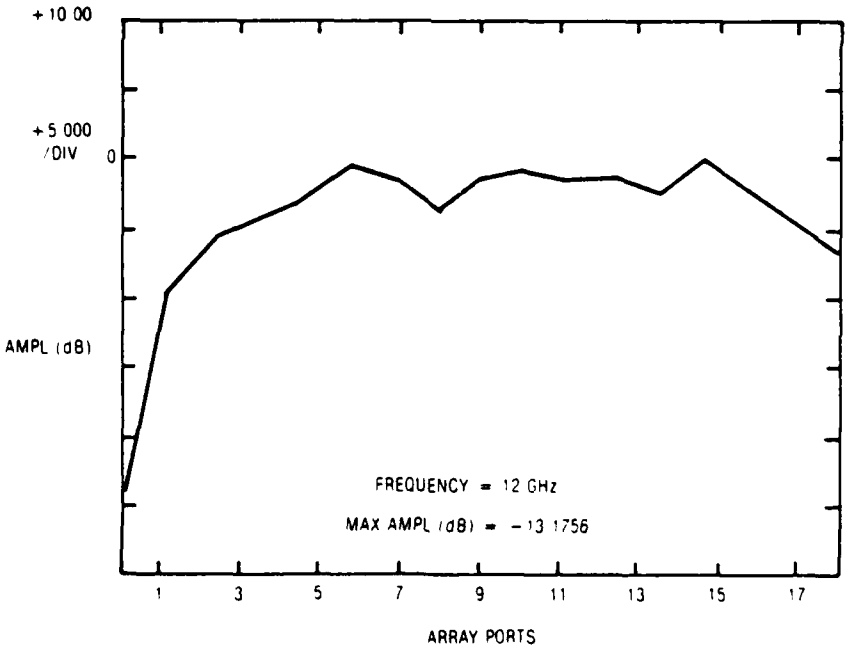

Figure 37B. Measured amplitude for integrated lens, Zϕ = 59°.

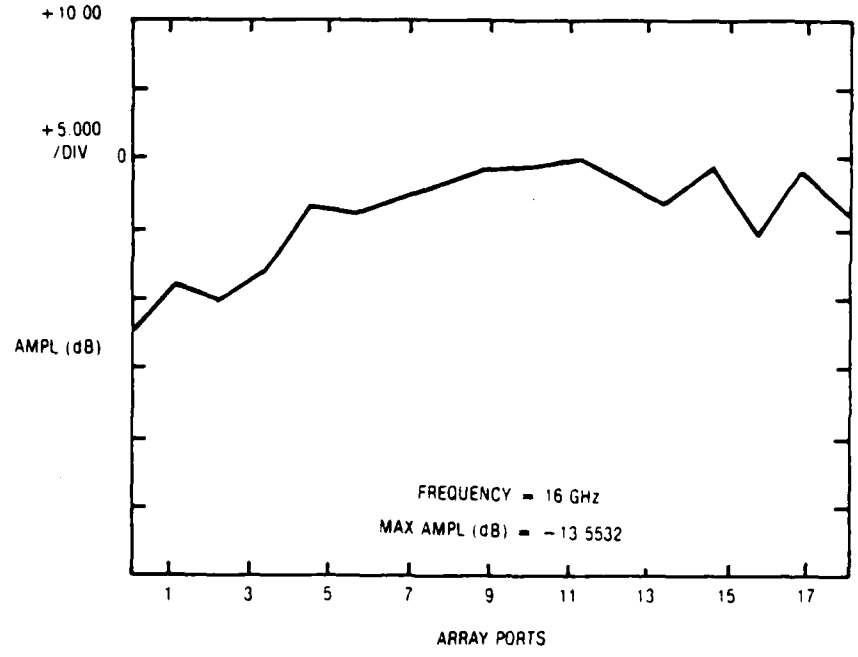

Figure 37C. Measured amplitude for integrated lens, Zϕ = 59°.

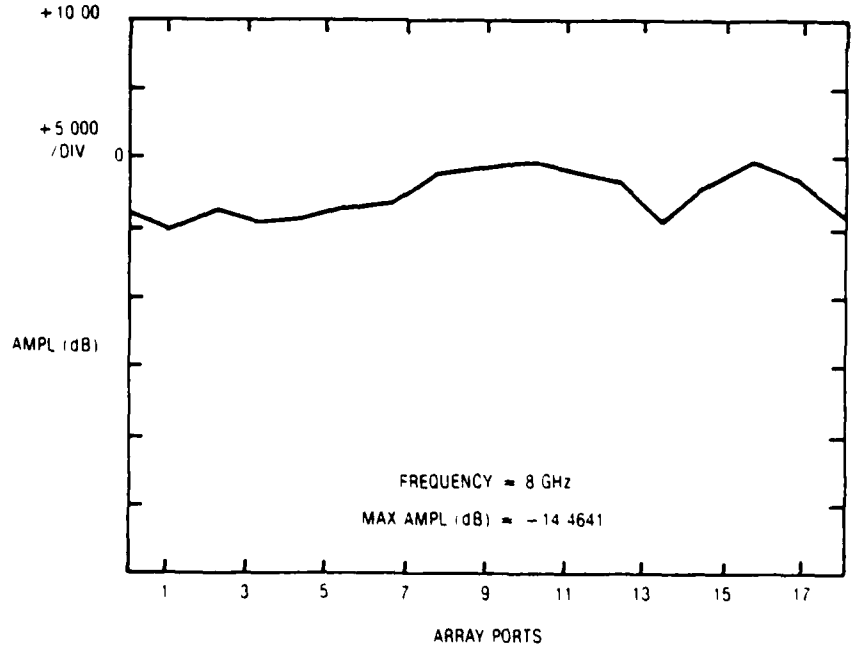

Figure 38A. Measured amplitude for integrated lens, Zϕ = 90°.

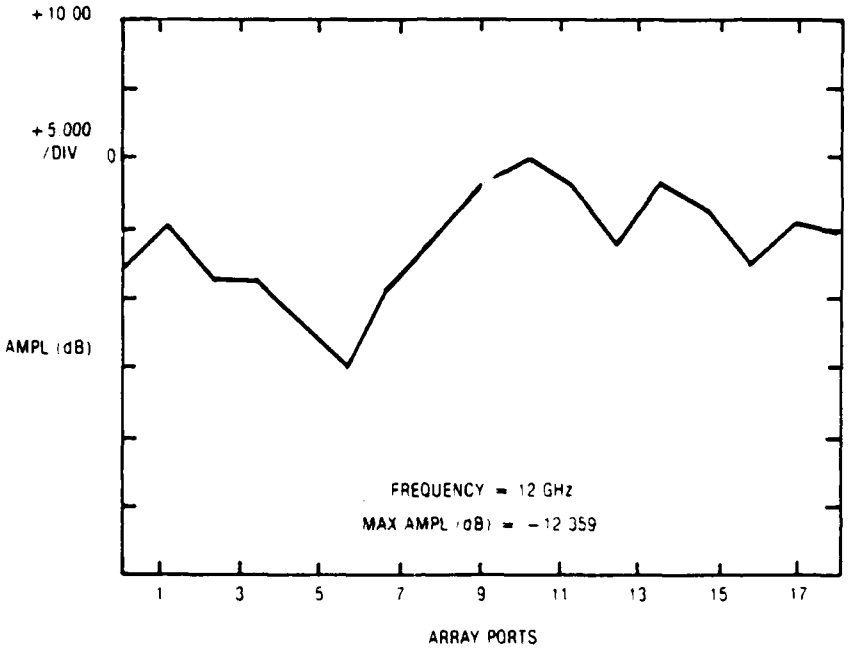

Figure 38B. Measured amplitude for integrated lens, Zϕ = 90°.

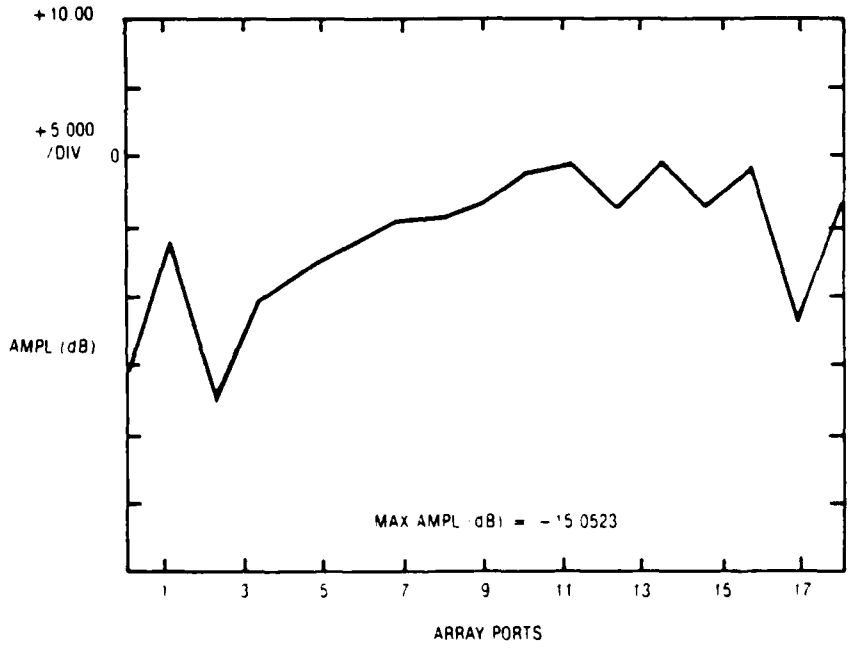

Figure 38C. Measured amplitude for integrated lens, Zϕ = 90°.

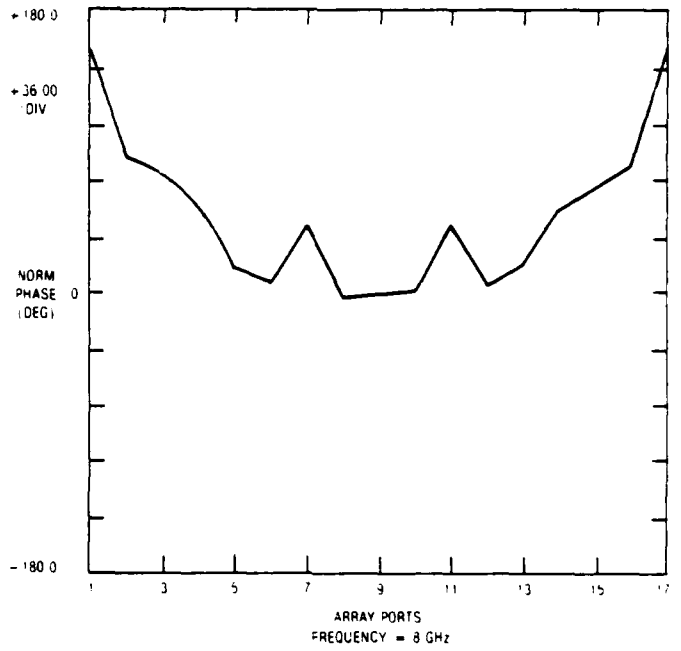

Figure 39A. Measured phase for integrated lens, $Z\phi = 0°$.

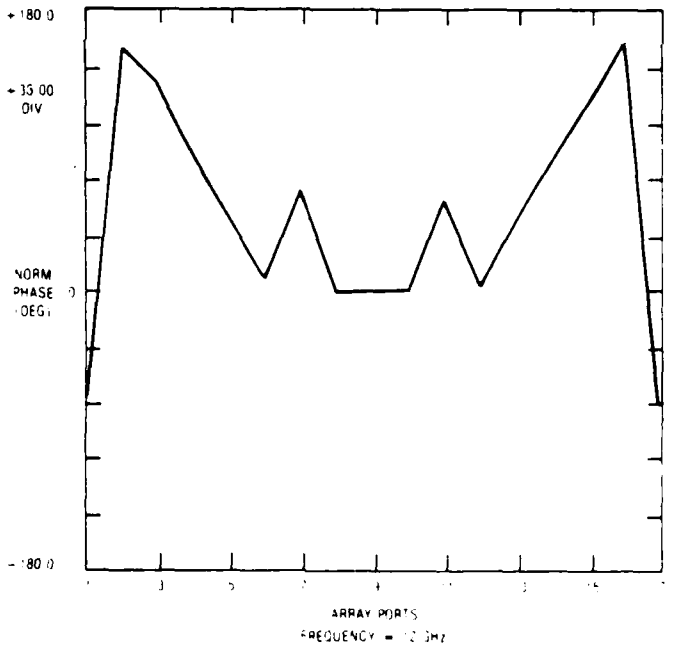

Figure 39B. Measured phase for integrated lens, $Z\phi = 0°$.

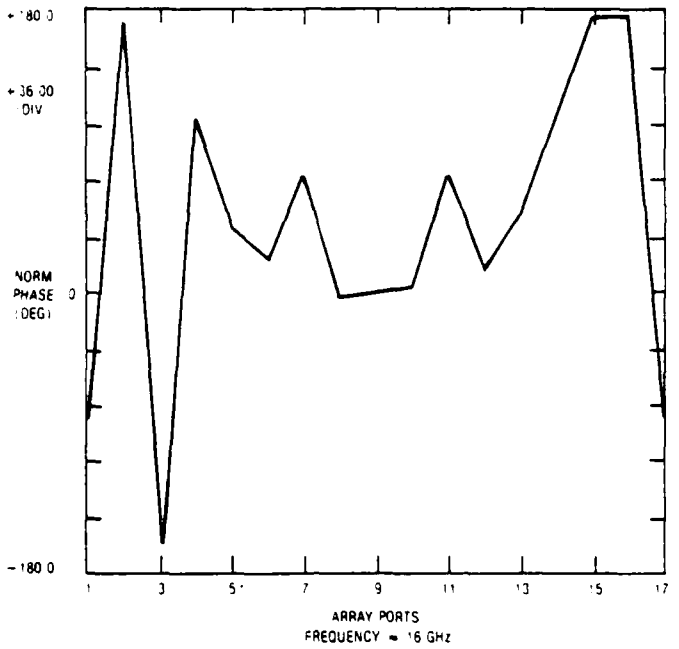

Figure 39C. Measured phase for integrated lens, Zϕ = 0°.

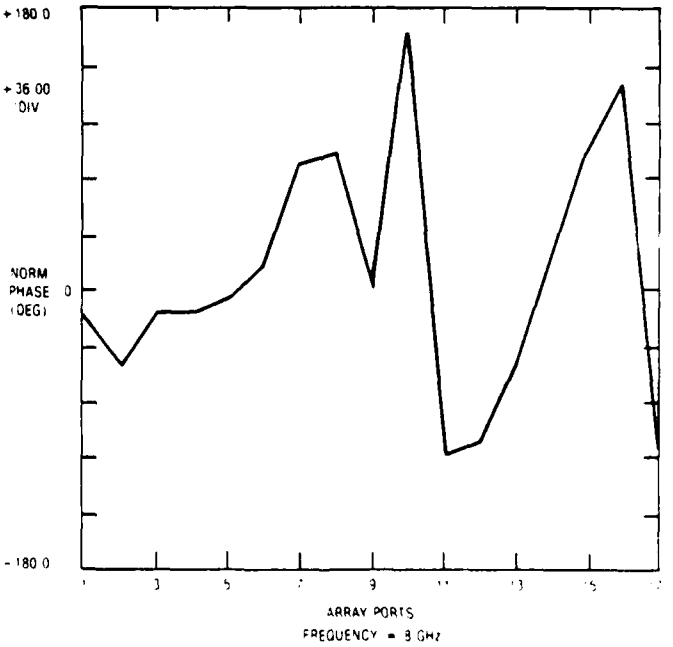

Figure 40A. Measured phase for integrated lens, Zϕ = 59°.

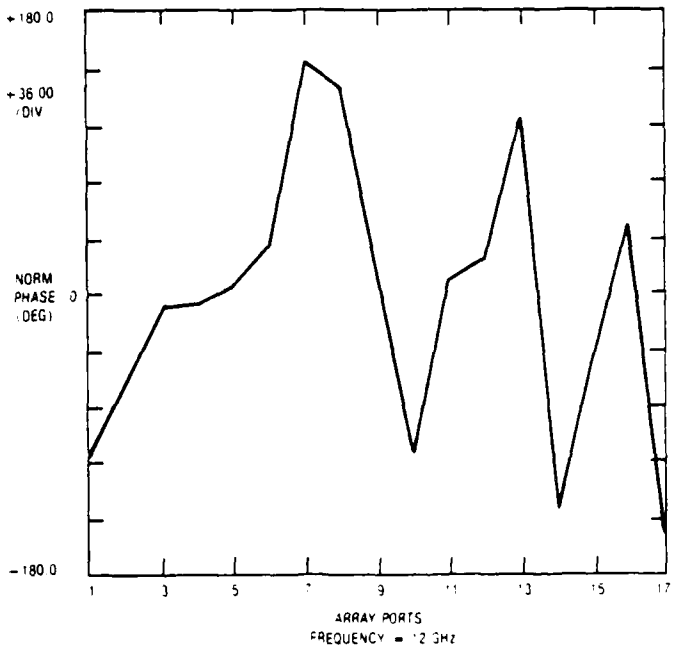

Figure 40B. Measured phase for integrated lens, Zϕ = 59°.

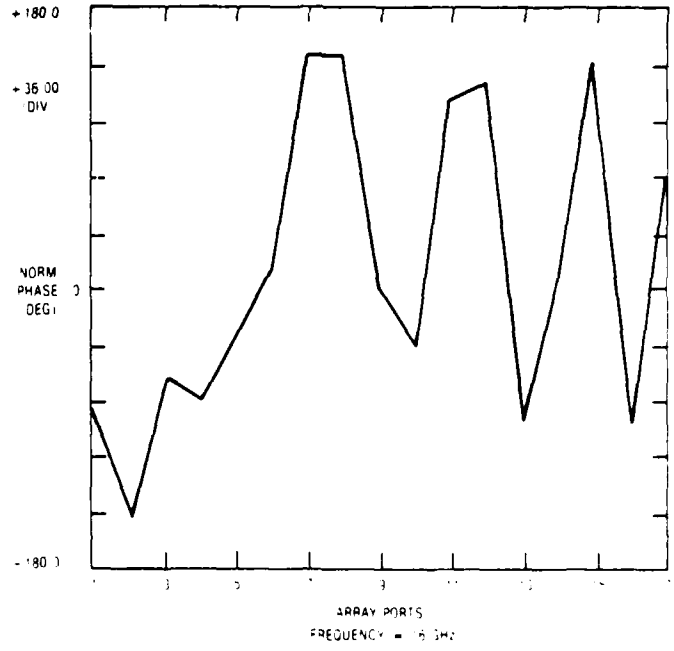

Figure 40C. Measured phase for integrated lens, Zϕ = 59°.

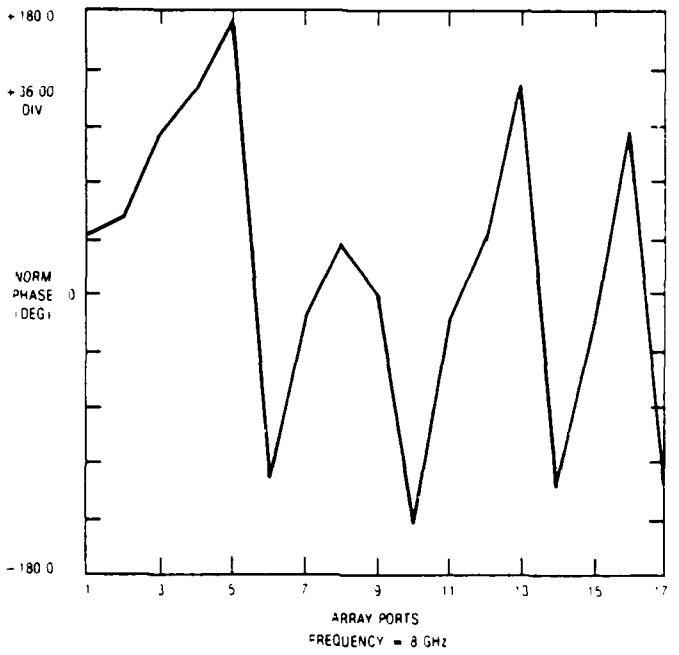

Figure 41A. Measured phase for integrated lens, Zϕ = 90°.

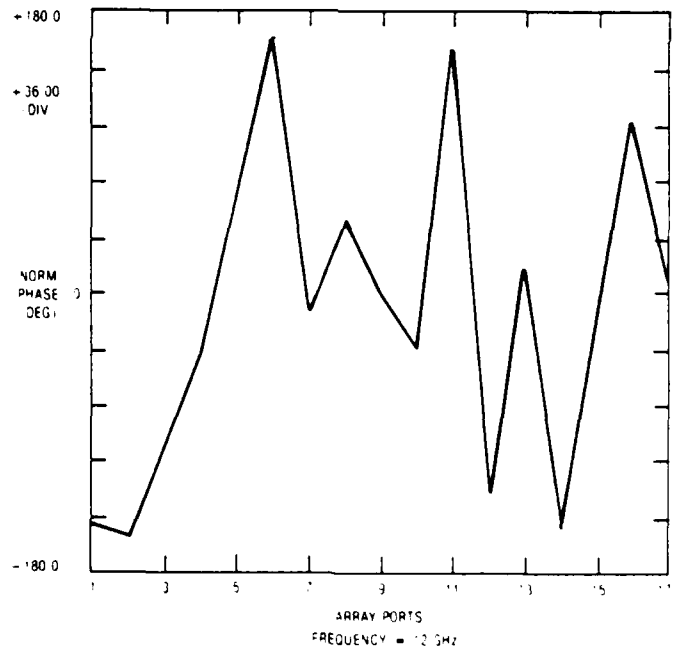

Figure 41B. Measured phase for integrated lens, Zϕ = 90°.

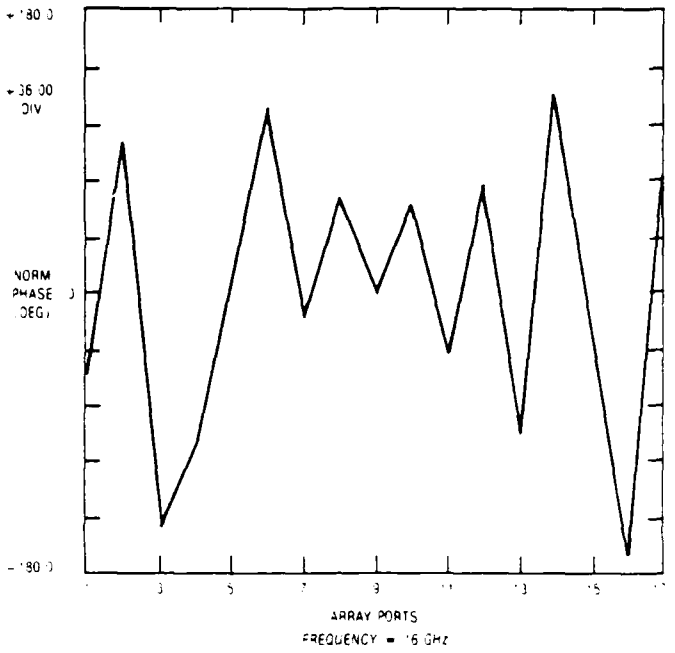

Figure 41C. Measured phase for integrated lens, Zϕ = 90°.

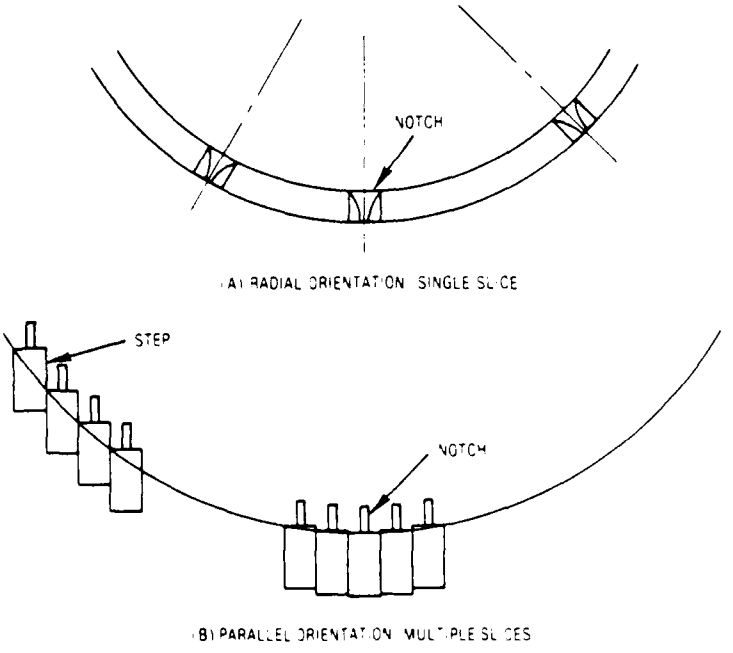

Figure 42. Element mounting for curved feed array.

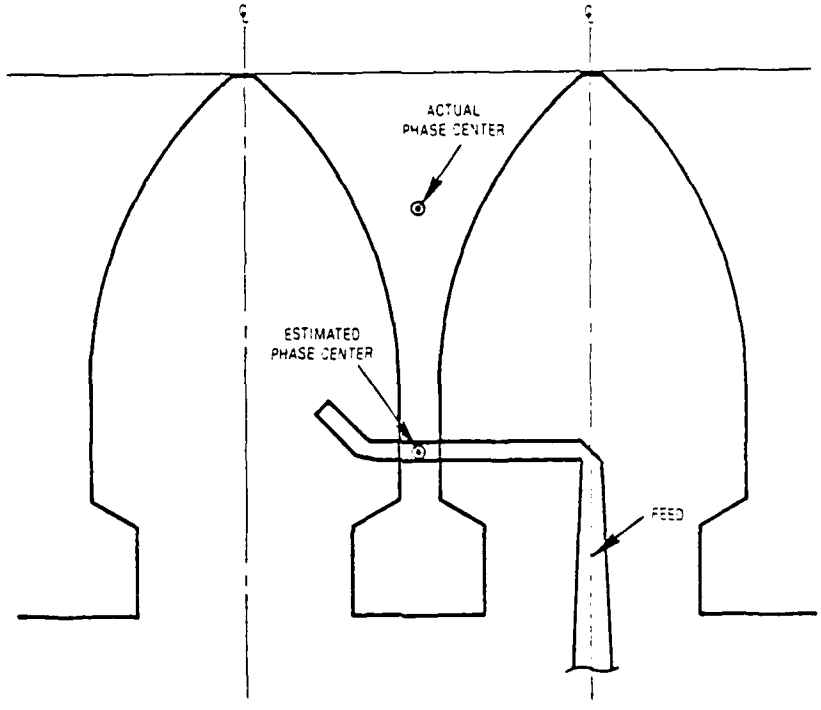

Figure 43. Element design for 3-D dome feed array indicating phase center location.

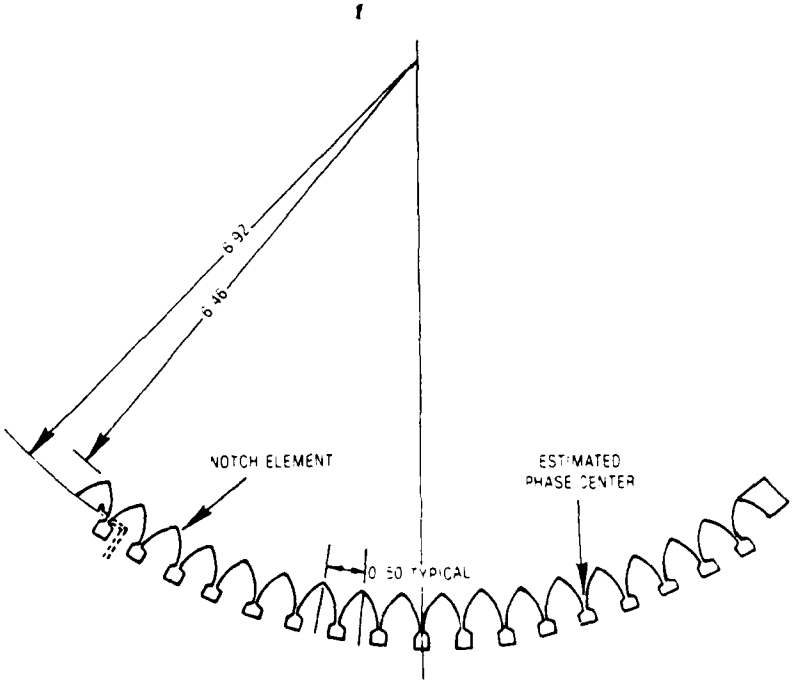

Figure 44. Central slice concave E-plane array.

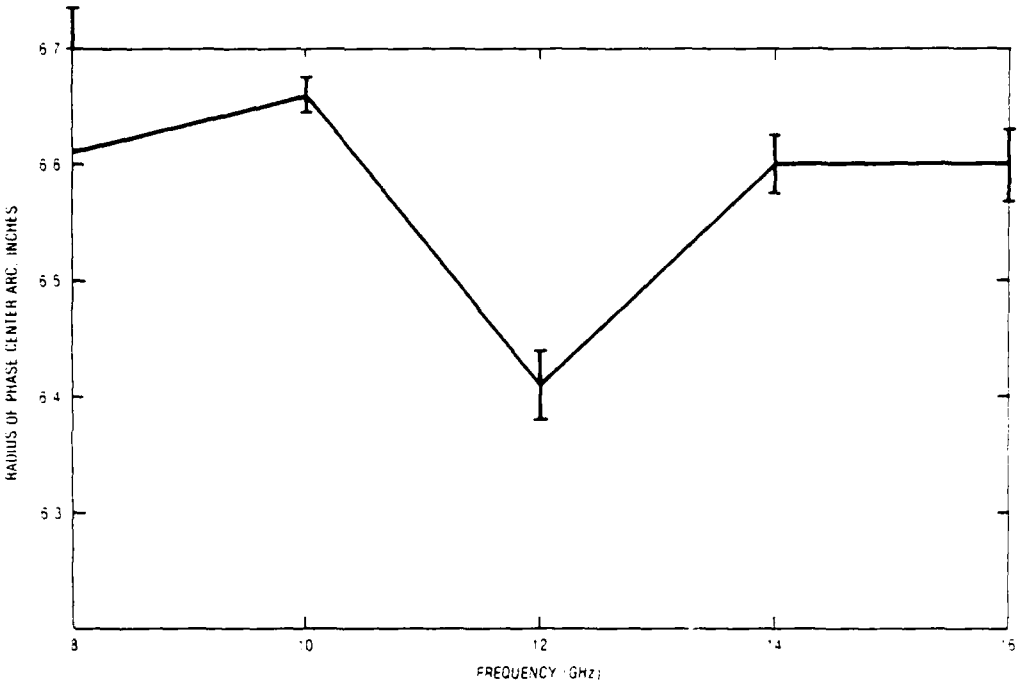

Figure 45. Radius of curvature to phase center arc versus frequency.

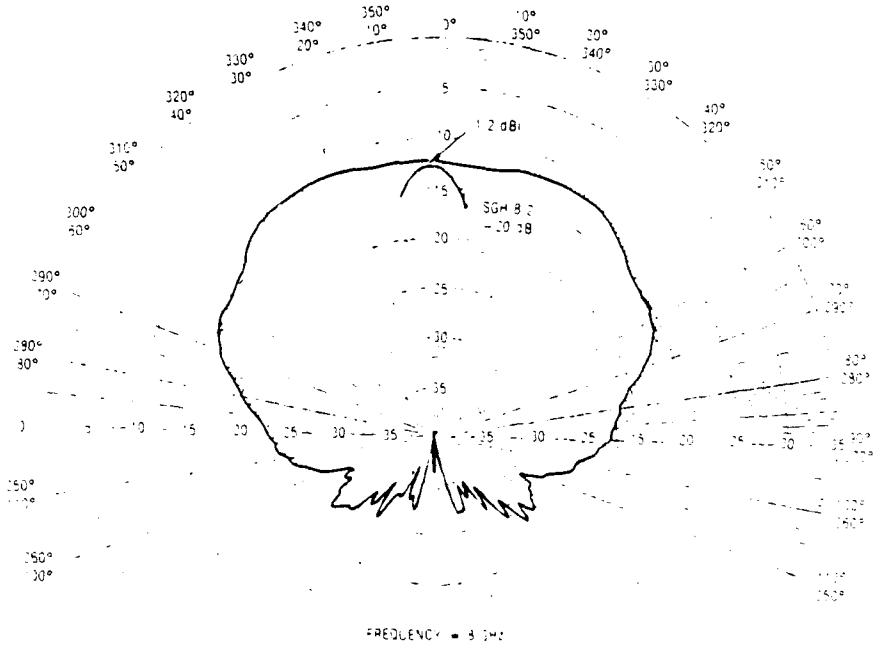

Figure 46A. Radiation patterns for center embedded element, E-plane.

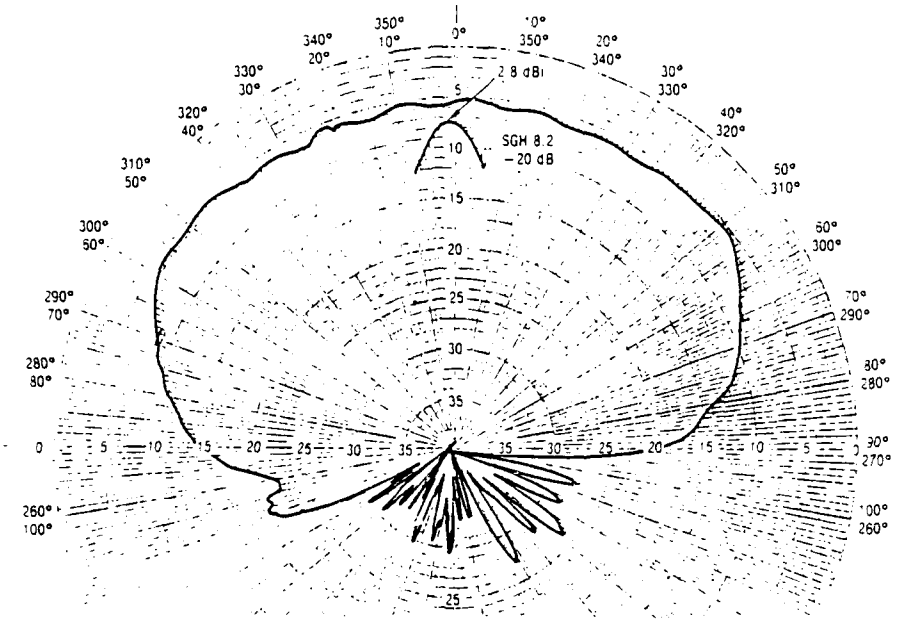

Figure 46B. Radiation patterns for center embedded element, E-plane.

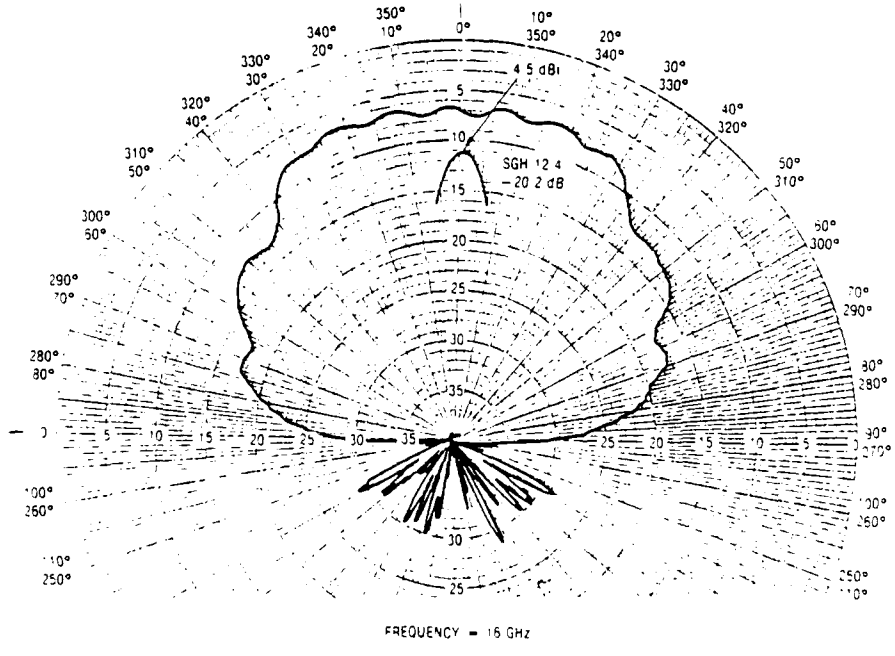

Figure 46C. Radiation patterns for center embedded element, E-plane.

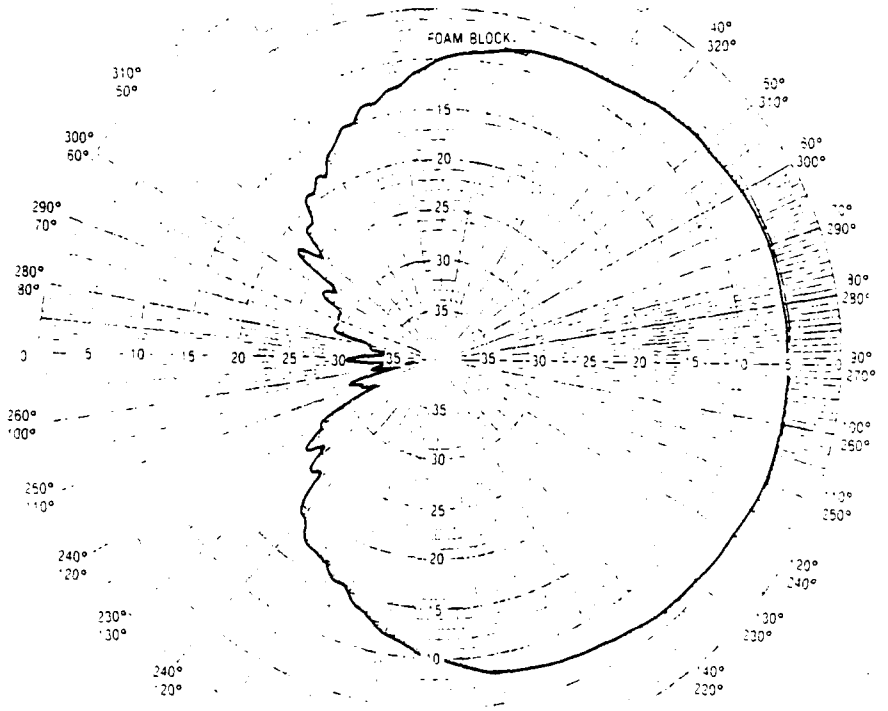

Figure 47A. Radiation patterns for center embedded element, H-plane.

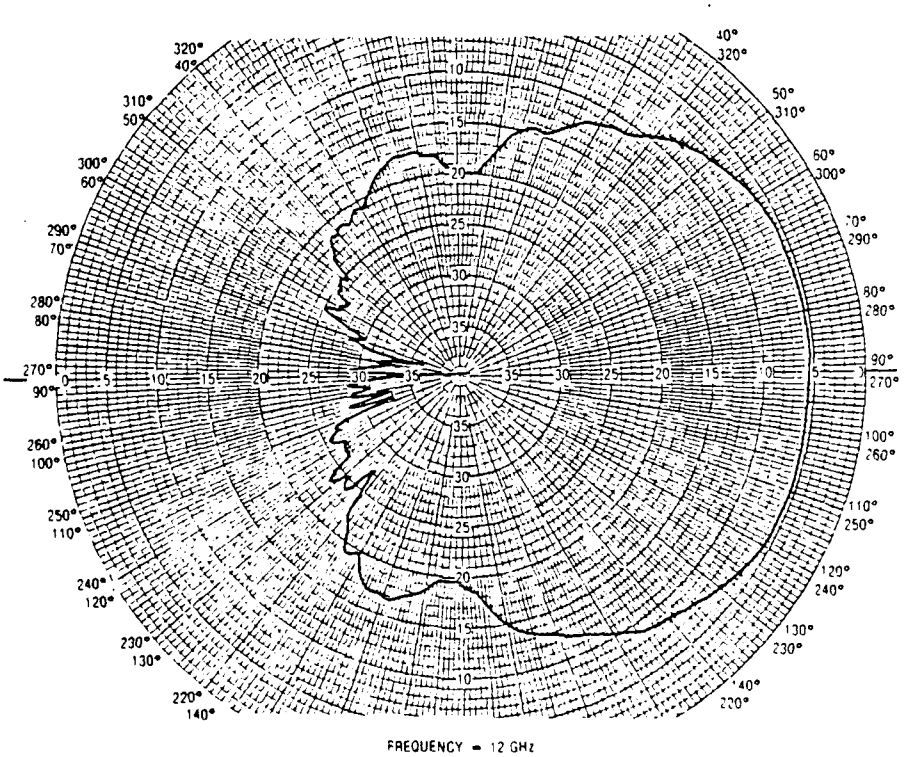

Figure 47B. Radiation patterns for center embedded element, H-plane.

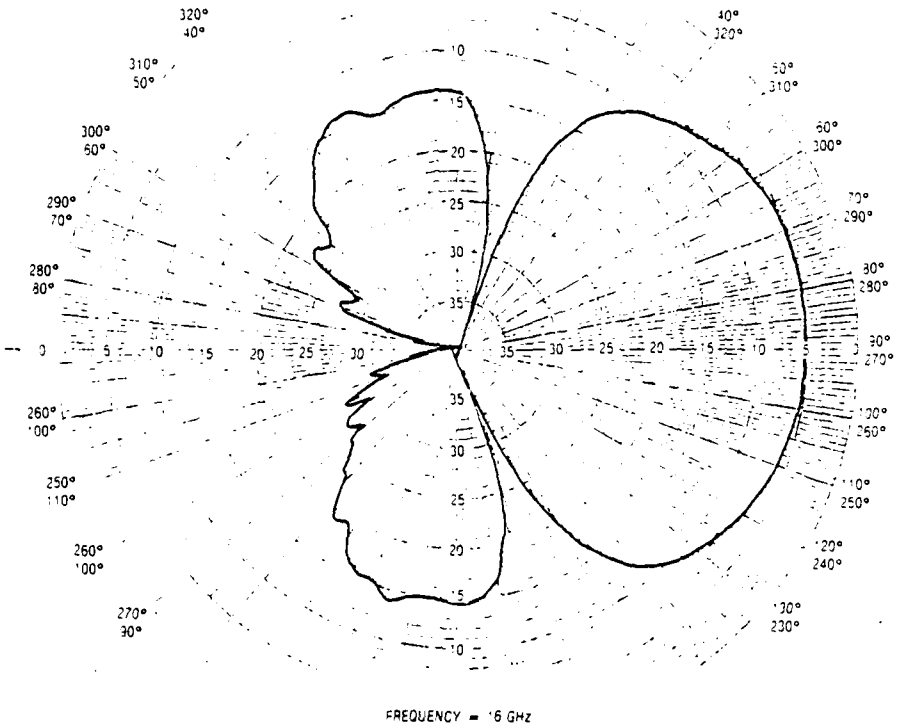

Figure 47C. Radiation patterns for center embedded element, H-plane.

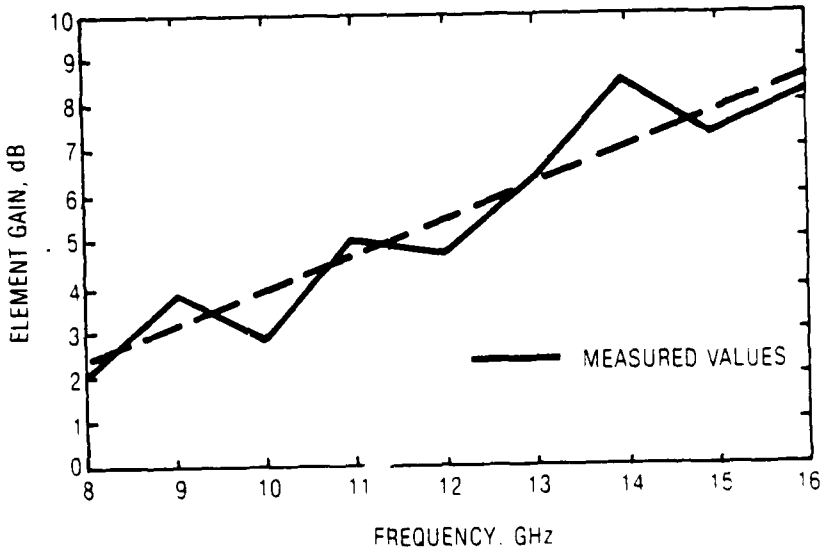

Figure 48. Measured linear gain.

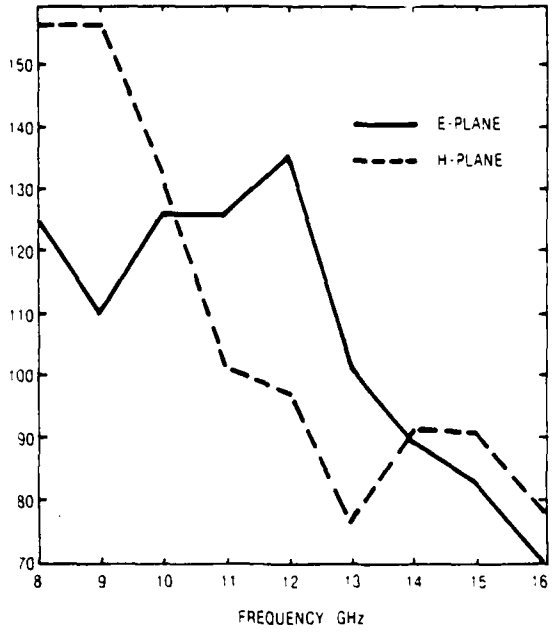

Figure 49. Measured halfpower beamwidth for notch element in concave slice.

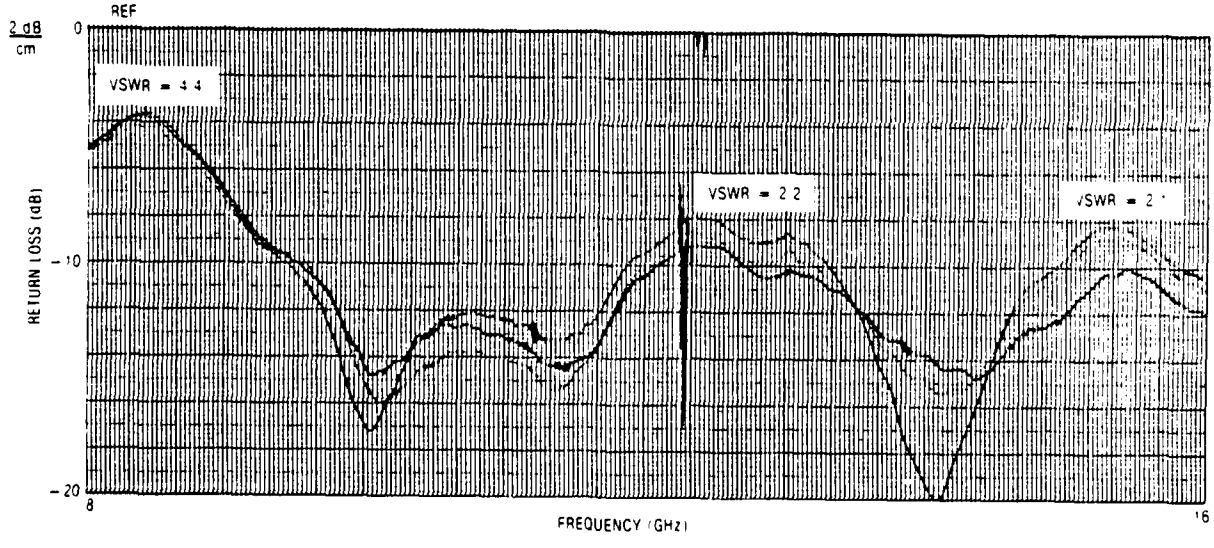

Figure 50. Passive VSWR for several elements of the central slice array.

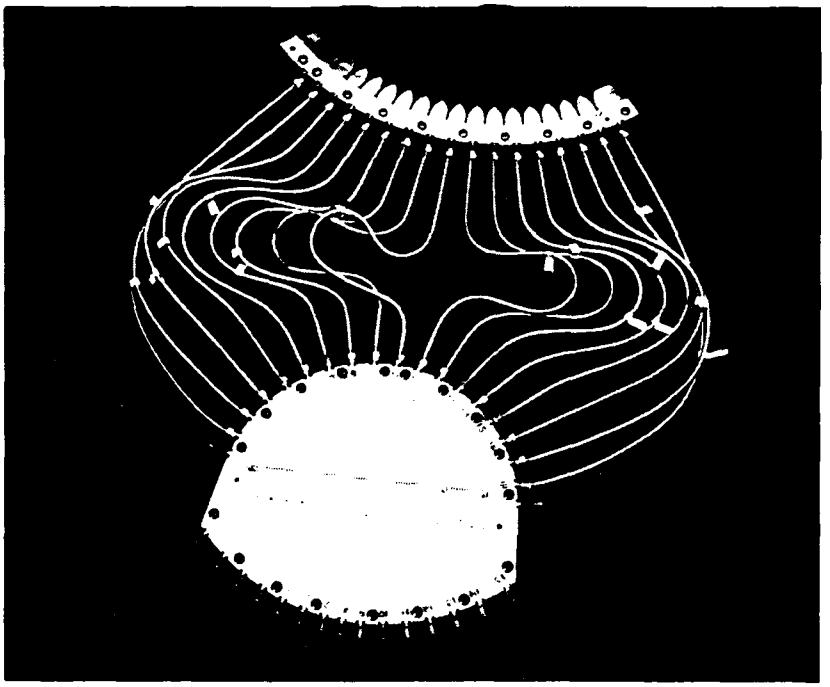

Figure 51. Complete central slice antenna.

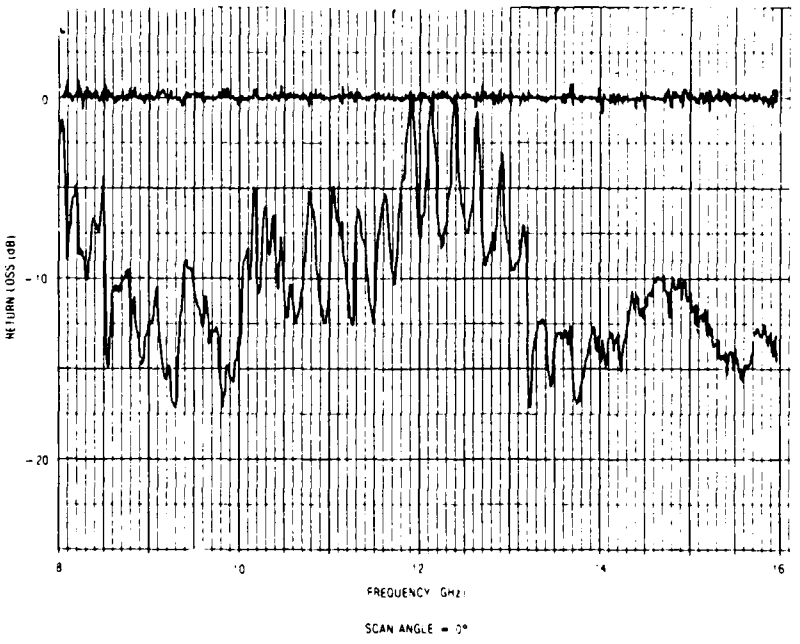

Figure 52A. Active VSWR for central array element.

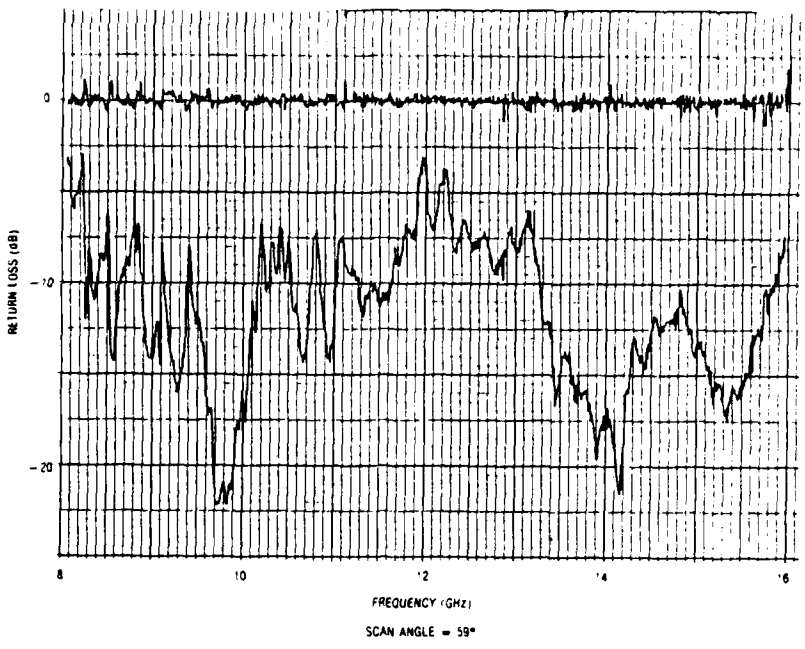

Figure 52B. Active VSWR for central array element.

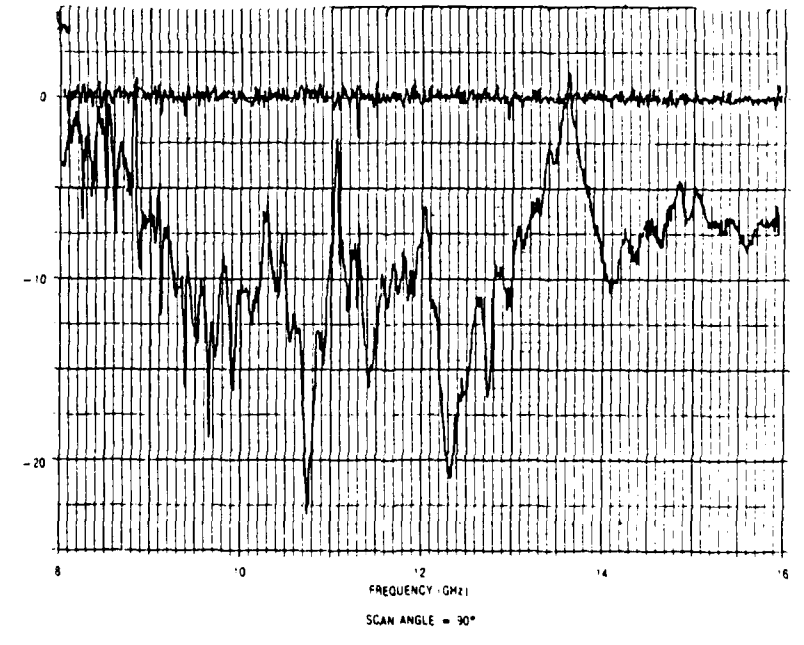

Figure 52C. Active VSWR for central array element.

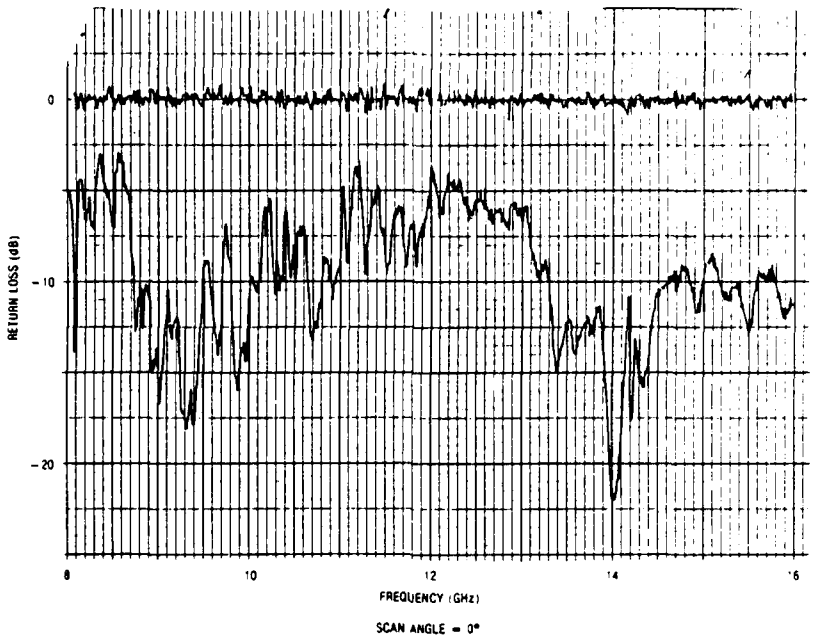

Figure 53A. Active VSWR for near edge array element.

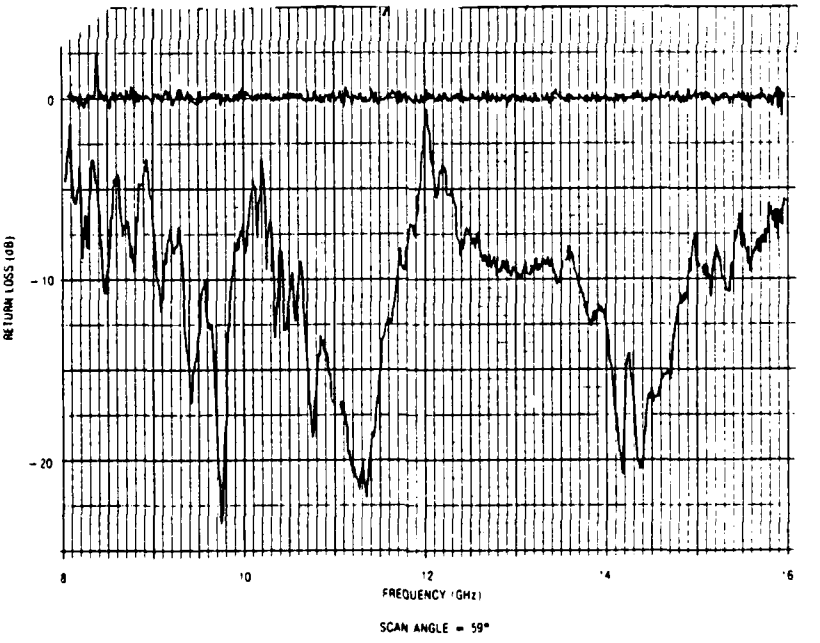

Figure 53B. Active VSWR for near edge array element.

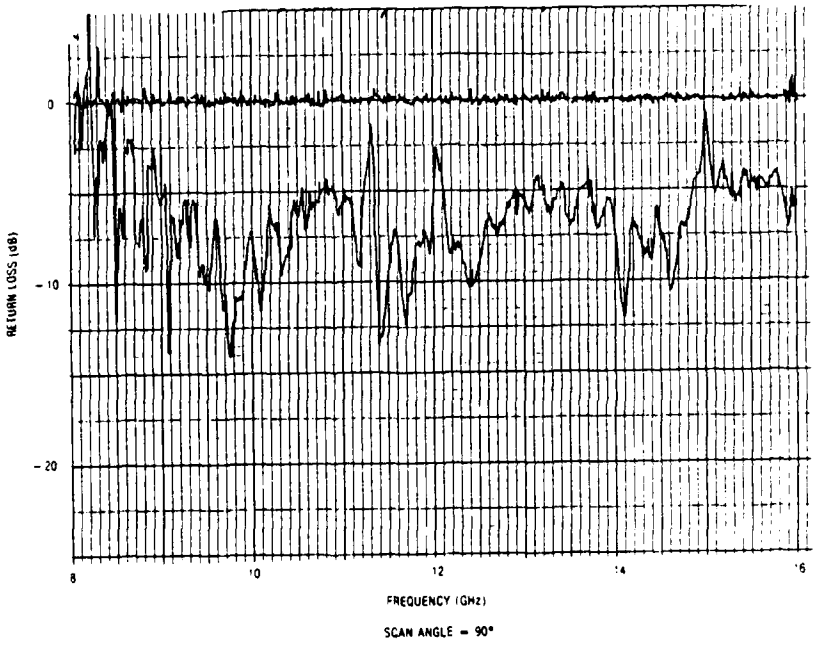

Figure 53C. Active VSWR for near edge array element.

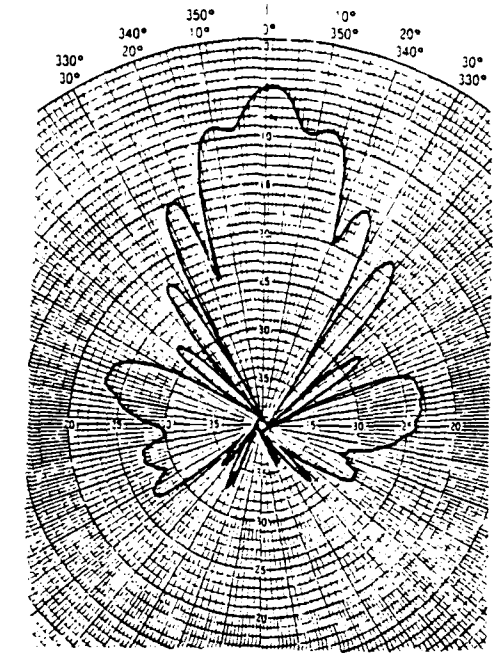

Measured

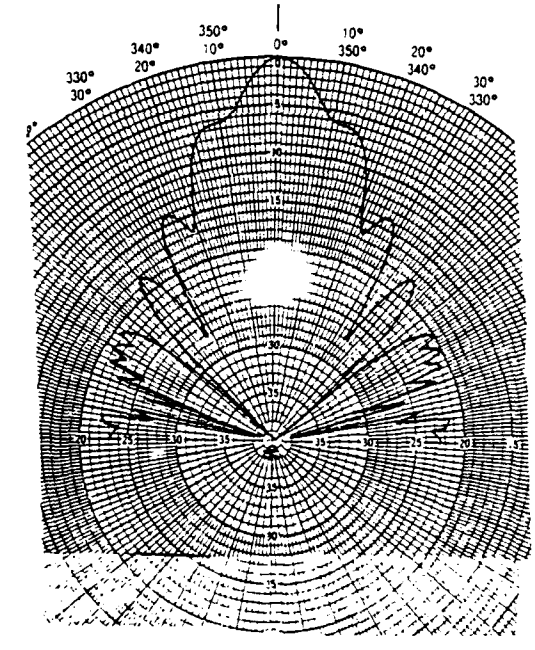

Computed

Figure 54. Central slice interior radiation patterns for 0° (zenith) beam at 8 GHz.

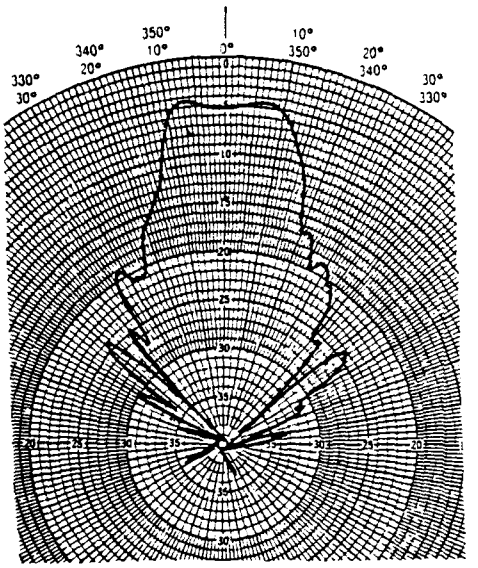

Measured

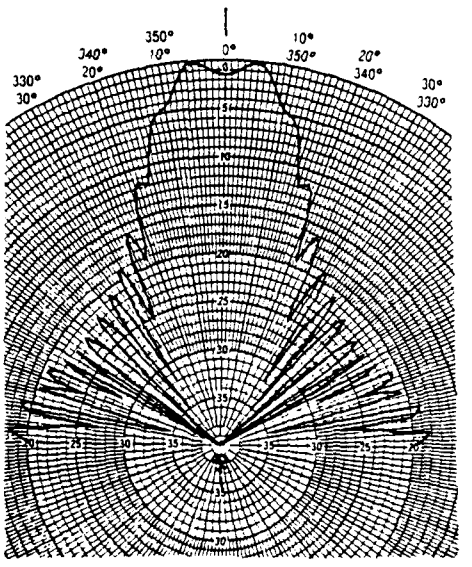

Computed

Figure 55. Central slice interior radiation patterns for 0° (zenith) beam at 16 GHz.

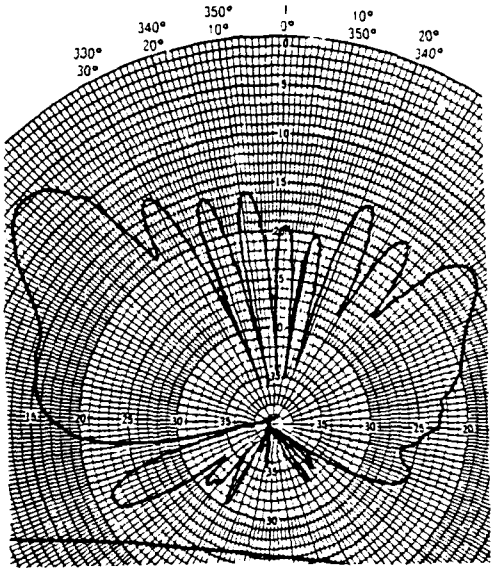

Measured

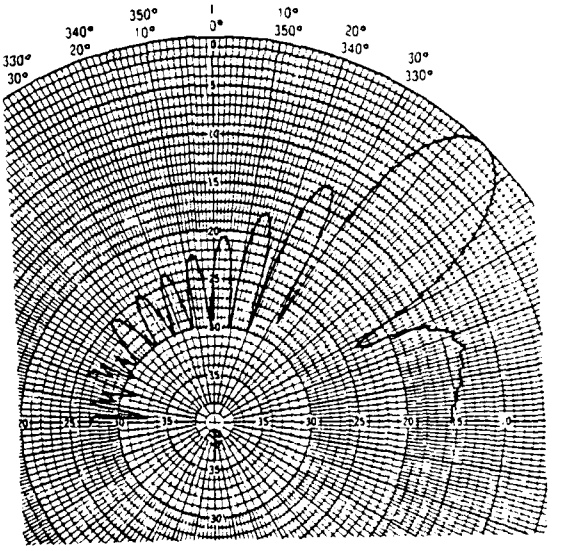

Computed (Reversed)

Figure 56. Central slice interior radiation patterns for 90° (horizon) beam at 8 GHz.

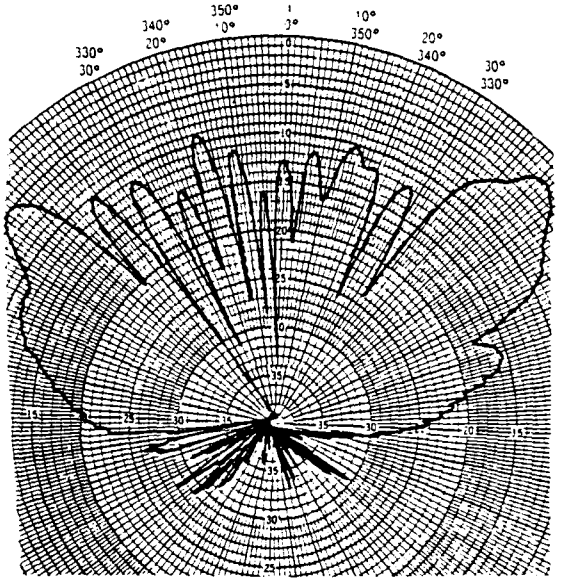

Measured

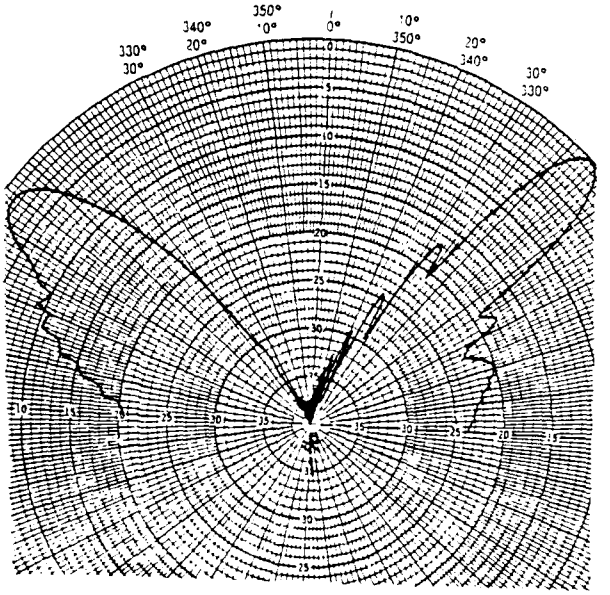

Computed (Reversed)

Figure 57. Central slice interior radiation patterns for 90° (horizon) beam at 16 GHz.

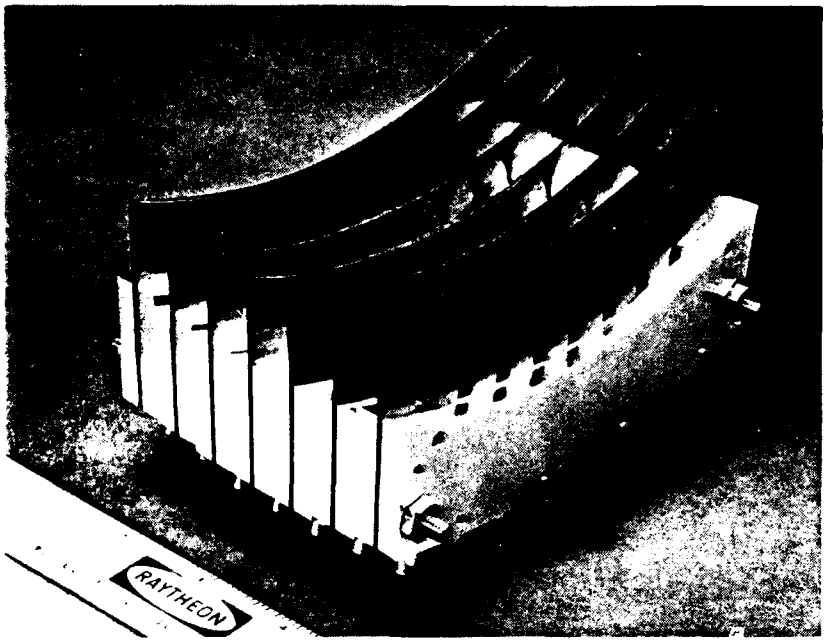

Figure 58A. Concave subarray of 7 x 7 elements.

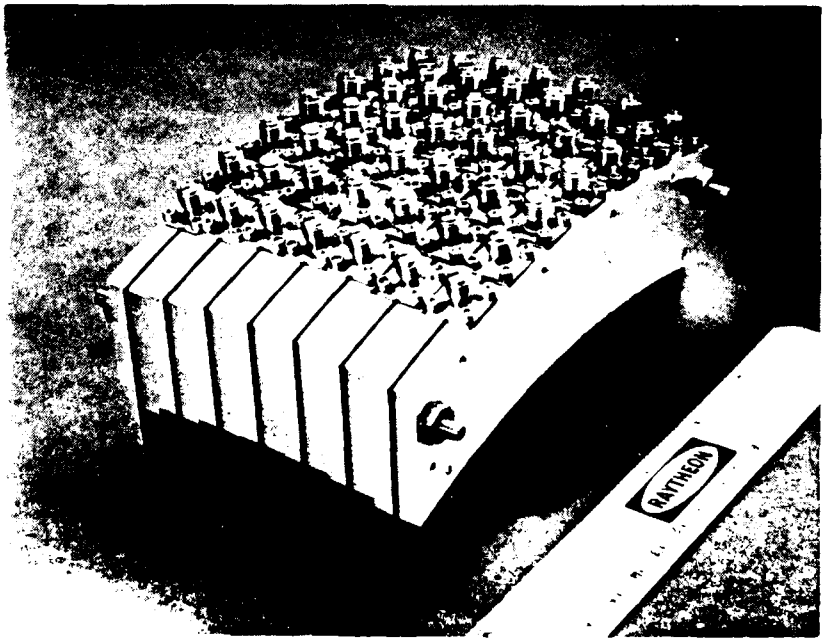

Figure 58B. Concave subarray of 7 x 7 elements.

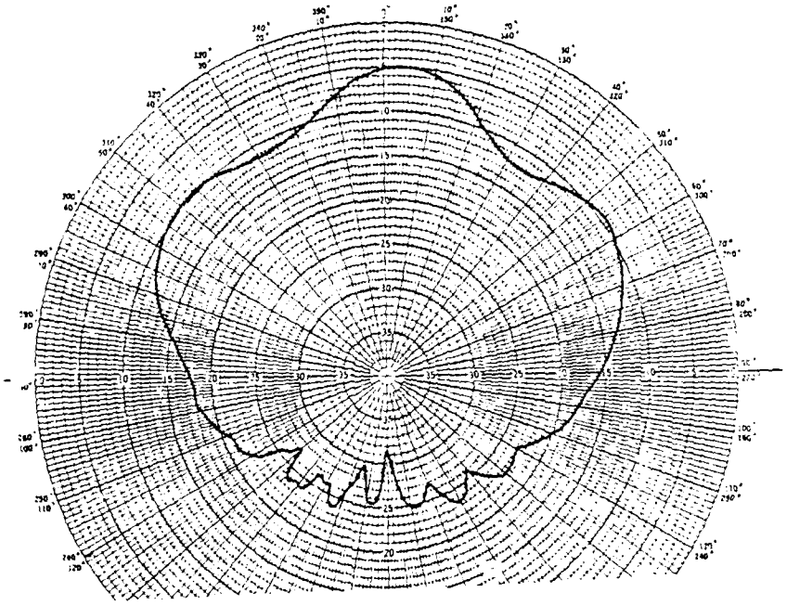

Frequency - 6 GHz

Figure 59A. Central embedded element patterns in E-plane.

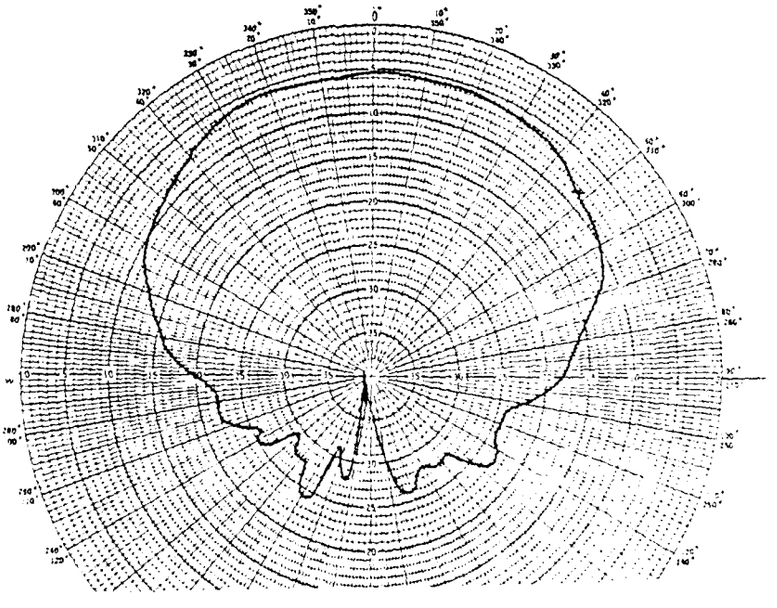

Frequency - 8 GHz

Figure 59B. Central embedded element patterns in E-plane.

AD-A149 809 3-D DOME/ROTMAN LENS ANTENNA BREADBOARD DEMONSTRATION 2/2
(U) RAYTHEON CO GOLETA CA ELECTROMAGNETIC SYSTEMS DIV
D T THOMAS ET AL. JAN 85 ONR-252-008-3 N00014-80-C-0143
UNCLASSIFIED F/G 9/5 NL

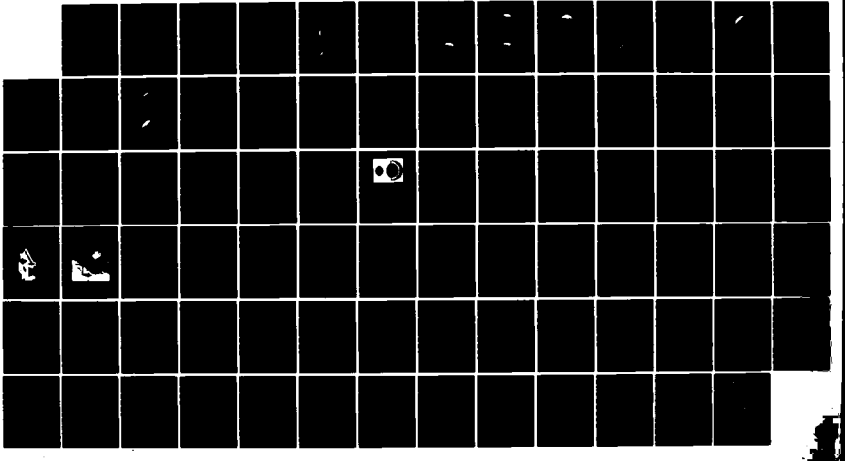

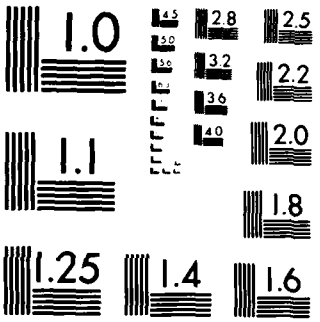

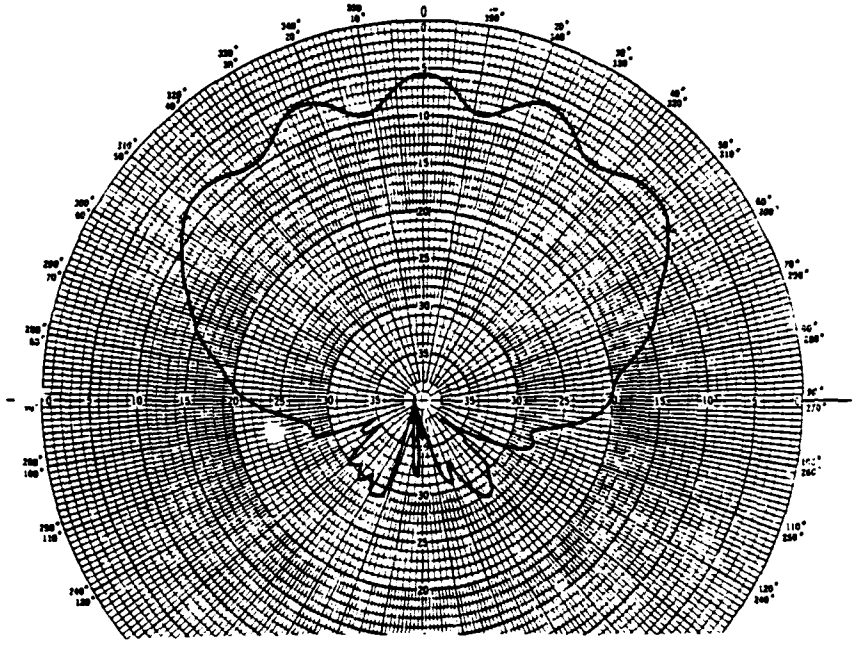

Frequency - 12 GHz

Figure 59C. Central embedded element patterns in E-plane.

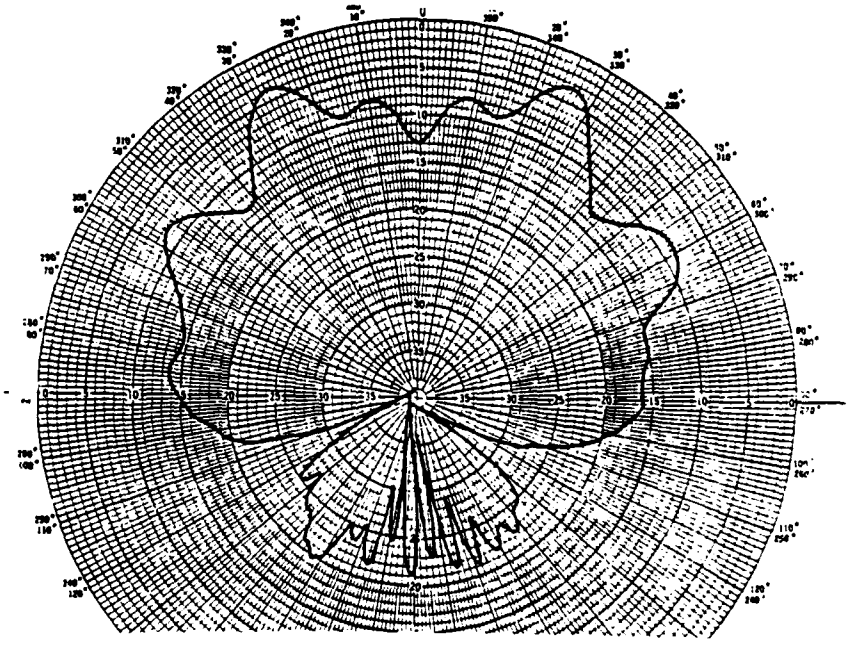

Frequency - 16 GHz

Figure 59D. Central embedded element patterns in E-plane.

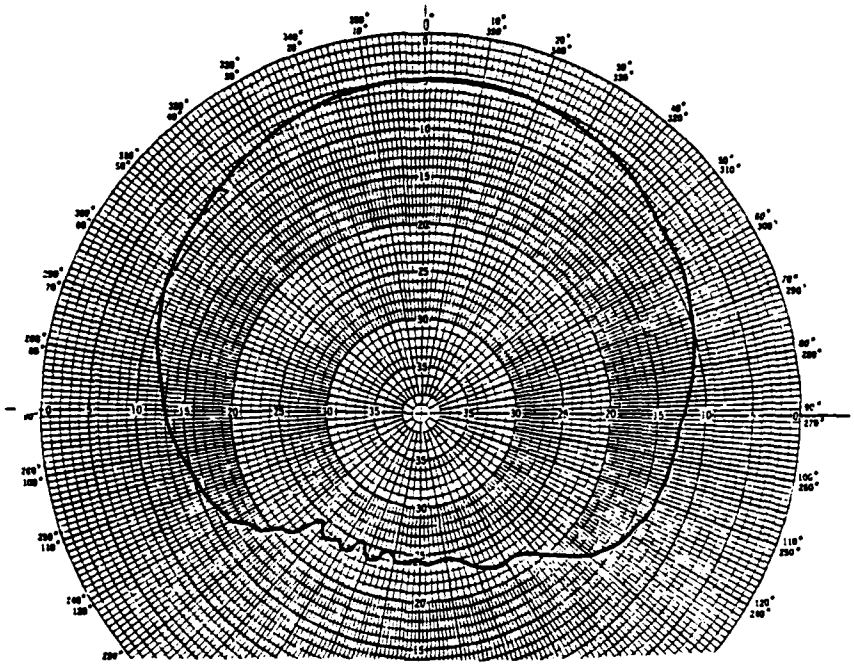

Frequency - 6 GHz

Figure 60A. Central embedded element patterns in H-plane.

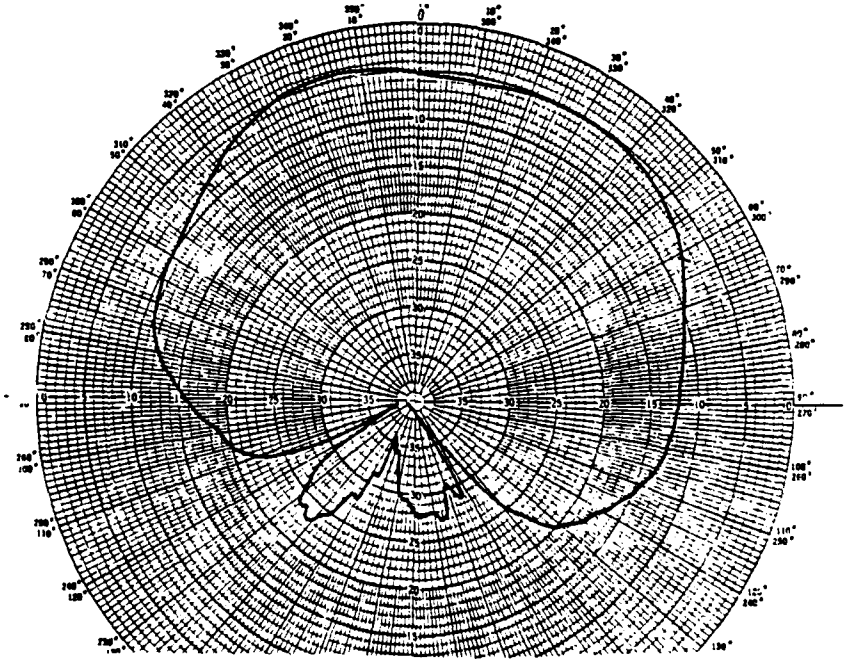

Frequency - 8 GHz

Figure 60B. Central embedded element patterns in H-plane.

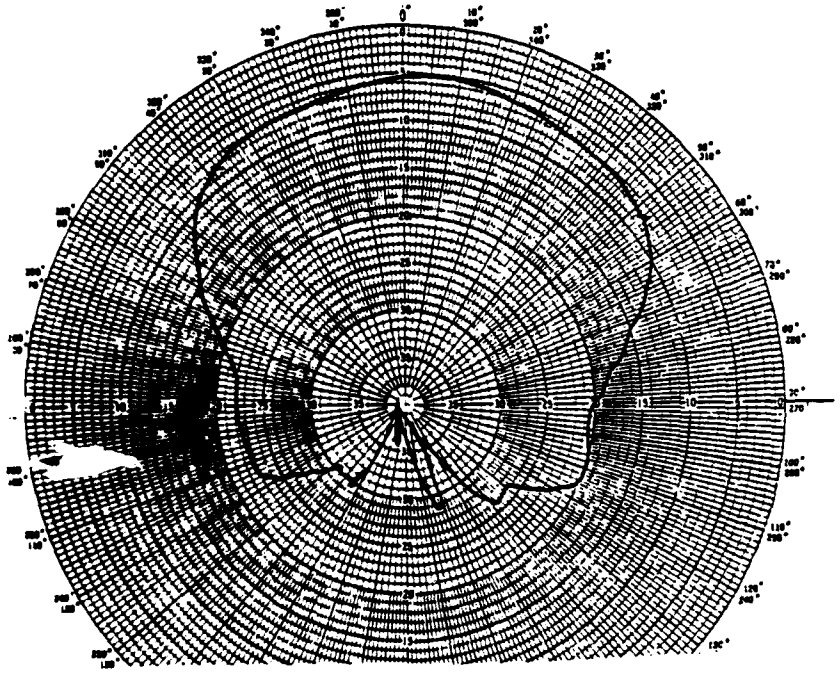

Frequency - 12 GHz

Figure 60C. Central embedded element patterns in H-plane.

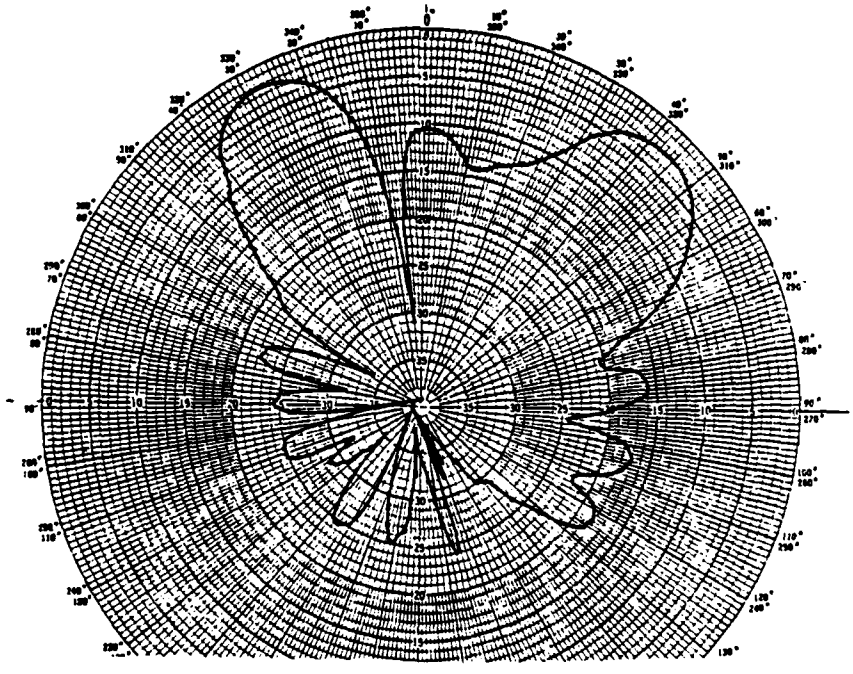

Frequency - 16 GHz

Figure 60D. Central embedded element patterns in H-plane.

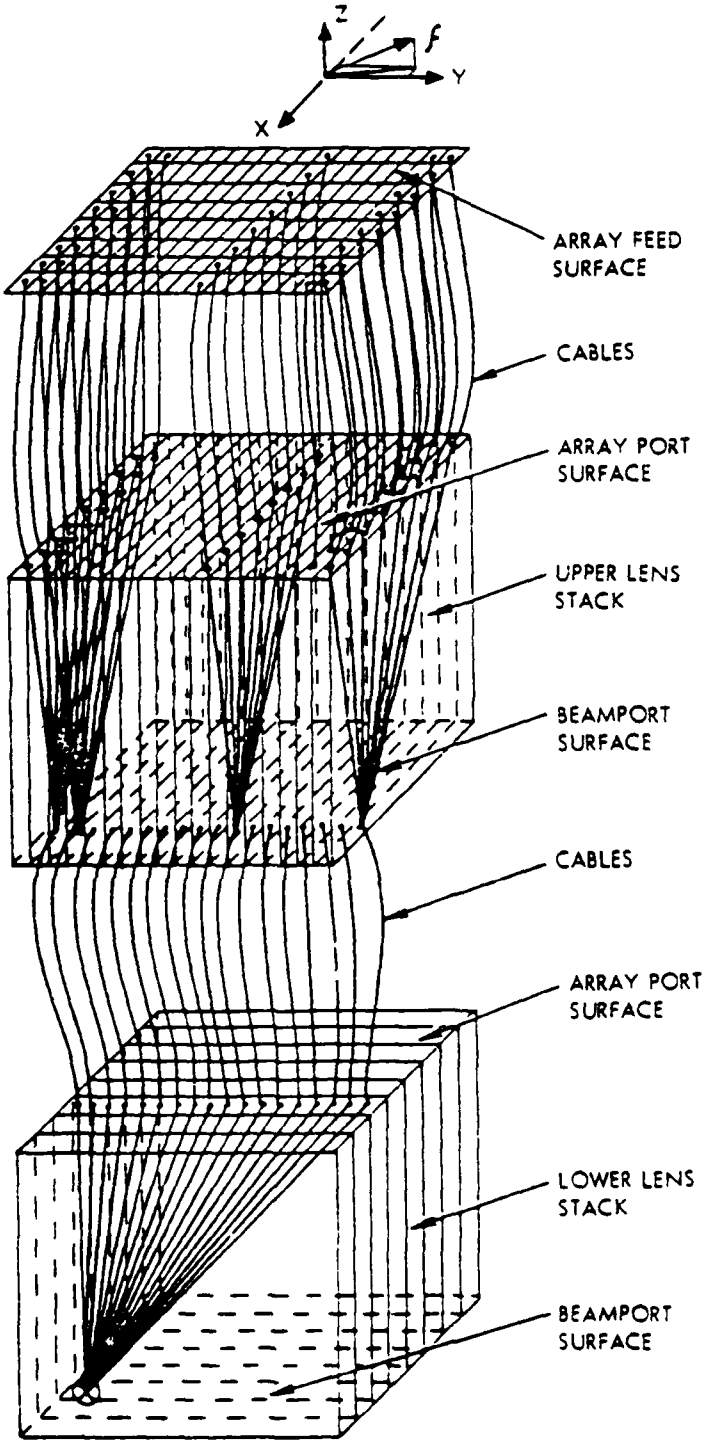

Figure 62. Two-stack feed lens configuration.

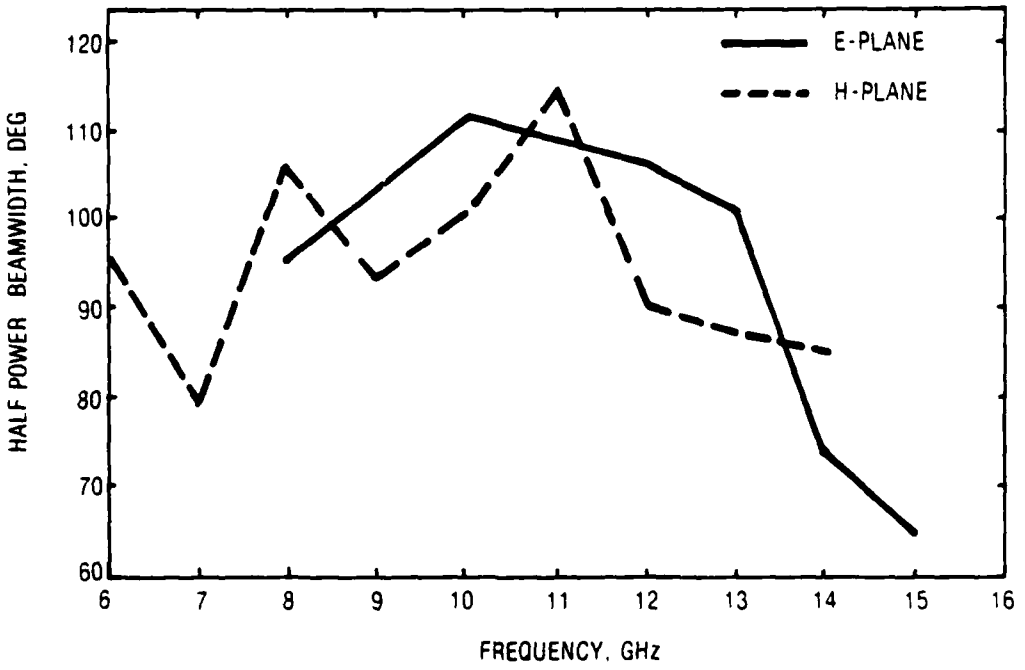

Figure 61. Halfpower beamwidth for center embedded element, 7 x 7 concave subarray.

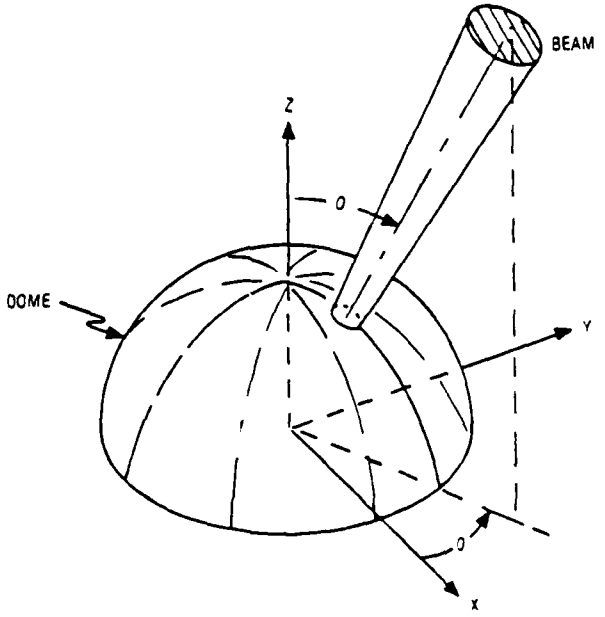

Figure 63. Spherical coordinates of 3-D dome antenna.

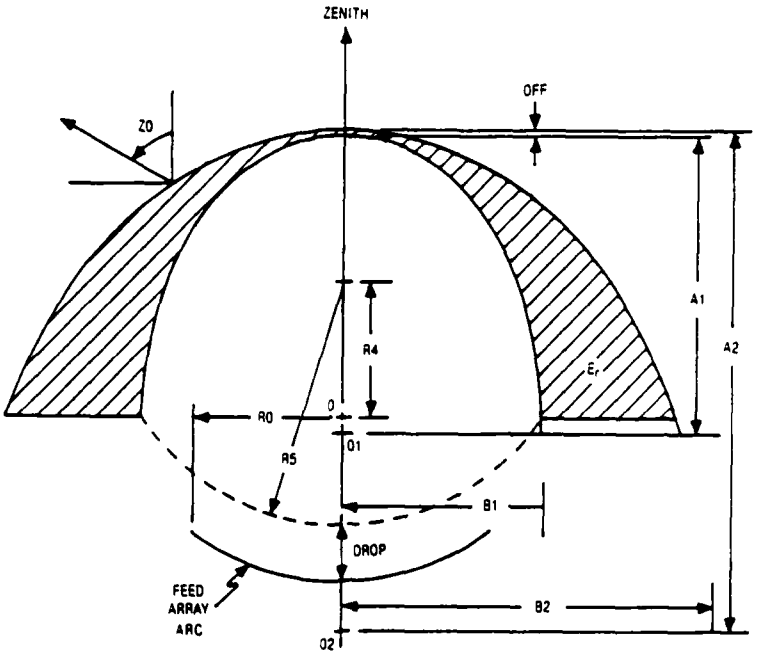

Figure 64. Design Parameters of 3-D Dome.

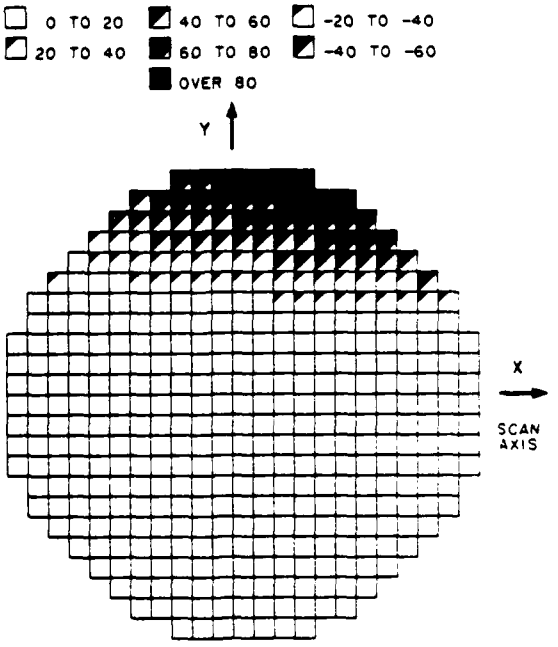

Figure 65. Phase Error at Feed Array (12 GHz)
$\xi = 90°$, $\phi = 0°$, R4 = 4 in., Single Lens Design Case.

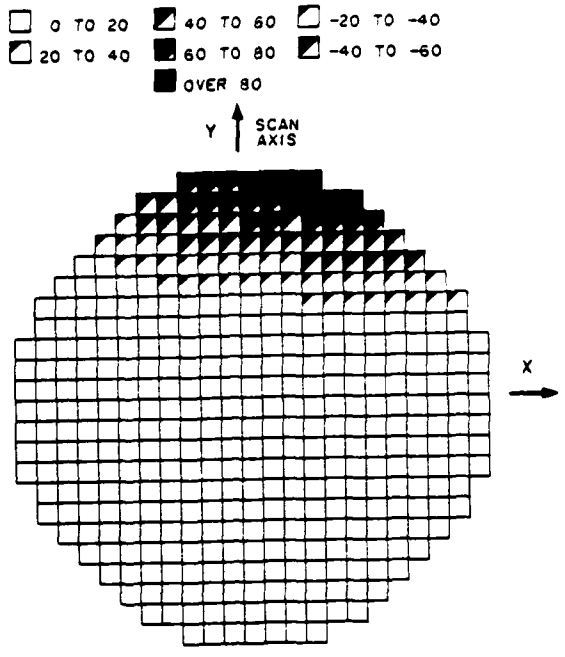

Figure 66. Phase Error at Feed Array (12 GHz)
$\xi = 90°$, $\phi = 90°$, R4 = 4 in., Single Lens Design Case.

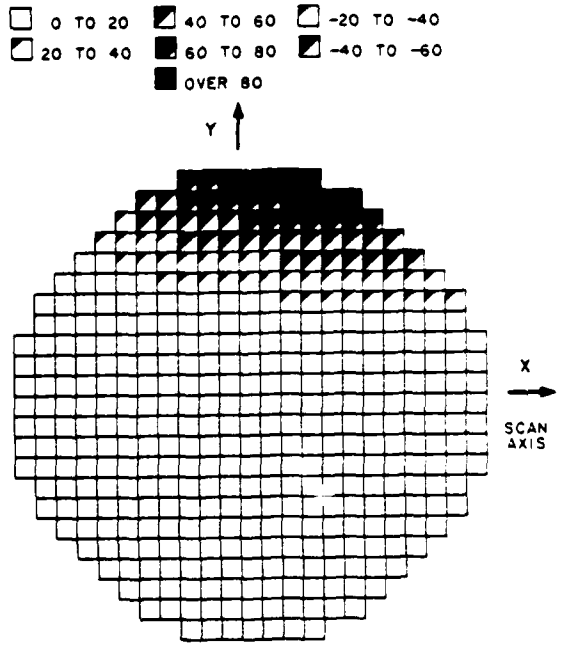

Figure 67. Phase Error at Feed Array (12 GHz)
$\xi = 90°$, $\phi = 0°$, R4 = 4 in., Three Lens Design Case.

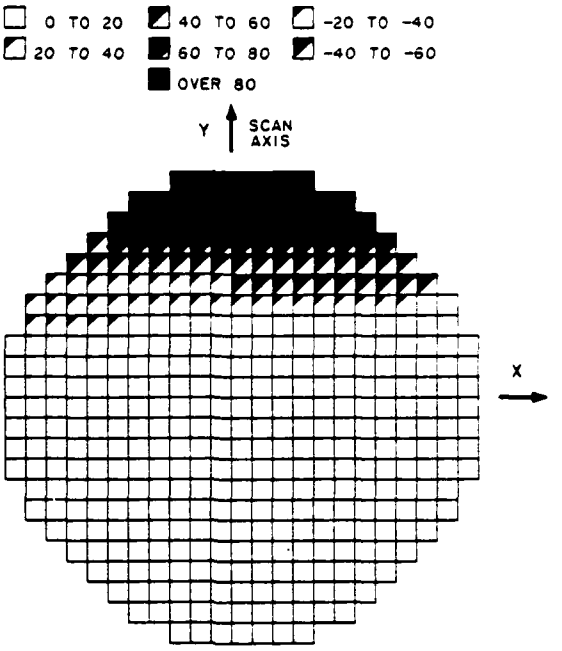

Figure 68. Phase Error at Feed Array (12 GHz)
$\xi = 90°$, $\phi = 90°$, R4 = 4 in., Three Lens Design Case.

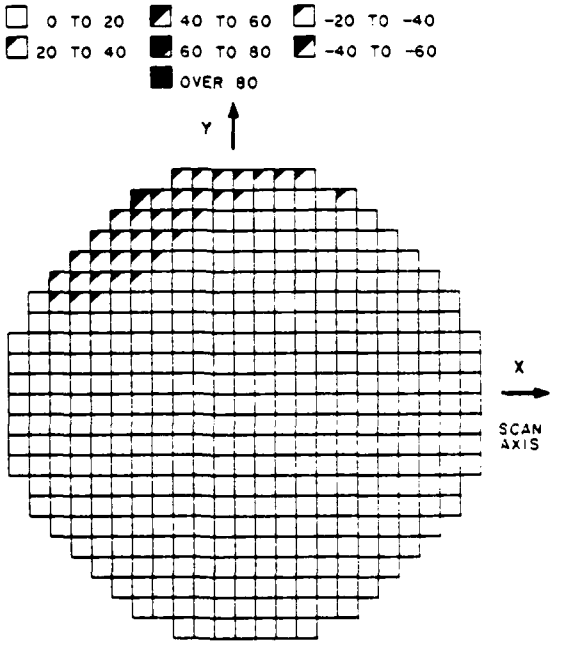

Figure 69. Phase Error at Feed Array (12 GHz)
$\xi = 71.2°$, $\phi = 0°$, R4 = 4 in., Minor Axis Lens Design.

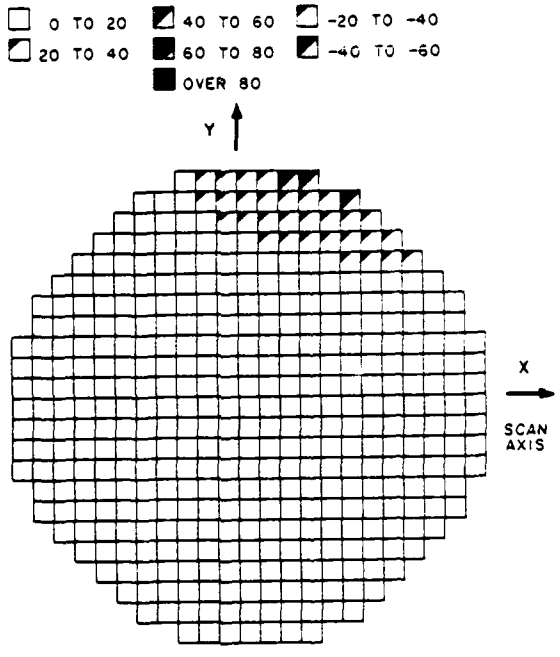

Figure 70. Phase Error at Feed Array (12 GHz)
$\xi = 90°$, $\phi = 0°$, R4 = 4 in., Minor Axis Lens Design.

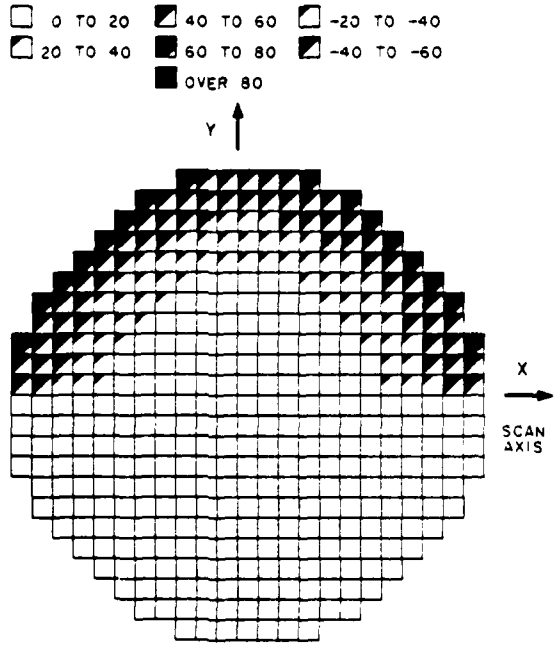

Figure 71. Phase Error at Feed Array (12 GHz)
$\xi = 0°$, $\phi = 0°$, R4 = 4 in., Minor Axis Lens Design.

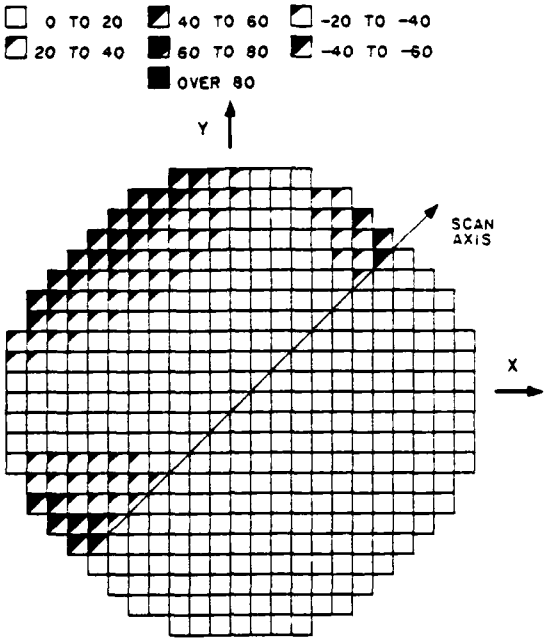

Figure 72. Phase Error at Feed Array (12 GHz)
$\xi = 73°$, $\phi = 45°$, R4 = 4 in., Minor Axis Lens Design.

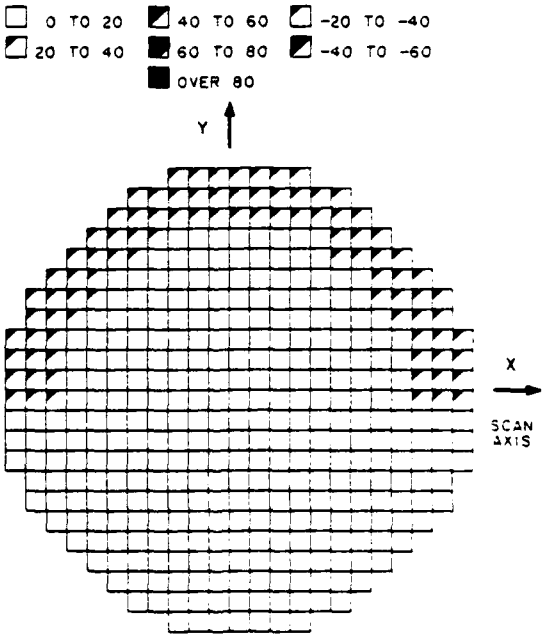

Figure 73. Phase Error at Feed Array (12 GHz)
$\xi = 0°$, $\phi = 0°$, R4 = 7 in., Optimized Feed Array, Minor Axis Lens Design.

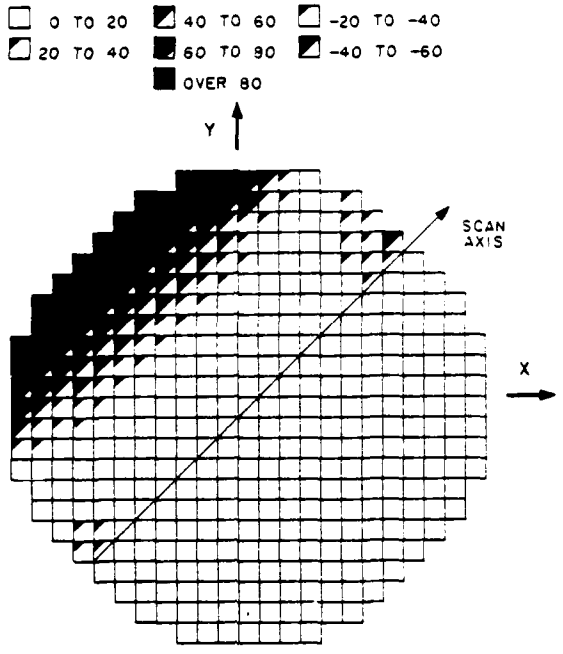

Figure 74. Phase Error at Feed Array (12 GHz)
$\xi = 87°$, $\phi = 45°$, R4 = 4 in., Minor Axis Lens Design.

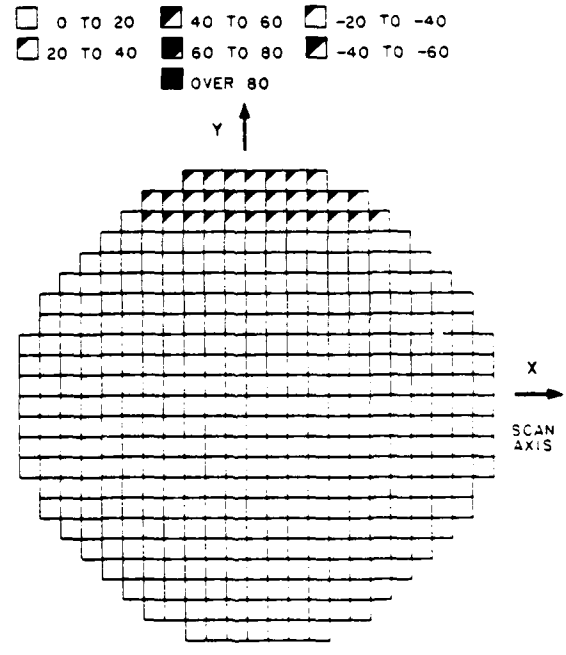

Figure 75. Phase Error at Feed Array (12 GHz)
$\xi = 20.5°$, $\phi = 0°$, R4 = 7 in., Optimized Feed Array, Minor Axis Lens Design.

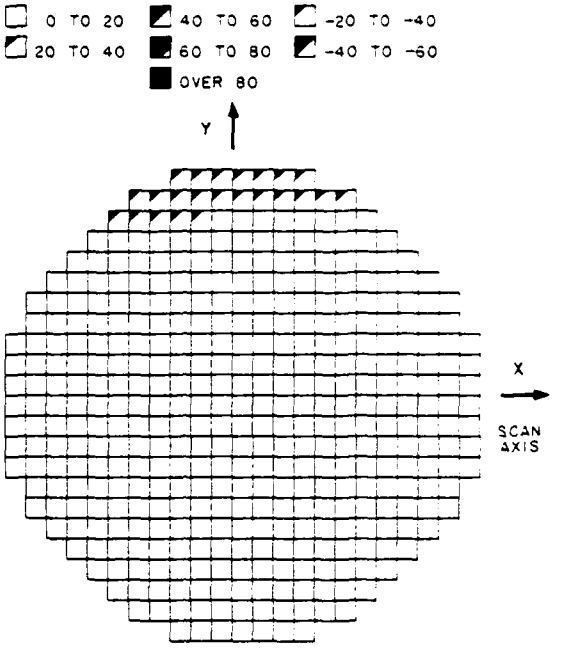

Figure 76. Phase Error at Feed Array (12 GHz)
$\xi = 42°$, $\phi = 0°$, R4 = 7 in., Optimized Feed Array, Minor Axis Lens Design.

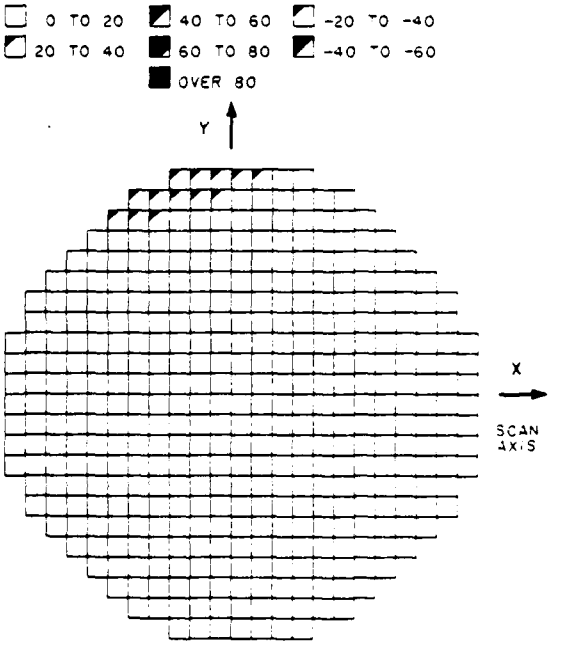

Figure 77. Phase Error at Feed Array (12 GHz).
$\xi = 59°$, $\phi = 0°$, R4 = 7 in., Optimized Feed Array, Minor Axis Lens Design.

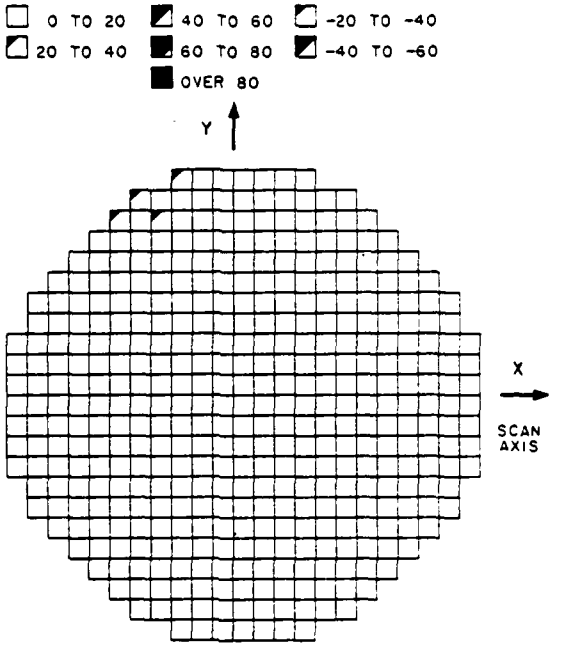

Figure 78. Phase Error at Feed Array (12 GHz)
ξ = 71.2°, ϕ = 0°, R4 = 7 in., Optimized Feed Array, Minor Axis Lens Design.

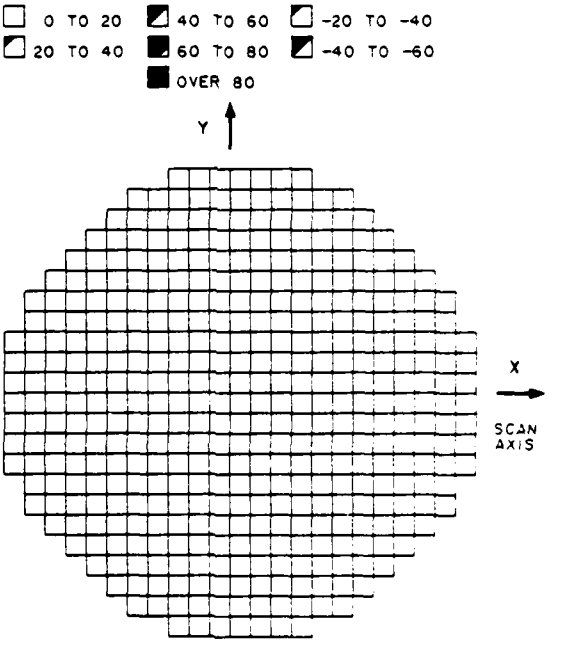

Figure 79. Phase Error at Feed Array (12 GHz)
ξ = 81.3°, ϕ = 0°, R4 = 7 in., Optimized Feed Array, Minor Axis Lens Design.

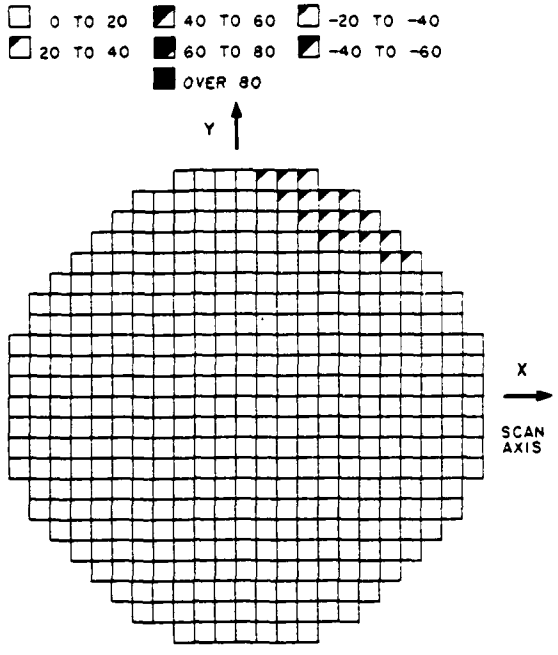

Figure 80. Phase Error at Feed Array (12 GHz)
ξ = 90.2°, ϕ = 0°, R4 = 7 in., Optimized Feed Array, Minor Axis Lens Design

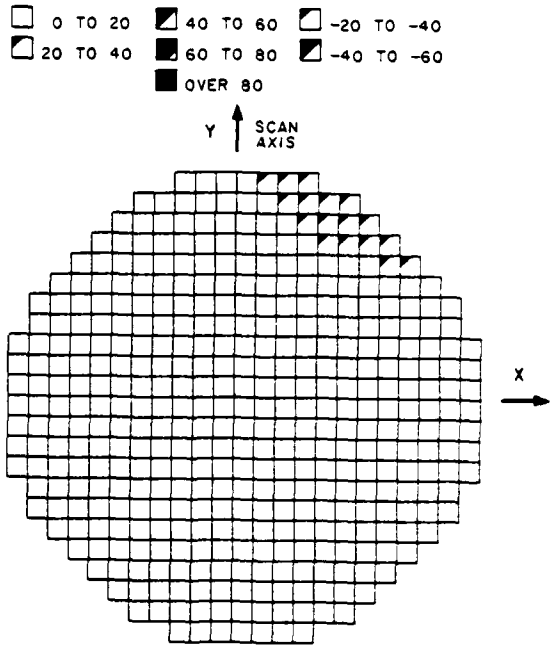

Figure 81. Phase Error at Feed Array (12 GHz)
ξ = 90.2°, ϕ = 90°, R4 = 7 in., Optimized Feed Array, Minor Axis Lens Design.

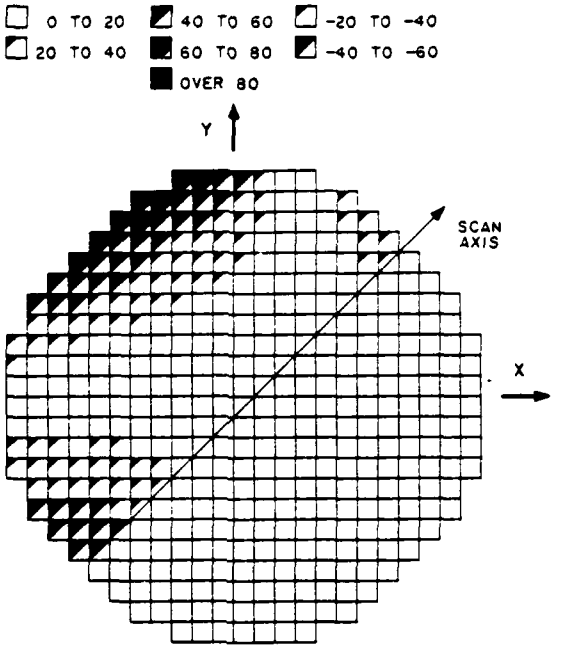

Figure 82. Phase Error at Feed Array (12 GHz)
$\xi = 73°$, $\phi = 45°$, R4 = 7 in., Optimized Feed Array, Minor Axis Lens Design.

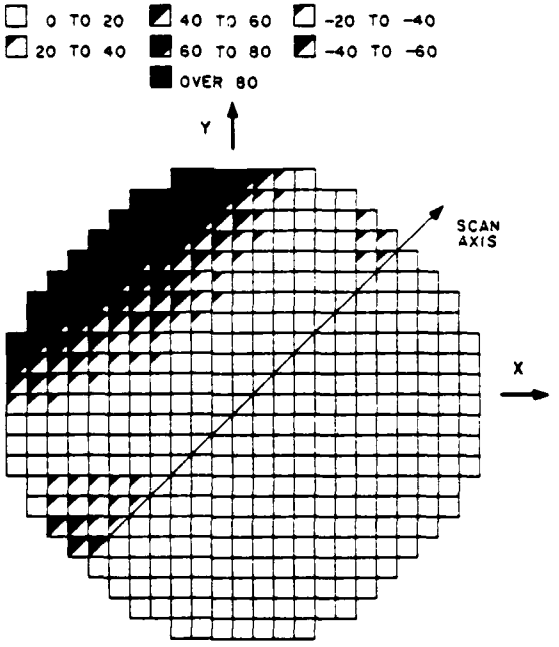

Figure 83. Phase Error at Feed Array (12 GHz)
$\xi = 87°$, $\phi = 45°$, R4 = 7 in., Optimized Feed Array, Minor Axis Lens Design.

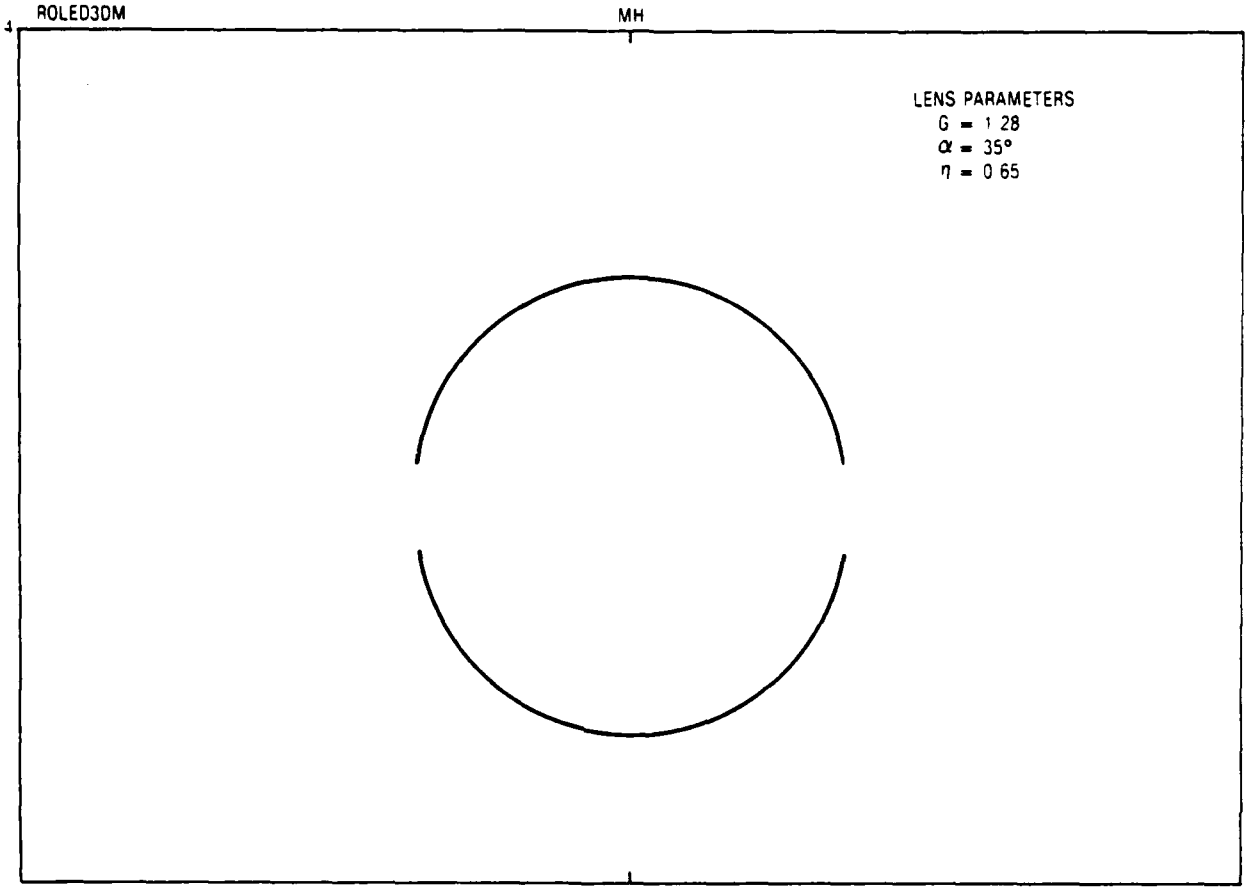

Figure 84. Lens Shape For Selected Design.

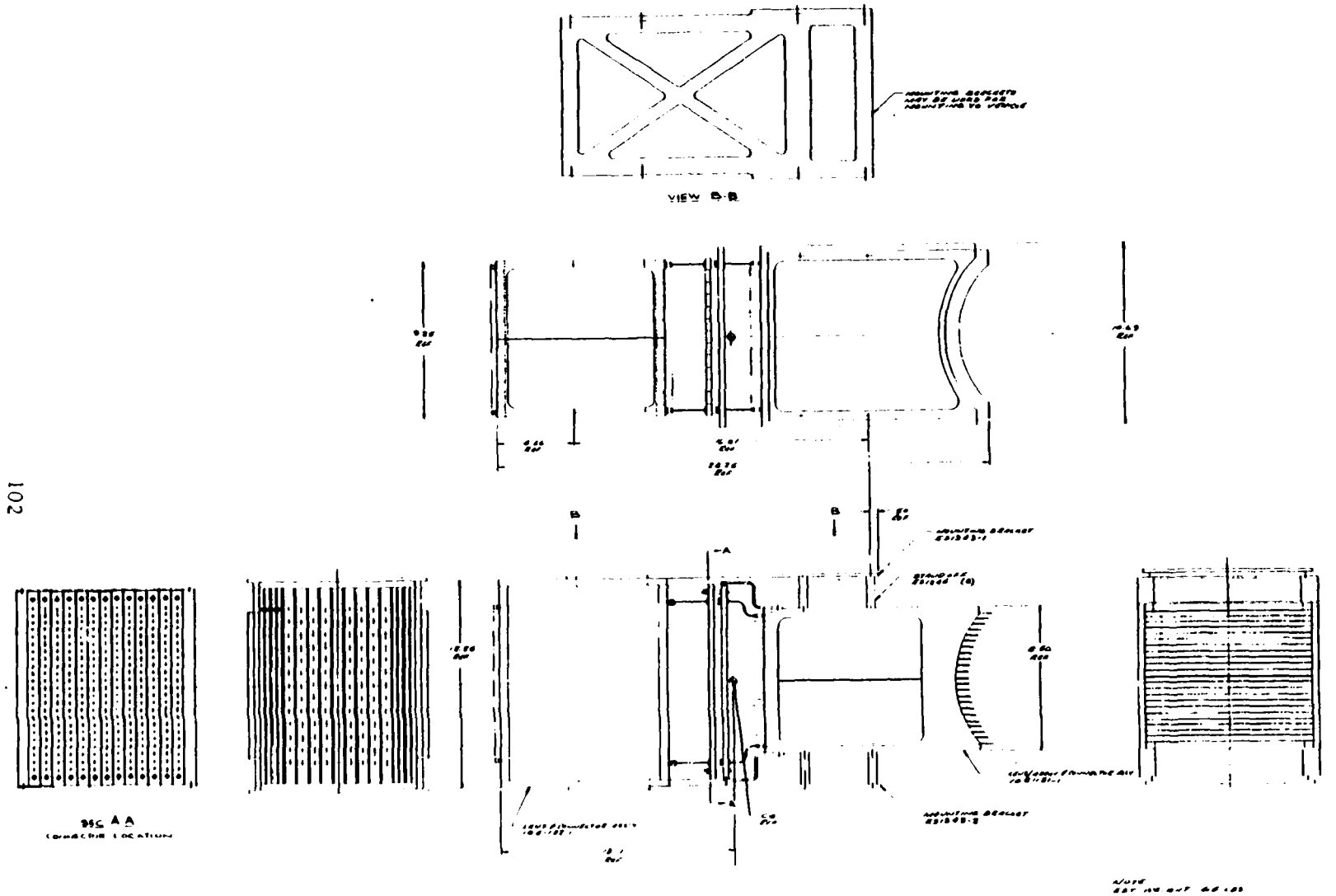

Figure 85. 3-D Dome System Packaging Concept.

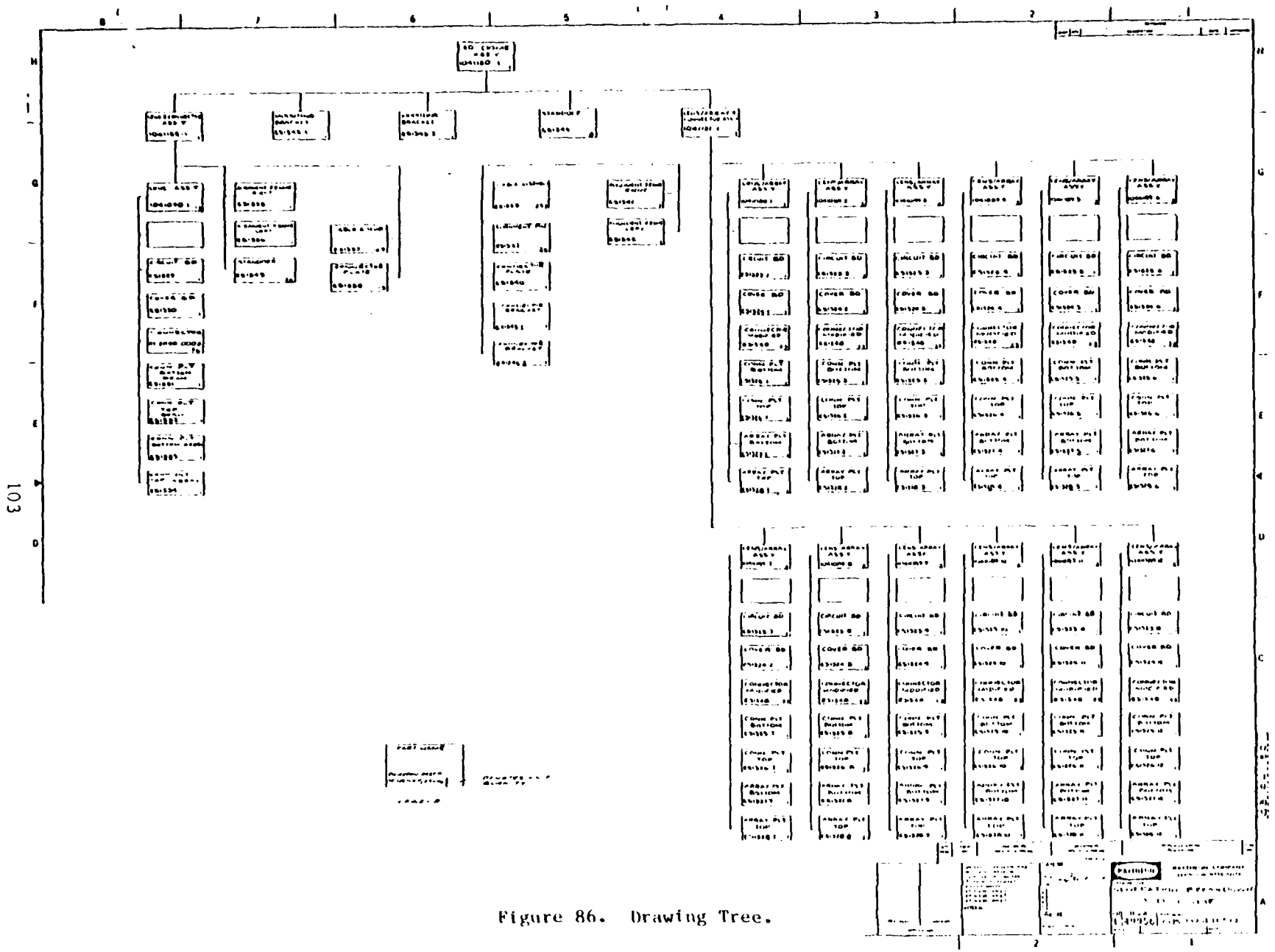

Figure 86. Drawing Tree.

TABLE 1. LENS TRADEOFF STUDY (CENTRAL SLICE)

R4 (in.)	Drop (in.)	R5 (in.)	Lens Shape	Beamwidth 0°	Beamwidth 90°	Comments
∞	0	∞	(Sperry direct)	26	13	Pattern direct from Sperry data
∞	0	∞	Egg shape	25	15	Lens design from Sperry data (flat array)
∞	0	∞	Egg shape	25	15	Lens design from ESD dome (flat array)
4	0	6.9	Good	30	11	Good curvature, selected design
3.55	0.25	6.9	Very Good	31	10	
6.25	-1.5	6.9	Fair	25	14	Translation only
5.19	-0.75	6.9	Fair	28	12	
4.42	-0.25	6.9	Good	29	11	
7	0.9	9.9	Fair	30	11	Decreased curvature only
4	-0.5	6.4	Good	29	11	
10	0	11.5	Poor	27	11	Translated and curved
10	2	13.5	Fair	32	11	

TABLE 2. CABLE LENGTHS IN DIELECTRIC

CABLE NUMBER	INCH	INCH NOMINAL	CM	CM NOMINAL	DEG	CM IN AIR
1	0.0	6.0	0.0	15.240	0.0	0.0-DUMMY
2	1.332	7.332	3.382	18.622	696.2	4.831
3	1.002	7.002	2.595	17.835	534.1	3.706
4	0.749	6.749	1.903	17.143	391.7	2.718
5	0.518	6.518	1.316	16.556	270.9	1.880
6	0.330	6.330	0.838	16.078	172.4	1.196
7	0.185	6.185	0.469	15.709	96.6	0.671
8	0.082	6.082	0.208	15.448	42.8	0.297
9	0.020	6.020	0.052	15.292	10.6	0.074
10	0.0	6.000	0.0	15.240	0.0	0.0
11	0.020	6.020	0.208	15.448	10.6	0.074
12	0.082	6.082	0.208	15.448	42.8	0.297
13	0.185	6.185	0.469	15.709	96.6	0.671
14	0.330	6.330	0.838	16.078	172.4	1.196
15	0.518	6.518	1.316	16.556	270.9	1.880
16	0.749	6.749	1.903	17.143	391.7	2.718
17	1.022	7.022	2.595	17.835	534.1	3.706
18	1.332	7.332	3.382	18.622	696.2	4.831
19	0.0	6.000	0.0	15.240	0.0	0.0--DUMMY

CABLE DIELECTRIC CONSTANT = 2.04

NOMINAL CABLE LENGTH = 6.00 INCHES

NOMINAL FREQUENCY = 12.00 GHz

TABLE 3. INTERIOR AND EXTERIOR SCAN ANGLES

BEAMPORT NUMBERS	INTERIOR SCAN ANGLE, (DEGREES)	EXTERIOR SCAN ANGLE, (DEGREES)
8	0	0
7, 9	6	20
6, 10	14	42
5, 11	21	59
4, 12	28	71
3, 13	36	81
2, 14	44	90
1, 15	(dummy ports, not used)	

TABLE 4. COMPARISON OF MEASURED AND COMPUTED DATA FOR CENTRAL SLICE ARRAY

-3 dB BEAMWIDTH (DEGREES)

FREQ(CHz)	BEAMPORT 8		BEAMPORT 12		BEAMPORT 14	
	COMP	MEAS	COMP	MEAS	COMP	MEAS
8	10.5	11	12	10.9	14	14
12	20	20	10.5	8.5	9	11.0
16	23.5	16.7(*)	12.5	8.5	8.0	8.0(G)

-10 dB BEAMWIDTH (DEGREES

FREQ(CHz)	BEAMPORT 8		BEAMPORT 12		BEAMPORT 14	
	COMP	MEAS	COMP	MEAS	COMP	MEAS
8	33	35	29.5	17.5	22	21.5
12	29	36	32.5	23.5	26	14.5
16	35	30	24	18.5	15	13 (G)

SCAN ANGLE (DEGREES)

FREQ(CHz)	BEAMPORT 8		BEAMPORT 12		BEAMPORT 14	
	COMP	MEAS	COMP	MEAS	COMP	MEAS
8	+1	0	-25	-28.5	-42	-44
12	-0.5	0	-24	-28	-42	-44
16	0	0	-28	-28	-43	-44

(*) Dip in center of beam

(G) Grating lobe present

TABLE 5. FEED LENS DESIGN CANDIDATES (DIMENSIONS IN INCHES)

Parameter (See Fig. 4-4)	Single Lens Design	Three Lens Design	Minor Axis Lens Design	Optimized Array Design
A2	13.125	13.125	13.125	13.125
B2	10.167	10.167	10.167	10.167
A1	8.00	8.00	8.00	8.00
B1	5.65	5.65	5.65	5.65
OFF	0.125	0.125	0.125	0.125
RO	4.0	4.0	4.0	4.0
R5	6.923	8.24	6.923	8.996
R4	4.0	4.0	4.0	7.0
DROP	0.0	2.0	0.0	0.0

TABLE 6. PHASE ERRORS IN 3-D DOME/ROTMAN LENS ANTENNA

(Degrees at 12 GHz)

SCAN ANGLE		SINGLE LENS		THREE LENS		MINOR AXIS LENS		OPTIMIZED ARRAY	
θ (ξ_o)	ϕ (azimuth)	RMS	PEAKS	RMS	PEAKS	RMS	PEAKS	RMS	PEAKS
0°	0°	2.76°	+11, -2	NA	NA	20.50°	+0, -67°	10.22°	0, -35
20.5°	0°	3.10°	+12, -1	NA	NA	16.18°	+1, -59	8.79°	+1, -32
42°	0°	4.46°	+18, -3	NA	NA	14.80°	+2, -54	7.89°	+1, -29
59°	0°	7.36°	+29, -5	NA	NA	12.41°	+3, -47	6.69°	+3, -27
71.2°	0°	11.71°	+46, -6	NA	NA	9.49°	+3, -40	5.98°	+3, -23
81.3°	0°	18.16°	+73, -6	NA	NA	8.17°	+7, -29	6.113°	+16, -15
90.2°	0°	25.05°	+100, -0	26.14	+100.0	10.96°	+44, -9	8.48°	+36, -5
90.2°	90°	25.05°	+100, -0	NA	NA	NA	NA	8.48°	+36, -5
73°	45°	NA	NA	NA	NA	24.52°	+57, -53	27.3°	+70, -56
87°	45°	NA	NA	NA	NA	38.82°	+123, -42	40.4°	+129, -51

TABLE 7. DIAGONAL SCAN DATA

ξ = 87 deg, ϕ = 45 deg.

Minor Axis Lens design

Element (in)	X Data (in)	Y Data (in)	Ideal Lens (in)	Minimum Co-phase Error (in)
2.528	-1.628	-1.255	-1.441	-.186
1.827	-1.117	- .855	- .986	-.129
1.104	- .650	- .485	- .567	-.082
0.0	0.0	0.0	0.0	0.0
-1.104	+ .534	+ .381	.457	+.076
-1.827	+ .824	+ .569	.696	+.127
-2.528	+1.055	+ .699	.877	+.178

TABLE 8. 3-D DOME PHYSICAL CHARACTERISTICS

ITEM	VOLUME (CU. IN.)	WEIGHT (LB.)
ELEVATION LENS/ARRAY ASSEMBLY	1,448.4	32.3
AZIMUTH LENS ASSEMBLY	1,382.6	25.6
SYSTEM BRACKETS	735.8	2.1
SYSTEM TOTALS	3,566.8	65.0

APPENDIX A.
WIDE ANGLE ARRAY FED LENS

1. DESIGN STUDIES

The Wide Angle Array Fed Lens (WAAFL) is a marriage of the Dome Antenna [13] and Rotman Lens Fed Multibeam Arrays [14]. It offers the capability for greater than hemisphere scan coverage from a single feed array, greater than octave bandwidth, and multiple simultaneous beams.

This paper describes WAAFL design studies which led to a novel curved feed array with substantial improvements in performance over conventional planar feed arrays. The curved feed array results in feed lens designs using Rotman lens technology which are superior to previous designs employing planar feed arrays.

A WAAFL is designed to provide scan amplification, i.e., wide angle scanning (hemisphere or greater) from a single array face. A ray path diagram (to scale) of a WAAFL with Rotman feed lens attached is shown in Figure A-1. The design shown is for a scan amplification factor K of 1.5.

The advantage realized by the curved feed array are reduced amplitude distortion, improved feed lens design which is 30 percent smaller and of a more efficient shape (less mismatch or spillover), and significantly lower path length errors.

---

13 Schwartzmann, L. and Stangel, J., "The Dome Antenna." Microwave Journal, pp. 31-34, October 1975.

14 Archer, pp. 24-32.

The ability to scan extremely wide angles is not accomplished without loss, however. A reduction in effective aperture occurs which translates directly to reduced gain (with respect to full feed array gain). Boresight aperture loss of 2.5 to 4.0 dB should be anticipated (one plane only) for Wide Angle Array Fed Lens antennas.

The uniform amplitude distribution can be seen in the ray path diagram of figure A-1. Figure A-2 shows the actual low distortion for two curved feed arrays. In contrast, the flat feed array distortion is asymmetrical and varies about 7 dB over the aperture, a fact which contributes significantly to sidelobe levels.

The greatly reduced path length errors for curved feed array are shown in Figure A-3. The order-of-magnitude improvement in path length error makes the difference between an infeasible feed lens and an attractive design and performance.

Three sets of computed low sidelobe radiation patterns are shown in Figure A-4. A Taylor-like aperture taper for 38 dB sidelobe level was imposed on the feed array. The effects of amplitude distortion and (for 60° scan) the lens phase error are evident in the sidelobe levels. However, the curved feed array clearly fares best at all three scan angles (0°, 60° and 90°). Significant beam broadening and shoulders are present when the flat feed array distortion is included.

Results of other cases, e.g. scan amplification of K=1.8 and 2.0, and representative lens designs will be described.

2. HARDWARE DEMONSTRATION OF A 2-DIMENSIONAL WIDE ANGLE ARRAY FED LENS

A 2-Dimensional WAAFL has been built and tested which demonstrates 180° scan coverage, 7 to 18 GHz frequency bandwidth, and multiple beams.

The design concept for this demonstration WAAFL was selected from the results of earlier design studies[15]. Design parameters are summarized in Table A-1. A photo of the completed hardware appears in Figure A-5.

The demonstration hardware consists of three items: (1) a semicircular array of double-ridge elements, (2) a printed stripline Array-Fed Lens which provides the scan amplification, and (3) a printed stripline Rotman Lens for scanning the beams. In the resultant system, each beamport produces a scanned beam in space. One advantage of the array fed lens is the absence of frequency-dependent beam squint.

Test results confirm the performance capability of the wide angle, array fed lens. Scan capability of 180° was measured over frequencies from 7 to 18 GHz. Figures A-6 through A-8 show measured radiation patterns at 8, 12, and 15 GHz, respectively. In Figure A-6, the full-beam rosette of 29 beams is shown for 8 GHz. Other figures show only selected beams covering the 180° scan sector.

In all cases, beam patterns are well formed with good sidelobes, and confirm the expected performance, including low-scan rolloff.

The excellent results of the hardware demonstration confirm the feasibility of 2-Dimensional Wide Angle Array Fed Lenses with Rotman lens feed.

---

15 Thomas, D., Design Studies of a Wide Angle Array Fed Lens, Paper presented to 1979 IEEE AP-S International Symposium.

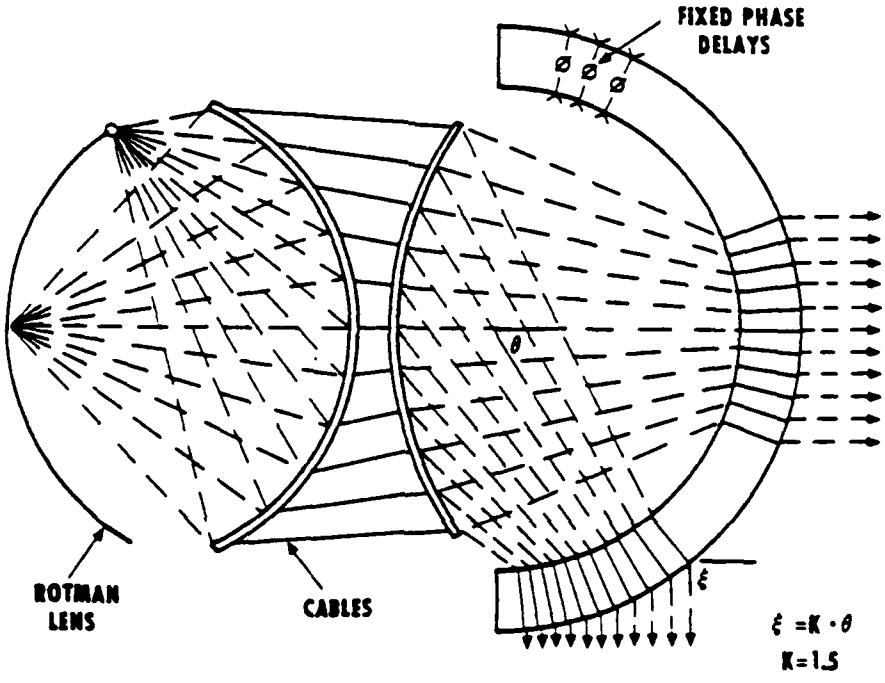

Figure A-1. Wide Angle, Array Fed Lens (WAAFL).

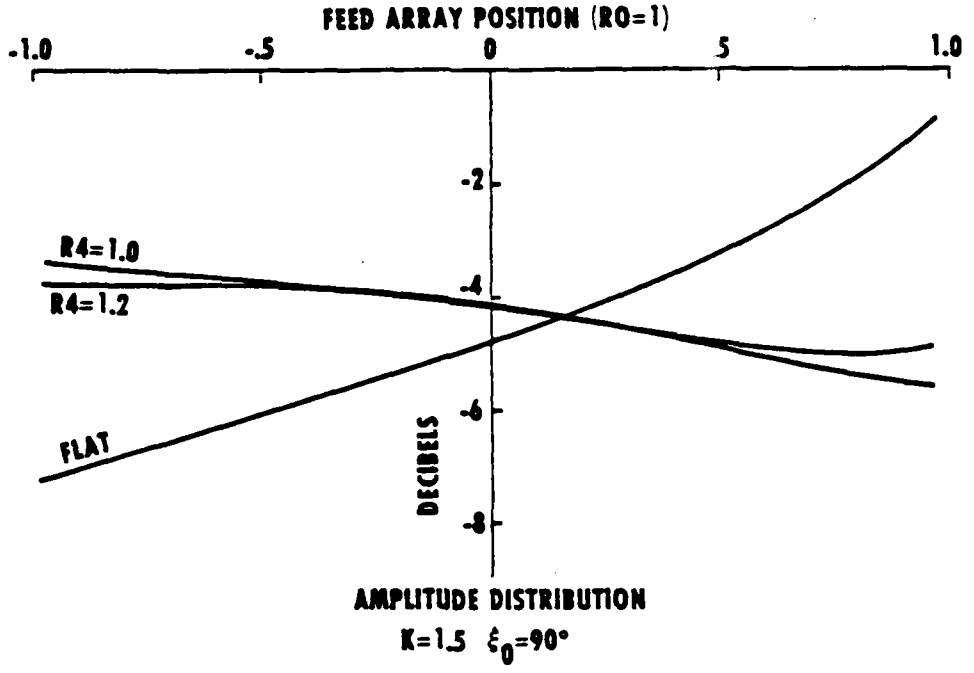

Figure A-2. Amplitude Distortion in Array Fed Lens.

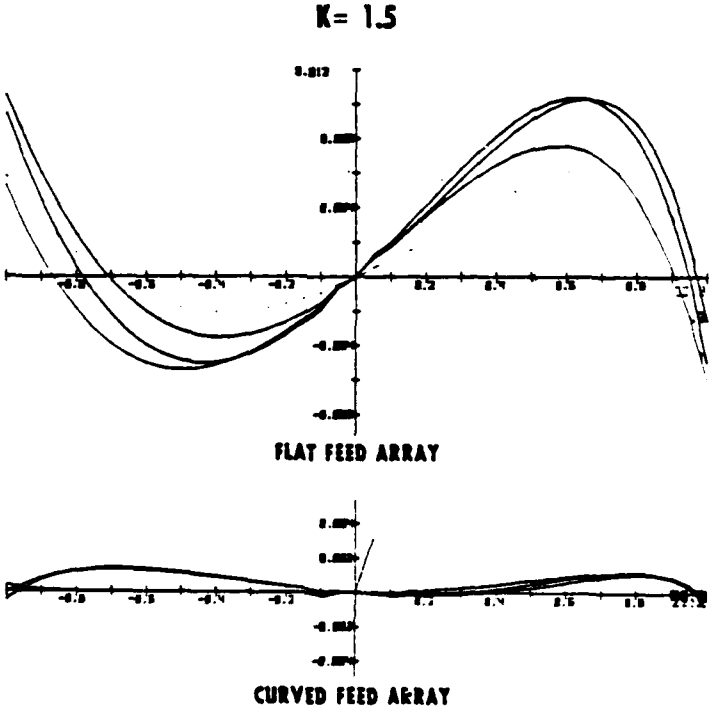

Figure A-3. Feed Lens Path-Length Error.

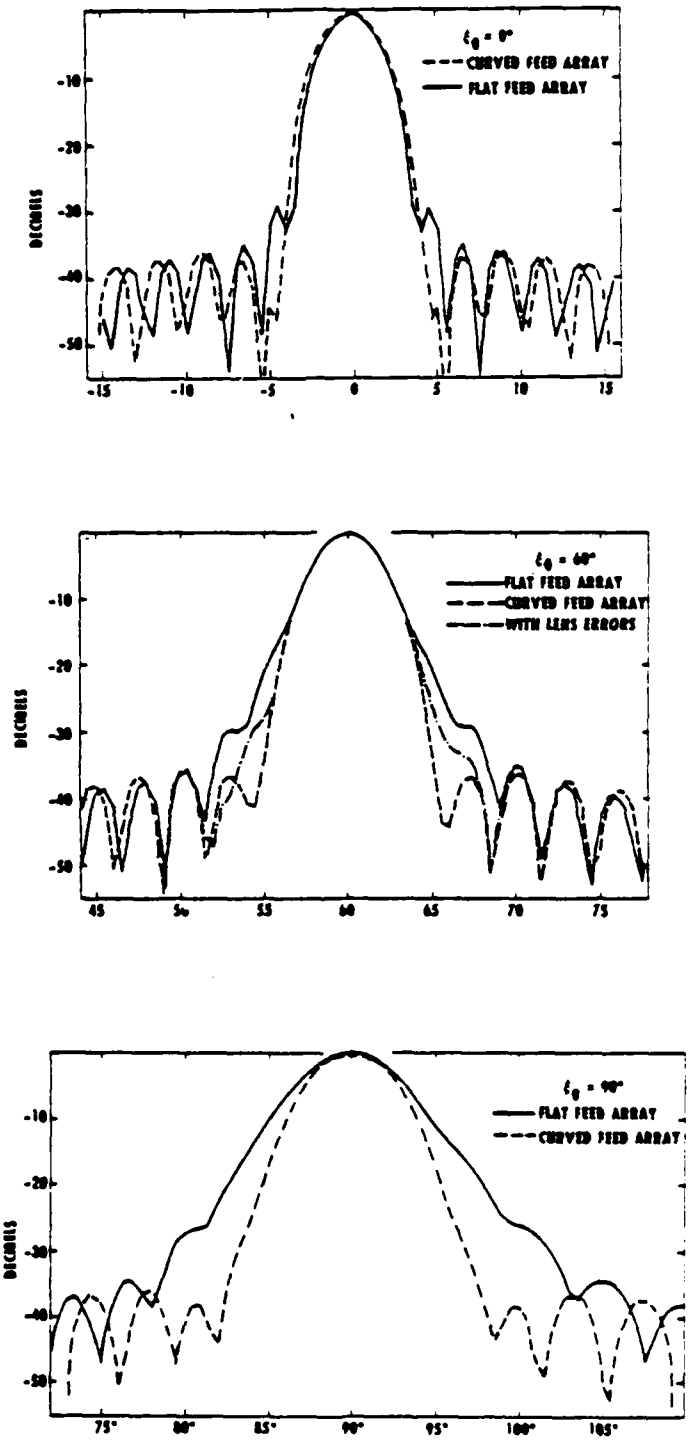

Figure A-4. Computed Low-Sidelobe Patterns.

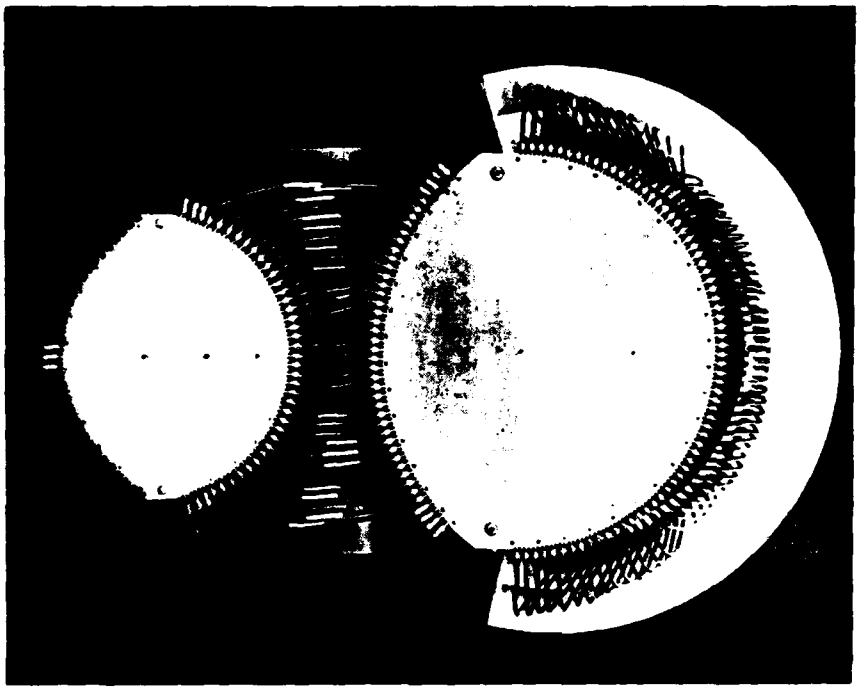

Figure A-5. WAAFL Demonstration Hardware.

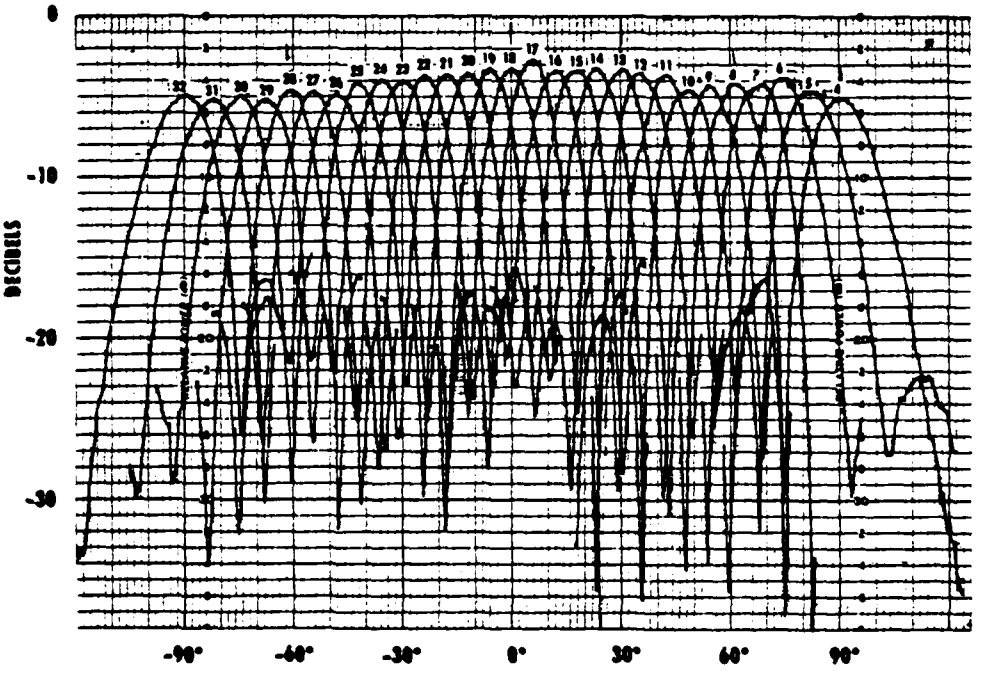

Figure A-6. WAAFL Measured Radiation Patterns (8 GHz).

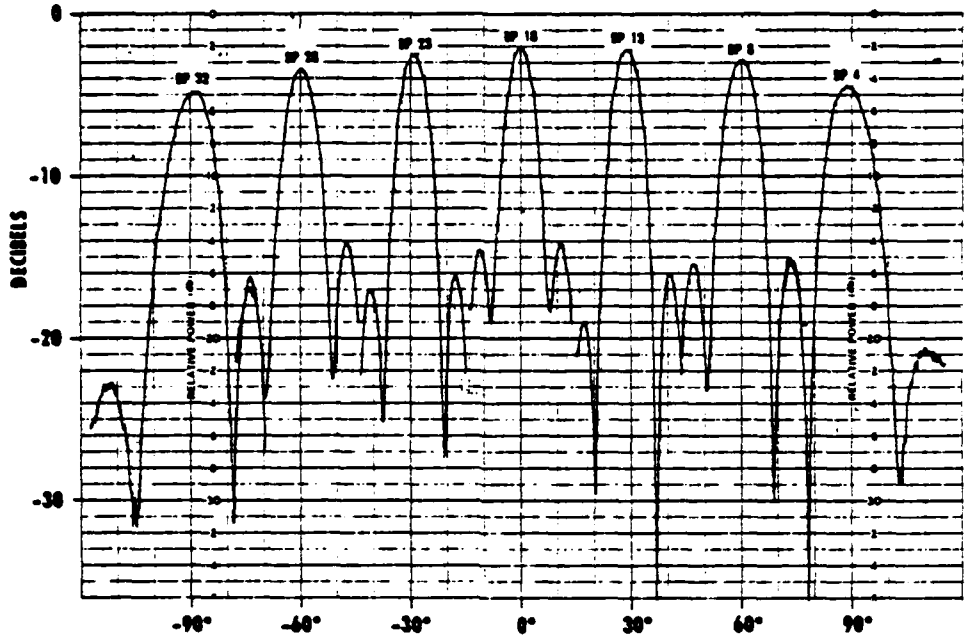

Figure A-7. WAAFL Measured Radiation Patterns (12 GHz).

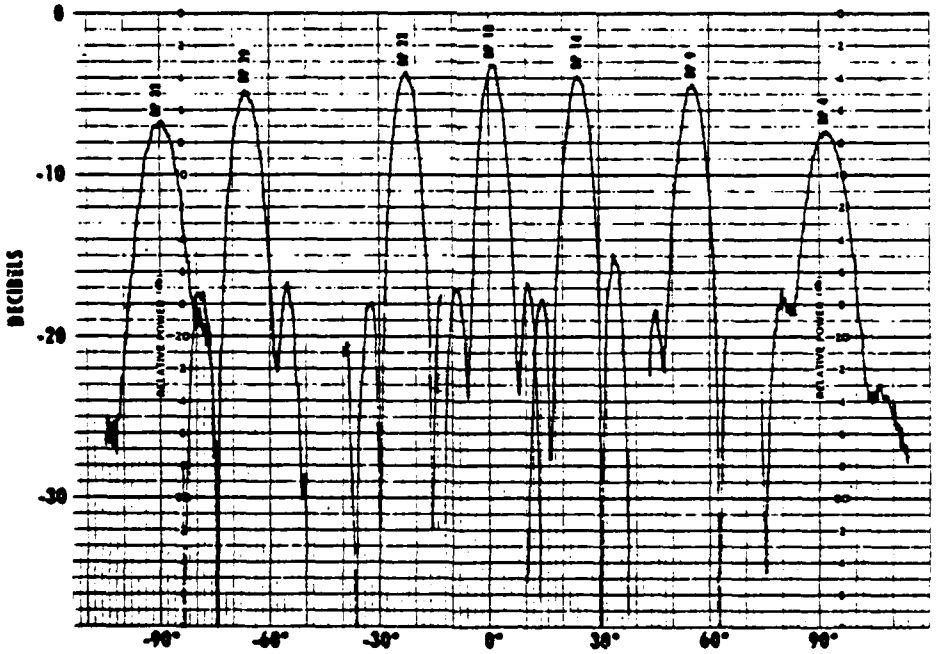

Figure A-8. WAAFL Measured Radiation Patterns (15 GHz).

TABLE A-1. WAAFL DESIGN DATA

SCAN COVERAGE	180°
BANDWIDTH	7 TO 18 GHz
BEAMWIDTH (NOMINAL)	
6°	(15 GHz)
11°	(8 GHz)
SEMICIRCULAR ARRAY	
69 ELEMENTS (180 DEGREES)	
9.08 IN RADIUS (PHASE CENTER)	
ARRAY FED LENS	
7.26 IN. SEMICIRCULAR ARC RADIUS	
35 ELEMENT FEED ARRAY	
12.1 IN. FEED ARRAY WIDTH	
SCAN AMPLIFICATION, K=1.5	
ROTMAN FEED LENS	
35 ARRAY PORTS, 29 BEAMPORTS	
G=1.10, α=40, η=0.65	

APPENDIX B.
LENS FED MULTIBEAM ARRAYS

1. LENS-FED MULTIBEAM ARRAY (ROTMAN LENS)

One type of phased array which is capable of generating multiple simultaneous beams from a single array aperture is the lens-fed array. Several types of lens array feeds exist, but the one of concern here is the bootlace lens first described by Rotman and Turner [16] and illustrated in Figure B-1. This type is characterized by a parallel-plate region and RF cables of specified length connecting the array to the parallel-plate region. The geometry of the lens and cable lengths is so designed that all ray paths from a plane wavefront (beam 1) to beam ports no. 1, 4 and 7 are of identical length, giving a total of three perfect-focus beam ports. Departure from perfect focus at intermediate beam ports (nos. 2, 3, 5, and 6 in Figure B-1) can usually be made negligible.

The lens-fed array is a quasi-optical device which depends on differing RF path length for its focusing properties, rather than on phase shifters (which are constant with frequency). As a result, scanned beam positions in space tend to be independent of frequency (no beam squint). Thus, lens-fed arrays can have very wide bandwidth, typically an octave or more.

Lens-fed arrays also have the capability for multiple simultaneous beams, with each beam enjoying the full aperture gain. Each beamport in Figure B-1 is essentially an independent antenna with a beam pointing in a fixed direction in space. Any beam coupling which occurs is normally significant only for adjacent beamports, and can be made small. This multibeam capability renders the lens-fed array equivalent to several conventional antennas.

---

[16] Rotman and Turner, pp. 623-632.

2. TWO-DIMENSIONAL MULTIBEAM ARRAYS

A two-dimensional multibeam array can be constructed of multiple linear arrays (rows and columns of elements on a surface) and a two-axis-scan beam-forming network composed of multiple two-dimensional Rotman lenses. The basic arrangement is illustrated schematically in Figure B-2. The columns of radiating elements are each fed by a vertical lens. Each column would then, by itself, form a cluster of conical fan beams stacked in the vertical plane. The corresponding beam ports on each of the vertical lenses are led through RF cable of appropriate lengths to a stack of similar horizontal lenses. The lenses of the second stack provide beam forming (focusing) for all elements in the array face in the horizontal plane. Each beam port of the second stack then corresponds to a pencil beam in space. The azimuth and elevation beamwidths of the beams are determined by the array face dimensions and the operating frequency, and the pointing direction of each beam is established by the geometry of the array and multiple lens beam-forming network, independent of RF frequency.

a. Multiple Tracking Steerable Telemetry Tracker (MUSTRAC)

The two-dimensional cluster of beams generated by the two stack feed lens described above is illustrated in Figure B-3. The shaded beams represent the four-beam clusters which enable two-axis monopulse tracking and data reception of (in this case) four simultaneous, independent communications transmitters within the solid angle of array coverage.

A two-dimensional multibeam array antenna of this type is shown in Figure B-4. This array is employed in a multiple-simultaneous-target steerable telemetry tracking system (MUSTRAC) which has satisfactorily completed Air Force evaluation and been in service for several years in the Eastern Test Range.

The 376 circularly polarized array radiating elements are fed by a beam forming network to provide a cluster of 132 pencil beams (4-degree beamwidth) filling a 50-degree cone. The beam forming network is shown in the rear view of the array in Figure B-5. Measured radiation patterns for one row of beams are presented in Figure B-6. Appropriate beams from this cluster are selected by means of a PIN diode switching network to form four simultaneous monopulse tracking beams that independently track separate telemetry sources over the 50-degree field of view. A four-beam cluster pattern is shown in Figure B-7. Note especially the low side-lobe level resulting from a combination of taper and geometry.

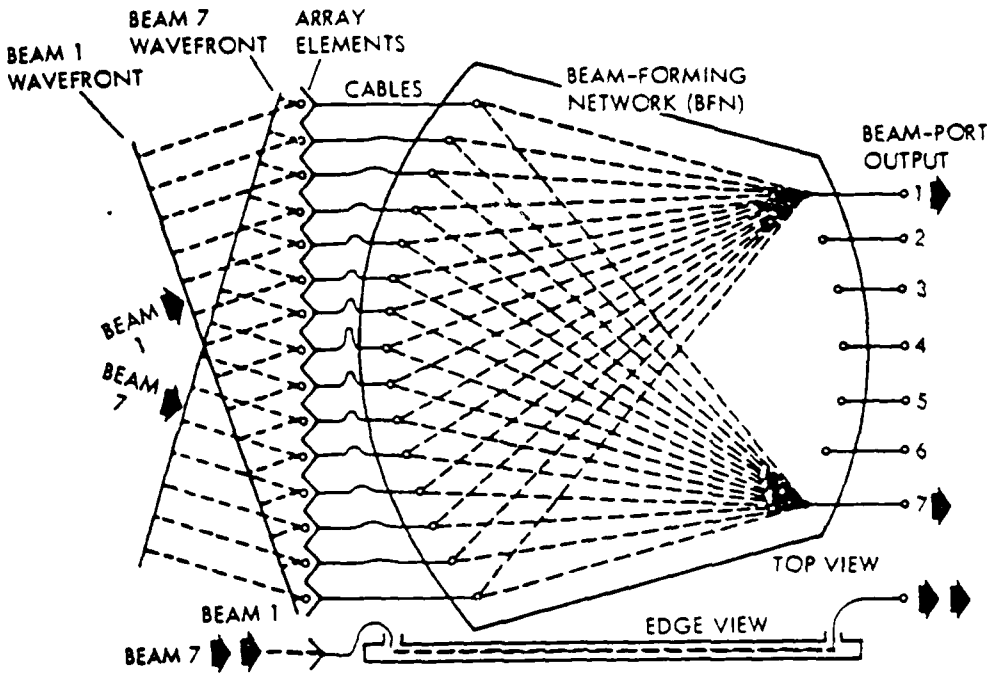

Figure B-1. Rotman Lens Beam-Forming Network.

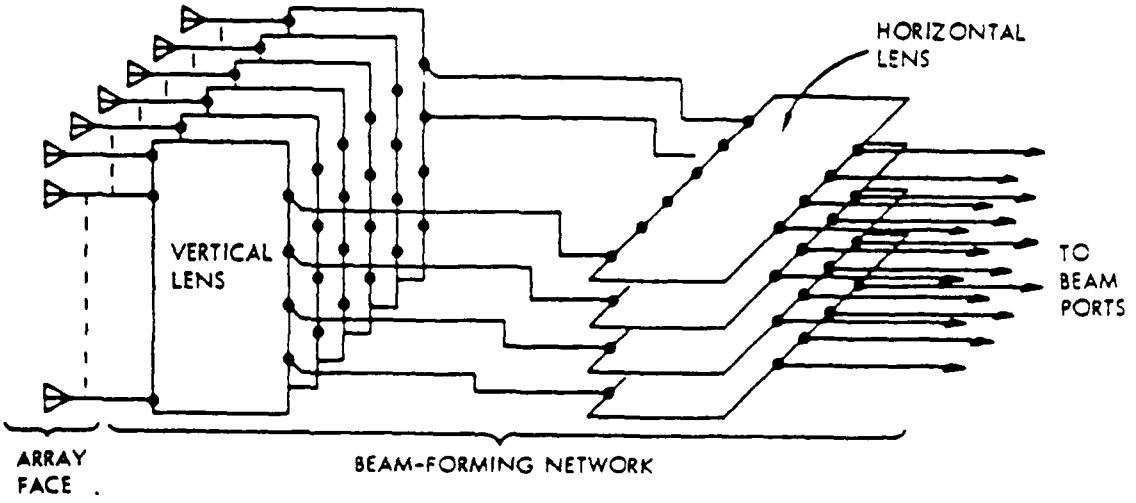

Figure B-2. Two-Stack Lens Beam Formation.

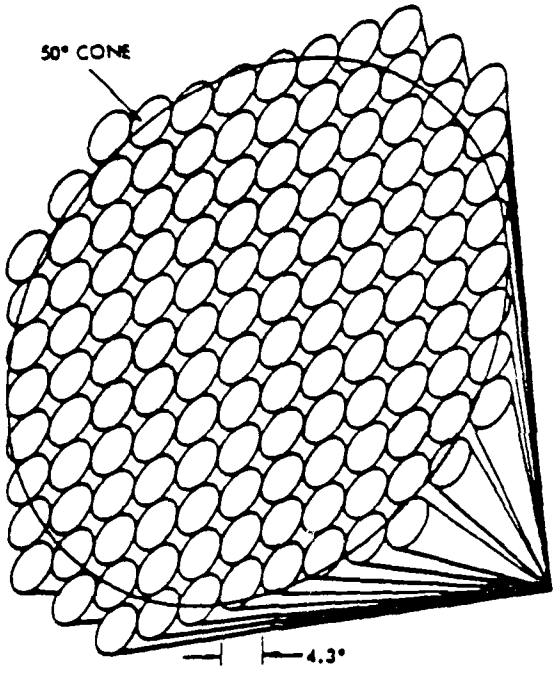

Figure B-3. Two-Dimensional Beam Cluster.

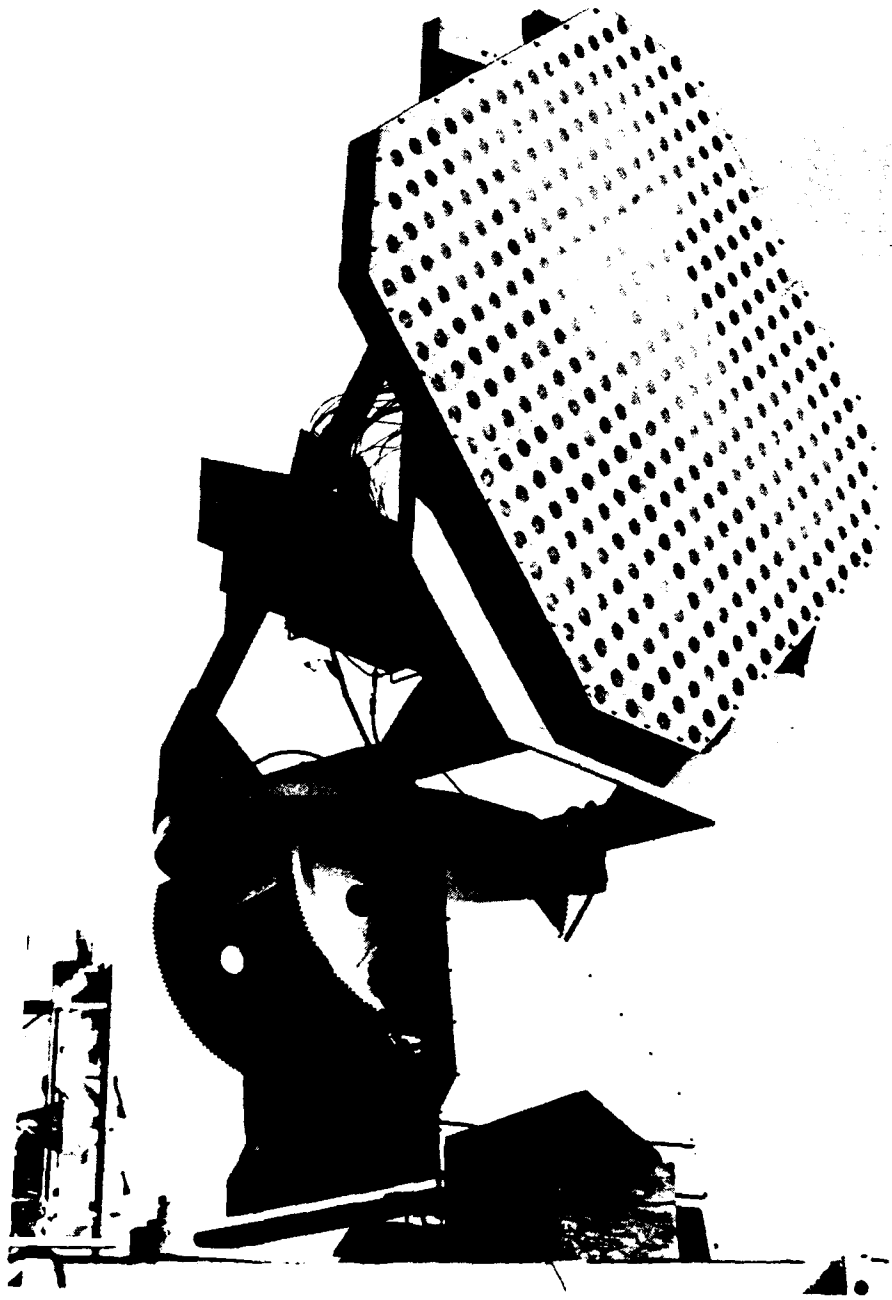

Figure B-4. MUSTRAC Antenna (Front View).

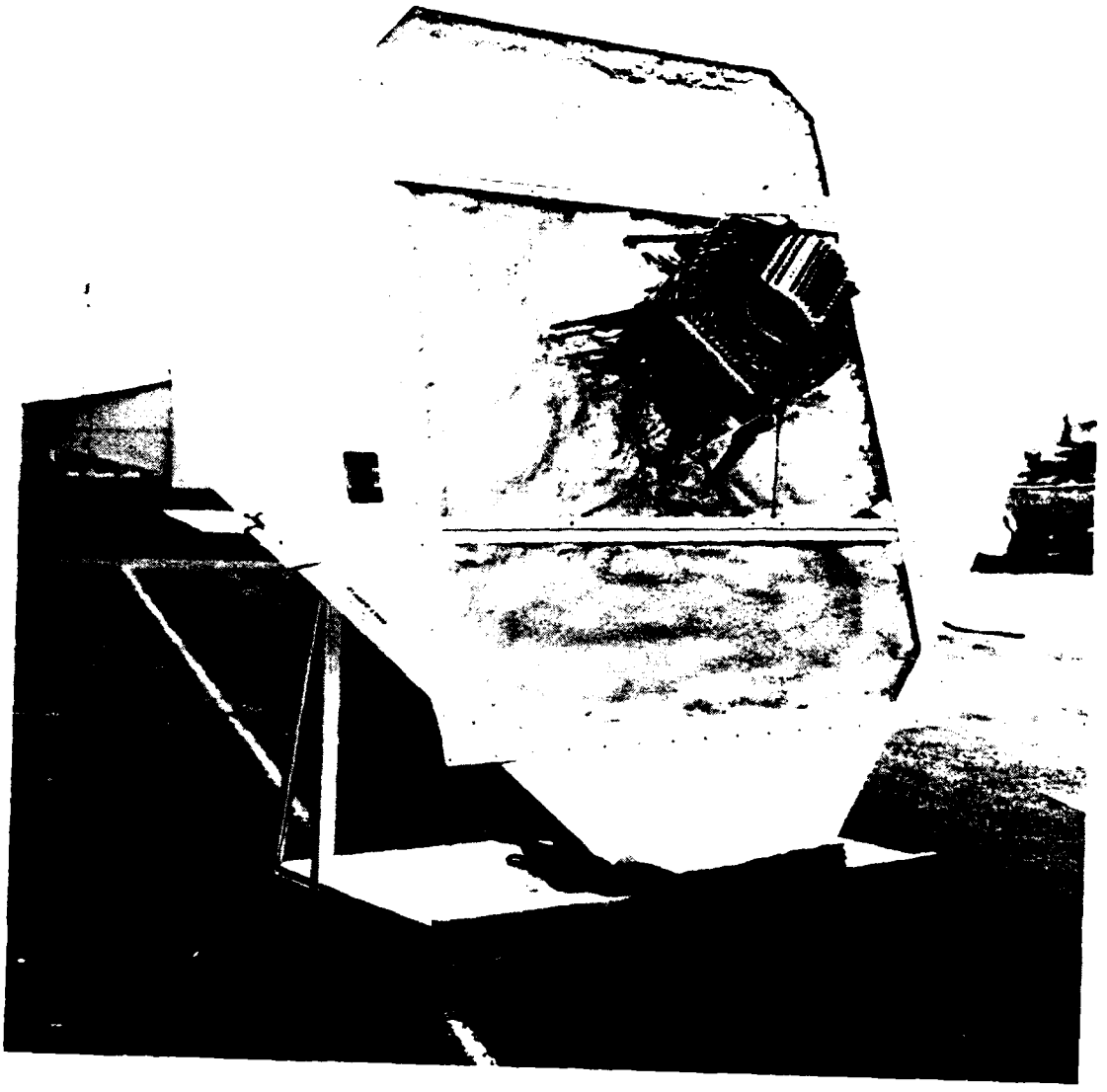

Figure B-5. MUSTRAC Antenna (Rear View, Two-Stack Lenses).

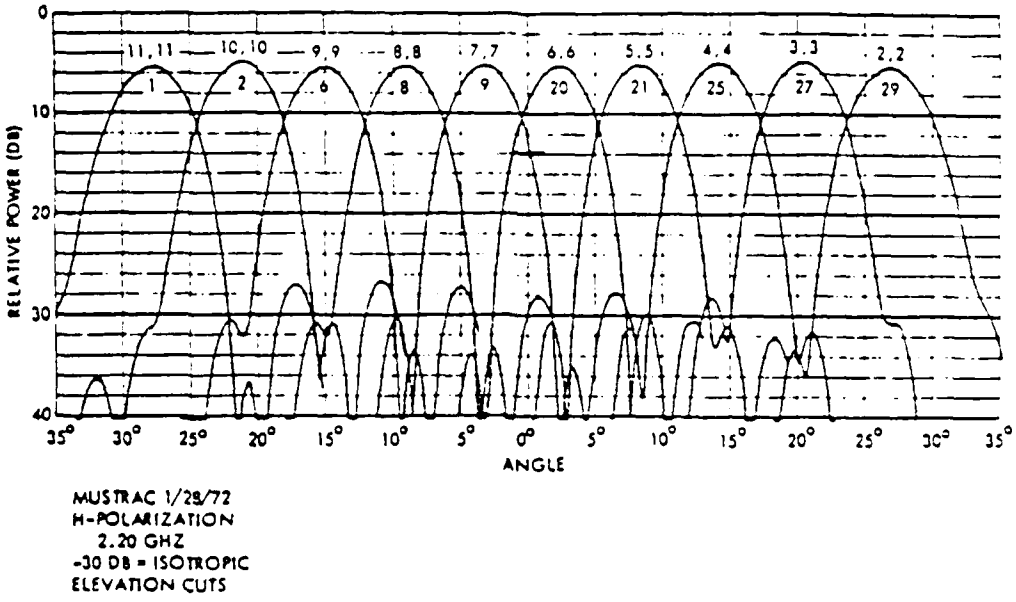

Figure B-6. MUSTRAC Measured Patterns.

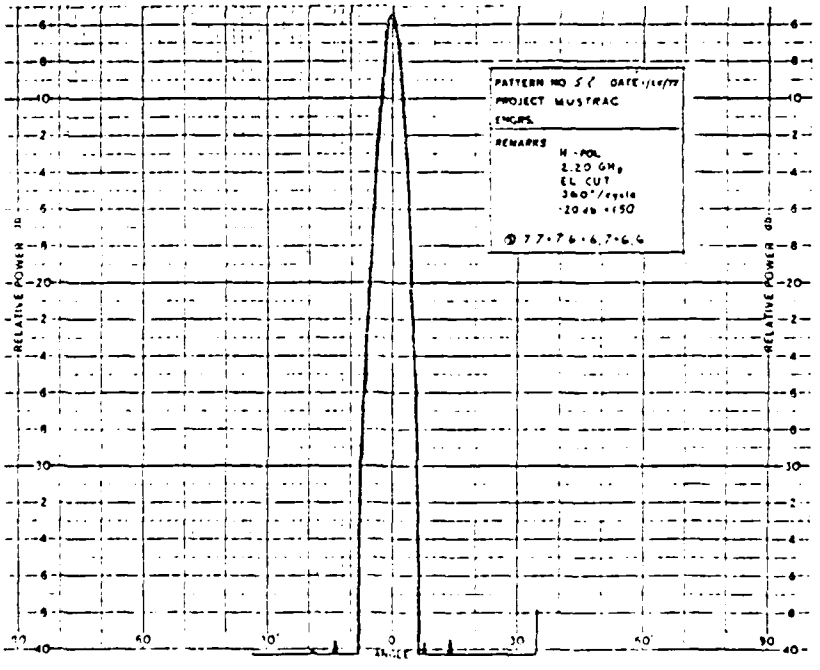

Figure B-7. MUSTRAC Measured Four-Beam Cluster.

APPENDIX C.

SOFTWARE DOCUMENTATION, 3-D DOME PROGRAMS

I. INTRODUCTION

1.1 Purpose

The practicality of designing and building an antenna with hemispherical coverage over a broad bandwidth is currently being investigated at Raytheon ESD. Previous studies have indicated that such an antenna is a feasible goal. (See references 1, 2, and 3).

In the current investigation the feasibility of using a solid dielectric dome for the wide angle array fed lens (WAAFL) is being studied. Computer programs model phase path lengths through a two-stack Rotman lens system to a curved or flat feed array. This data can be compared with the phase path length data from the feed array to a planar wave front outside the dome, possibly generated by another computer program which models the dielectric dome. The current programs model dielectric domes with either spherical or ellipsoidal surfaces. Unless otherwise indicated, lengths are in inches and angles are in degrees.

It is not the purpose of this document to provide conclusions as to the practicality of building the desired antenna system. It is the purpose of this document to describe the current state of the programs which model the system. At a later time it is anticipated that more data concerning the appropriate choice of dome parameters will become available. At that time the programs documented herein will be exercised to determine if an antenna system as described above can be built which will keep phase errors within reasonable bounds.

1.2 Scope of Document

Six programs were developed for modelling of various portions of the antenna system. This document describes each of these programs. In addition, the interdependence of the programs is examined. Descriptions of file inputs and outputs of the programs are given.

Scope of Document (cont'd)

In the user's guide section the inputs required at the terminal at the time of program execution are given. This section includes a description of the expected output, as well as a brief description of what diagnostic messages may be encountered during program execution.

In the quality assurance section the results of test runs are examined and expected accuracy of data is discussed.

The overall scope of this document is to give an individual who is familiar with the IBM/370 system the information necessary to provide input to the programs described. The operator will then be able to run these programs and interpret the results.

II. APPLICABLE DOCUMENTS

1. Thomas, D., "Final Report on Lens Fed Array Applications," (Company Private) Raytheon ESD, Project No. 77D-660, 31 Dec 1977.

2. Bixler, D. and Thomas, D., "Final Report on Antenna Technology (Part I), Wide Angle Array Fed Lens," (Company Private) Raytheon ESD, Project No. 78D-659, 31 Dec 1978.

3. Thomas, D. and Bixler, D., "Feed Lens Portion of 3-D Dome Antenna Study - Final Technical Report for Period Oct 77-Apr 79," Raytheon ESD, Contract N00014-77-C0760, ONR Task 252-008-1, Oct 1979.

* 4. McInturff, K., "Non-Concentric Tangential 3D Dome Model-Receiver Case," 11 Mar 80.

* 5. McInturff, K., "Non-Concentric Tangential 3D Dome Model-Transmitter Case," 13 Mar 80.

* 6. McInturff, K., "Non-Concentric Tangential 3D Dome Model-Solution of Two Problems," 14 Mar 80.

* 7. McInturff, K., "3D Dome Model; Solution of System of Equations," 31 Mar 80.

* 8. McInturff, K., "Normals," 31 Mar 80.

* See Appendix C

III. REQUIREMENTS

3.1 General

3.1.1 Program Location/Language

All programs were written for use on the IBM/370 system at Raytheon ESD. Currently these programs are accessed by logging on to 92SWDEV1. The programs are written in FORTRAN IV. Each of the six programs has an associated executive program of the same name which sets up the appropriate input/output files using information input as arguments from the terminal when the program is called. The six programs are:

1. TRANS3D - generates phase path length data from feed array to planar wave front.

2. ROLED3D - designs a Rotman lens from phase data output from TRANS3D; optimizes beamport locations using IMSL subroutine.

3. ROLED3D2 - design a Rotman lens from phase data output from TRANS3D; optimizes beamport locations manually.

4. CHECK3D1 - compares phase path lengths generated by TRANS3D with phase path lengths through two-stack lens systems for on-axis exit angles (i.e., PHI=0).

5. CHECK3D2 - same as CHECK3D1 except the exit axis is perpendicular to the exit axis in CHECK3D1.

6. CHECK3D3 - compares phase path lengths generated by TRANS3D with phase path lengths through two-stack lens system for diagonal exit angles (i.e., PHI=45°)

Program Language/Location (cont'd)

The first program, TRANS3D, is the most detailed and requires a number of subroutines specifically written for use by TRANS3D. They are:

1. FUNCTX - minimizes $-N_2 \cdot N_3$ as a function of coordinates x and y on the inner dome surface. [N_2 and N_3 are both unit vectors. N_3 represents the direction in which every ray should be traveling after passage through the dome. N_2 is the approximation to N_3 found by selecting a point (x,y,z) on the inner surface of the dome and tracing the ray path from the feed array through (x,y,z), and through the dome. (See Figure 2 in Section 3.3.3.) When $N_2 \cdot N_3$ equals 1, $N_2 = N_3$ and (x,y,z) will be the point (x_1,y_1,z_1) of Figure 2.]

2. FUNCTZ - minimizes $-N_2 \cdot N_3$ as a function of coordinates z and y on the inner dome surface.

3. EN2N3 - is the function $N_2 \cdot N_3$.

4. XYZ2 - calculates the coordinates (x_2, y_2, z_2) of the point of exit from the dome of a transmitted ray.

5. NORMA1 - determines the third coordinate of a point on the inner spherical surface given two coordinates.

6. NORMA2 - determines the third coordinate of a point on the inner ellipsoidal surface given two coordinates.

7. NORMB1 - gives solutions of quadratic equations needed to find the coordinates of the point (x_2, y_2, z_2) on the outer spherical surface.

8. NORMB2 - gives solutions of quadratic equations needed to find the coordinates of the point (x_2, y_2, z_2) on the outer ellipsoidal surface.

All programs and subroutines mentioned above are to be found on 92SWDEV1.

File I/O for TRANS3D (cont'd)

The output files are:

File 11: TR0T30 DATA C
File 12: TR1T30 DATA C
.
.
.
File 30: TR19T30 DATA C
File 8 : TRANS3D DATAPR C
File 9 : TRANS3D MODDAT30 C

If the second argument is 'D', Files 11-30 will have the filename of DUMMY and the filetype of File 9 will be the concatenation of two items. The first item is 'DIAG' and the second is the first argument. For example, inputting

(Example 2) TRANS3D 75 D

sets up the files

File 11-30: DUMMY DATA C
File 8 : TRANS3D DATAPR C
File 9 : TRANS3D DIAG75 C

The argument 'D' corresponds to an off-axis run and the '75' corresponds to Z0.

At the completion of the program TRANS3D, the contents of the file TRANS3D DATAPR C is appended to the file TRANS3D PRINT C. The file TRANS3D DATAPR C is not modified by this procedure.

When files 11-30 are distinct (e.g., Example 1), each individual file will contain data corresponding to a given distance (CUTDIS) from the central slice. Each file contains the following data:

File I/O for TRANS3D (cont'd)

Z0, CUTDIS, M0, RR0, PHDLA.

Z0 is the exit angle outside the dome.

M0 is the number of array elements in the feed array slice under consideration such that x is non-negative.

RR0 is the radius of the slice under consideration (not the radius R0 of the feed array).

PHDLA is an array containing the phase delay data to be used in the design of the Rotman lens system below the feed array. The number of phase delay data elements in the file is 2*M0, with the central data element being repeated.

The file TRANS3D DATAPR C contains input and output data in a form ready for printing. This file is appended to TRANS3D PRINT C, which is the file typically used for printout. The command

PRINT TRANS3D PRINT C (CC

puts this file on the printer spool in the proper form.

File 9 contains a shorter list of data than the print file 8. This file is in turn an input file for programs CHECK3D1 and CHECK3D2 and contains the following data items:

Z0, PHI, DIEL, NX, NY, DELTX, DELTY, R4, R0, DROP, OFF, R1, as well as the arrays

PX, PY, PHDLA.

File I/O for TRANS3D (cont'd)

The non-array data items are dome and feed array parameters initialized by operator input at the terminal during execution of TRANS3D. (Reference section 4.1) PX and PY are arrays containing the (x,y) coordinates of feed array elements. PHDLA is the normalized phase path length of a ray emanating from a feed array element to a point in the planar wave front. Normalization is with respect to the central feed array element.

When the second argument is 'D' (e.g., Example 2) Files 11-30 are dummy files because the off-axis case phase data is not to be used for Rotman lens design. File 8 is as in Example 1. File 9 contains the same data as file 9 in Example 1. However, when PHI=45°, this file can be used as input to the program CHECK3D3.

3.2.2 File I/O for ROLED3D and ROLED3D2

When the program ROLED3D or ROLED3D2 is run, eight input files are needed. Each program requires one argument which designates the number of the Rotman lens design slice (starting with 0 as the central slice). This argument will be the second of the four items of which the file name for files 11-30 in the preceding section consists. For example,

(Example 3) ROLED3D 4

indicates that the fourth slice away from the central slice in the feed array is used in the Rotman lens design. The eight input files are then

File I/O for ROLED3D and ROLED3D2 (cont'd)

```
TR4T0    DATA C
TR4T15   DATA C
   .
   .
   .
TR4T90   DATA C
TR4T67   DATA C
```

The content of these files has previously been described, each file being file 15 in one of eight runs of TRANS3D with Z0 = 0, 15, 30, 45, 60, 75, 90 or 67.5.

The output file in Example 3 is RLD3D4 DATA C. In general, the file name of the output file from either ROLED3D or ROLED3D2 is the concatenation of RLD3D and the argument (e.g., 4 in Example 3). This output file contains the data

```
M0, G0, F0, A
(J, U(J), V(J), W(J), J=1, M0)
(A7(N), H(N), N=1,8)
```

This output file is used as the input file for each of the programs CHECK3D1, CHECK3D2, and CHECK3D3.

M0 is the number of array elements for half the Rotman lens. That is, the number of array ports is 2*M0-1.

G0 is the distance from the central beamport to the central array port.

A is the focal angle and F0 is the distance from the central array port to the beamport arc at angle A.

U(J), V(J) are coordinates of array port elements and W(J) is the cable length correction normalized to the central array port.

A7(N), H(N) are the polar coordinates of the beamport locations after corrections to minimize phase errors at intermediate beamports. A7 is the angle and H the distance.

3.2.3 File I/O for CHECK3D1, CHECK3D2, and CHECK3D3

Each of the 'CHECK3D' programs requires at least two input files, one being file 9 from an appropriate TRANS3D run and the other being the output file from a run of either ROLED3D or ROLED3D2. In addition, CHECK3D1 and CHECK3D2 require the non-empty files from files 11-30 from the same run of TRANS3D. It is appropriate to run CHECK3D1 and CHECK3D2 only when these runs correspond to an on-axis run of TRANS3D, that is only when the second argument of the TRANS3D run is not 'D' and PHI=0. It is appropriate to run CHECK3D3 only when this corresponds to a diagonal run of TRANS3D, that is, only when the second argument of the TRANS3D run is 'D' and PHI=45°.

In order to have proper file initialization, three arguments must be given for each run of CHECK3D1 or CHECK3D2. The first argument should be the same as the first argument in the corresponding TRANS3D run. This argument corresponds to Z0, as before. The second argument should be the same as the argument in the correspondng ROLED3D or ROLED3D2 run. This argument corresponds to the slice number, as before. The third argument should be the number of non-empty files among files 11-30 in the corresponding TRANS3D run.

The number of non-empty files among files 11-30 is dependent on the number of rows of phase data generated. For PHI=0, the number of non-empty files is the same as the number of non-negative y values for which there corresponds at least one feed array element yielding phase delay data.

Only two arguments need be given for a run of CHECK3D3 and their description is the same as the description of the first two arguments given for CHECK3D1 and CHECK3D2.

File I/O for CHECK3D1, CHECK3D2, and CHECK3D3 (cont'd)

For output each of these three programs yields a table of phase data in an output file. For each element in the feed array, the phase path length from the element through the dome to the planar wave front is compared with phase path length through the two-stack Rotman lens system. The difference between these two lengths is given in the table, as well as this phase difference in degrees at 12 GHz. Finally the root-mean-square value of this phase error over the entire feed array is displayed at the terminal and stored in the output file.

The output file is named

CHECK3D1 DATA C

when CHECK3D1 is run. A copy of the file CHECK3D1 DATA C is appended to the file CHECK3D1 PRINT C at the conclusion of the run (without CHECK3D1 DATA C being modified). In this way data for a number of CHECK3D1 runs can be accumulated before printing. This is also true for the programs CHECK3D2 and CHECK3D3.

3.3 Function Description

3.3.1 General Flow of Programs

The program TRANS3D generates phase path length data from the feed array through the 3-D dome to a planar wave front. This data has two main purposes. It is of immediate use in designing the Rotman lens which will be used in the two-stack Rotman lens system. Either of the programs ROLED3D and ROLED3D2 can be used to design the Rotman lens, using as input the data files generated by the program TRANS3D.

The difference between ROLED3D and ROLED3D2 is that the former optimizes beamport locations using an IMSL subroutine and does not allow for manual manipulation, whereas the latter is strictly a manual tool for optimizing beamport location. In general, the best employment of the programs is to use ROLED3D to find the general locations of the beamports, then to use ROLED3D2 to find these locations precisely.

The second purpose of the data generated by TRANS3D is as input to the programs CHECK3D1, CHECK3D2, and CHECK3D3. In each of these programs phase path length through the Rotman lens system is calculated and compared to the TRANS3D phase data.

For a given dome and feed array design, the program TRANS3D is first run with PHI=0 and Z0=0, 15, 30, 45, 60, 75, 90, and 67. The data generated by these runs is then used to design the Rotman lens using either ROLED3D or ROLED3D2. Then either CHECK3D1 or CHECK3D2 is used to check on-axis performance of the total system. CHECK3D1 and CHECK3D2 should yield the same result in the current modelling because of the assumption that all lenses in the two-stack Rotman lens system are identical.

General Flow of Programs (cont'd)

For further testing of the dome design, TRANS3D can be rerun with PHI=45° to generate phase data needed for input into CHECK3D3. It is difficult to predict the choice of Z0 in these runs which will minimize phase errors when CHECK3D3 is run. It usually requires a number of runs with different values of Z0 to check for the proper value of Z0 corresponding to a given beamport chosen in the lower stack of Rotman lenses.

3.3.2 Program Descriptions

3.3.2.1 TRANS3D

The program TRANS3D allows the operator to choose the desired dome. The operator chooses spherical or ellipsoidal surfaces for the dome, as well as the dielectric constant of the dome material. The operator may also select various feed array designs, flat or curved, raised or dropped, as well as element spacing and radius of feed array. A description of each of the variables to be input at the terminal is found in the initial comment section of the program TRANS3D and in the user's guide section of this document. The equations used in TRANS3D and its subroutines are described in previous work. (See references 4, 5, 6, 7, 8).

After inputting the dome and feed array data, the operator must answer three questions

(1) DESIRE TERMINAL OUTPUT (Y/N)?
(2) DESIRE PRINTER OUTPUT (Y/N)?
(3) DESIRE FILE OUTPUT (Y/N)?

Answering 'Y' to one or more of these questions allows data to be sent to the appropriate output device, file or files. Questions (1), (2), and (3) correspond to files 6, 8, and 9, respectively.

TRANS3D (cont'd)

Since the grid of points input for consideration as feed array elements is rectangular and the feed array is circular, it is often the case that certain grid points will fail to fall within the feed array radius. In this case the message

SAMPLE AREA HAS BEEN TRUNCATED

will be displayed at the terminal. If the number of valid feed array elements exceeds the allowable array size (currently set at 370), the message

TOO MANY DATA POINTS FOR ARRAY

is displayed at the terminal. In any case the number of valid feed array elements for which a point in the planar wave front outside the dome has been calculated is displayed at the terminal, in the form

78 POINTS IN SAMPLE

if, for instance, there are 78 valid points.

If PHI=0, the operator has the option of storing phase delay data in files 11-30 by answering the question

STORE PHASE DELAY DATA FOR ROTMAN LENS DESIGN (Y/N)?

with 'Y'.

1 TRANS3D (cont'd)

If the question

X-Y REGION TO BE PROJECTED (PLOT/LIST/CONT)?

is answered with 'P' at the terminal, the operator plots the outline of the grid of feed array elements, as well as the circle marking the feed array radius. If the answer is 'L', a list of feed array elements along the edge of the feed array is displayed at the terminal. If 'C' is input in response to the question, then neither plotting nor listing occurs. This question repeats until a 'C' is input.

The next question to be answered is

PROJECTION IN PLANE WAVE (PLOT/LIST/CONT)?

If the plotting option is chosen, the full grid of projected points is plotted in the u-v plane. If the listing option is chosen, the phase data is transferred to the appropriate files as determined by the answers to the 'OUTPUT' questions asked above.

Answering the question

CENTRAL SLICE (PLOT/CONT)?

with 'P' allows plotting of the central slice (Y=0) through the feed array and dome, including ray tracing from the central slice feed array elements to the planar wave front.

Finally the operator has the opportunity to change parameters. Answering the question

CHANGE INPUT ANGLES Z0 AND PHI (Y/N)?

TRANS3D (cont'd)

with 'Y' allows the operator to change Z0 and PHI without modifying the dome or feed array. Answering the question

REDO SAMPLE-WILL ERASE OLD ONE (N/Y)?

with 'Y' allows the operator to change any or all of the dome and feed array parameters before recalculating the phase data.

3.3.2.2 ROLED3D and ROLED3D2

Either of the programs ROLED3D and ROLED3D2 designs a Rotman lens for use in the two-stack Rotman lens system which lies beneath the feed array and dome. In either program the standard Rotman lens parameters G, ALPHA, and ETA must be input from the terminal. The array port coordinates, cable lengths and beamport arc are determined by equations documented in reference 1 (pp. 106-110).

In either program the operator has the option of modifying the beamport locations to minimize phase error. In ROLED3D if the question

CALCULATE BEAMPORT LOCATIONS WHICH
MINIMIZE PHASE ERRORS (Y/N)?

is answered with 'Y', an optimizing routine is called which determines the optimal beamport locations. No option is included for modifying the beamport locations if the routine does not produce the desired accuracy. The program ROLED3D2 does not contain the optimizing routine found in ROLED3D. Instead, when the question

CALCULATE PHASE ERRORS?

is answered with 'Y', the operator may input estimates of ALPHA and H for each of the eight angles under consideration

ROLED3D and ROLED3D2 (cont'd)

and have phase errors at each printed at the terminal until the operator is satisfied with the results.

By answering the question

ROTMAN LENS: LIST, PLOT, CONT

appropriately in either program, the operator may get a listing of array port coordinates and cable lengths or a plot of the Rotman lens (with beamport locations not optimized).

After this the operator may redesign the lens by answering

REDESIGN LENS (Y/N)?

with 'Y'. In this case the operator may change the variables G, ALPHA, and ETA. (See reference 1, p. 140, for a discussion of parameter optimization studies).

3.3.2.3 CHECK3D1, CHECK3D2, and CHECK3D3

Each of these programs generates phase data through the two-stack Rotman lens system and compares this data with phase data generated by TRANS3D. The only option while running CHECK3D1 or CHECK3D2 is whether to use optimal beamport locations as determined in ROLED3D or ROLED3D2. If the question

DATA INCLUDES BEAMPORT LOCATION (Y/N)?

is answered with 'N', only Z0=0 or 90° are acceptable values. If answered with 'Y', the acceptable values for Z0 are 0, 15, 30, 45, 60, 67.5, 75, and 90.

Figure 3.3.3.2

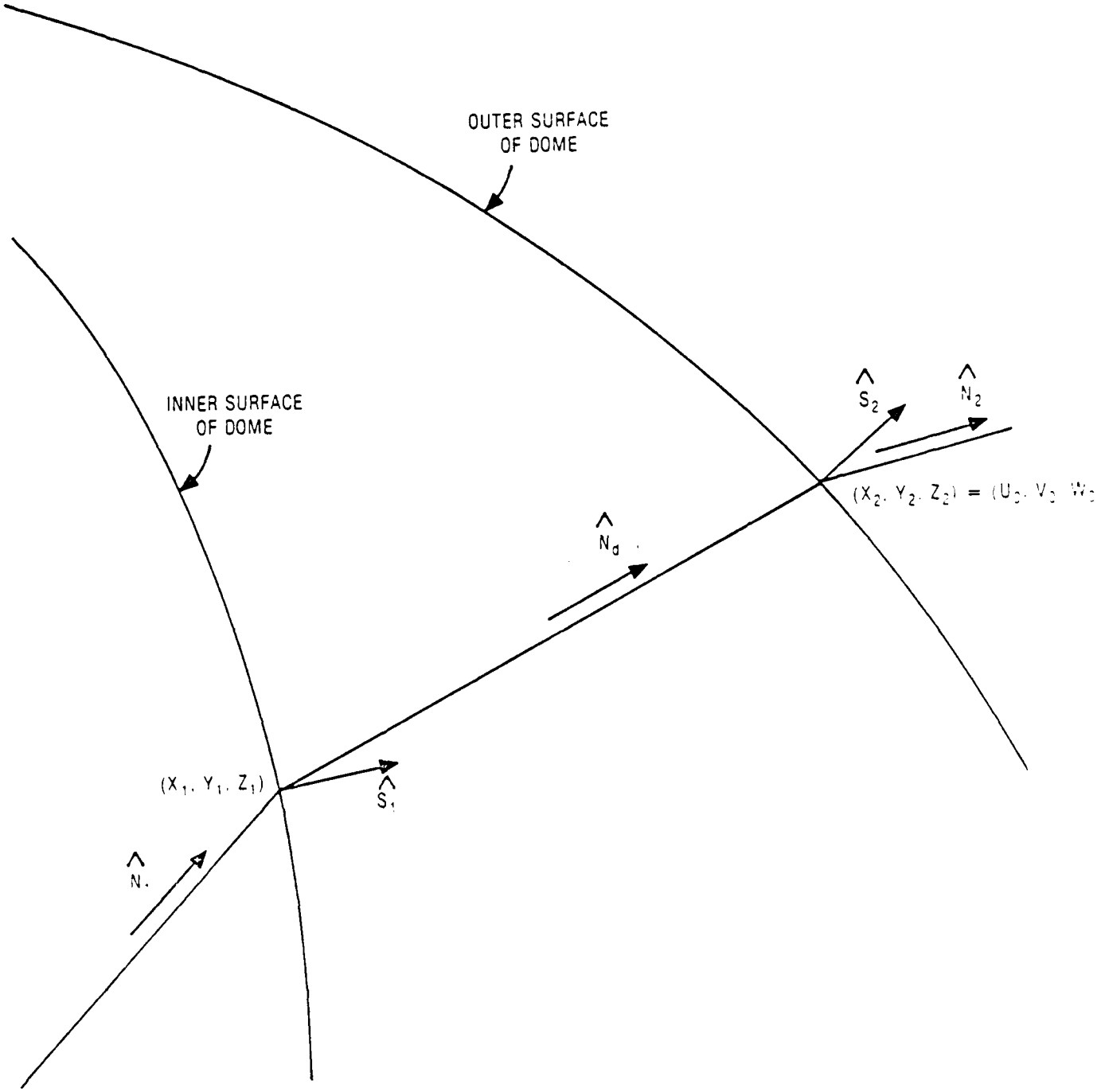
OUTER SURFACE
OF DOME
INNER SURFACE
OF DOME
$\hat{S}_2$
$\hat{N}_2$
$(X_2, Y_2, Z_2) = (U_2, V_2, W_2$
$\hat{N}_d$
(X_1, Y_1, Z_1)
$\hat{S}_1$
$\hat{N}_1$

Figure 3.3.3.3

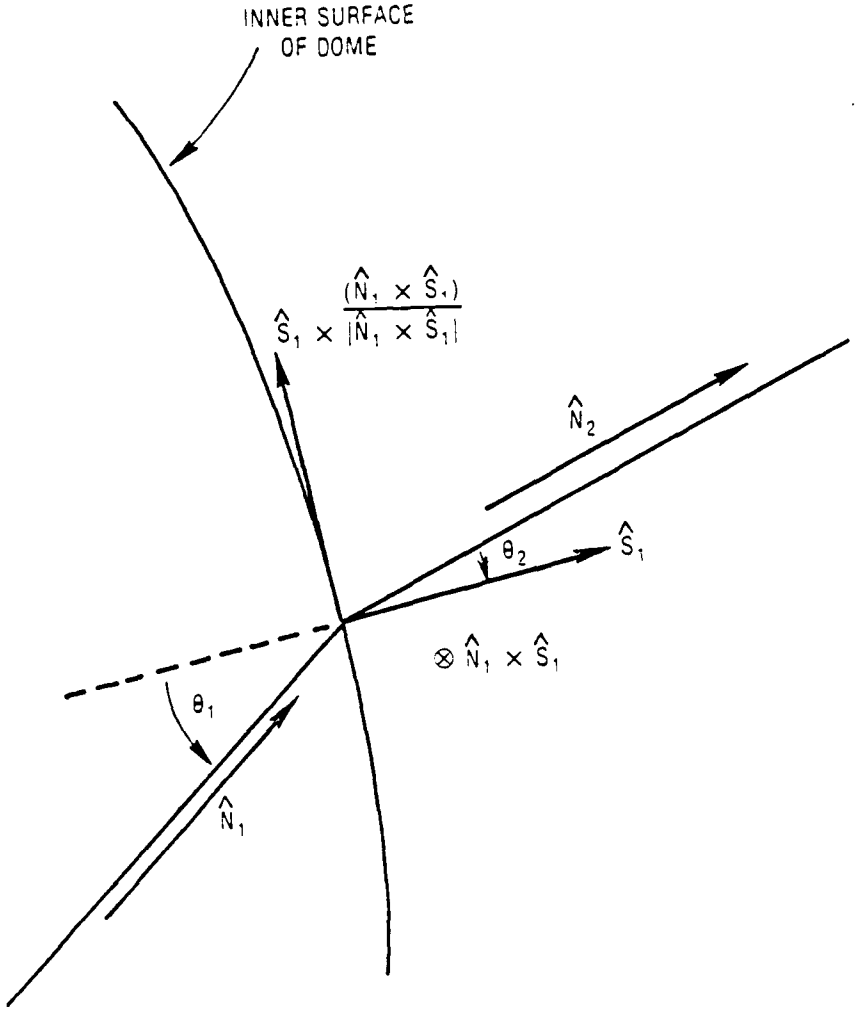
INNER SURFACE
OF DOME
$\hat{S}_1 \times \frac{(\hat{N}_1 \times \hat{S}_1)}{|\hat{N}_1 \times \hat{S}_1|}$
$\hat{N}_2$
θ_2
$\hat{S}_1$
$\otimes \hat{N}_1 \times \hat{S}_1$
θ_1
$\hat{N}_1$

Figure 3.3.3.4

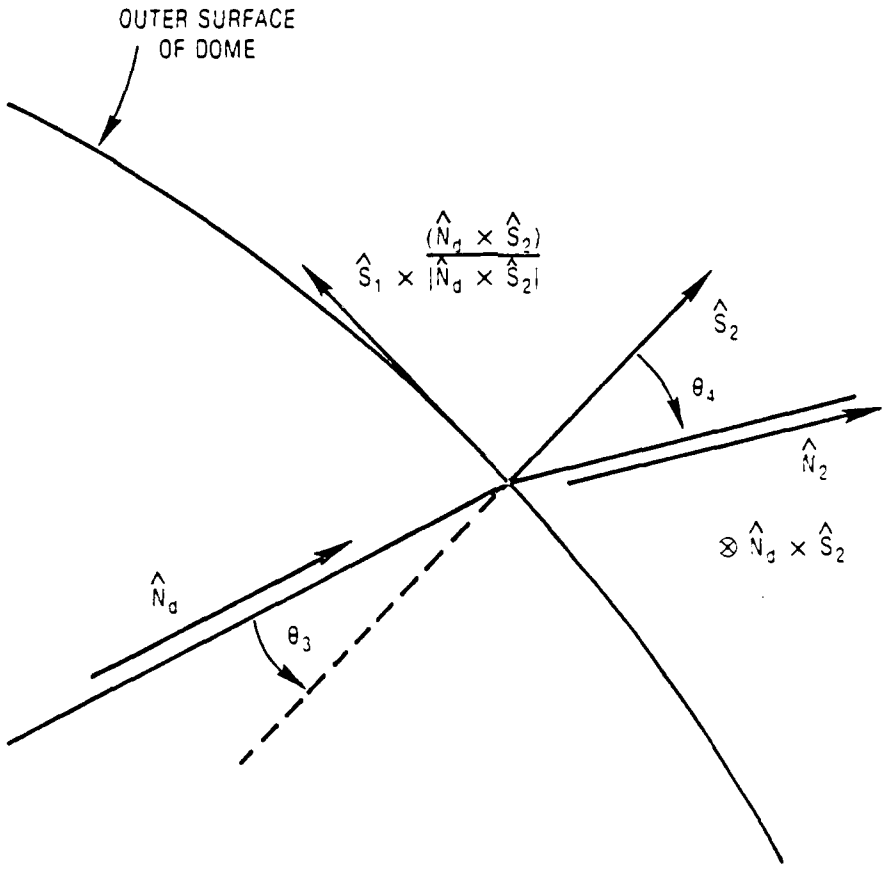
OUTER SURFACE
OF DOME
$\hat{S}_1 \times \frac{(\hat{N}_d \times \hat{S}_2)}{|\hat{N}_d \times \hat{S}_2|}$
$\hat{S}_2$
θ_4
$\hat{N}_2$
$\otimes \hat{N}_d \times \hat{S}_2$
$\hat{N}_d$
θ_3

IV. USER'S GUIDE

4.1 Inputs Required

This section is a listing of the required terminal inputs for each program. Each listing contains variable name, type, description and appropriate units. Figure 1 of Section 3.3.3 contains a pictorial representation of some of the variables of Section 4.1.1.

4.1.1 TRANS3D

DELTX (real) - spacing of feed array elements along the x-axis (inches)

DELTY (real) - spacing of feed array elements along the y-axis (inches)

NX (integer) - number of possible elements in the feed array along the x-axis

NY (integer) - number of possible elements in the feed array along the y-axis

Z0 (real) - the angle down from vertical of a ray path outside the dome (degrees)

PHI (real) - the angle by which the propagation plane is displaced from the feed array axis (degrees)

DIEL (real) - the relative dielectric of the dome

R4 (real) - z-coordinate of center of sphere on which feed array elements are located (inches)

RO (real) - radius of projection of feed array in the xy-plane (inches)

2 TRANS3D (cont'd)

DROP (real) - distance center of feed array is dropped from its canonical position (inches)

OFF (real) - distance the top of the outer surface is offset from the top of the inner surface (inches)

R1 (real) - radius of the inner spherical surface (inches)

A1 (real) - semi-axis length in z-direction of the inner ellipsoidal surface (inches)

B1 (real) - semi-axis length in x (or y) - direction of the inner ellipsoidal surface (inches)

A2 (real) - semi-axis length in z-direction of the outer ellipsoidal surface (inches)

B2 (real) - semi-axis lengh in x (or y) - direction of the outer ellipsoidal surface (inches)

4.1.2 ROLED3D or ROLED3D2

G (real) - ratio of focal distance G0 to focal distance F0 in the Rotman lens

A (real) - focal angle (degrees)

E0 (real) - ratio of maximum array dimension R0 to focal distance F0

4.1.3 CHECK3D3

NB (integer) - scan angle number for bottom lens

NT (integer) - scan angle number for top lens

NOTE: Scan angle numbers 1 through 8 correspond to on-axis exit angles Z0 being 0, 15, 30, 45, 60, 75, 90, and 67.5, respectively.

4.2 Program Execution

4.2.1 General Procedure

The first step in the procedure to be followed by the operator of this set of programs is to choose a dome and feed array configuration. The input sheet labelled

TRANS3D Inputs

is convenient for this purpose (See Section 5.2.). It gives the operator a convenient format from which data can be easily read into the computer.

A complete set of eight on-axis TRANS3D runs on the computer for the given dome and feed array is

```
TRANS3D  0 C
TRANS3D 15 C
TRANS3D 30 C
   .
   .
   .
TRANS3D 90 C
TRANS3D 67 C
```

The grid projection plots and ray-tracing plots are examined, especially for Z0=90°, to insure proper scan amplification is being affected by the given dome-feed array system.

General Procedure (cont'd)

For a system giving proper scan amplification, the next step is to design a Rotman lens to be used in both stacks of lenses which feed the dome-feed array system.

There are four degrees of freedom in the selection of this Rotman lens. First the slice in the feed array which is used to supply phase data can be varied. The usual choice is the slice furthest from the central slice which still has the same number of data points (i.e., array elements) as the central slice. The other three parameters to be varied are the standard Rotman lens parameters G, ALPHA, and ETA (abbreviated to G, A, and E0 in ROLED3D and ROLED3D2).

The usual procedure is to vary G, ALPHA, and ETA until a lens shape and size is produced which is optimal. 'Optimal' in this instance is a subjective matter, but the football shape familiar to the experienced Rotman lens designer is to be striven for. As a general rule, flat feeds necessitate rounder lenses than desired, leading to the use of curved feed arrays. (See reference 1). As a final step in the Rotman lens design, beamport locations are chosen to minimize phase errors at the angles 0, 15, 30, 45, 60, 75, 90 and 67.5.

After completion of the Rotman lens design, the total system design is complete, and it remains to check the phase data that is generated by this complete system. The first check is to run either of the programs CHECK3D1 and CHECK3D2. There are no parameters to vary because the system has been chosen at this point.

General Procedure (cont'd)

To further check the system, TRANS3D may be rerun with the same dome and feed array parameters and PHI=45°. If the scan angles are equal (say 60°) for the lens in the bottom stack and each lens in the top stack, PHI will be 45° and Z0 will be some yet-to-be-determined angle. There is actually no single value of Z0 which is the correct solution. One appropriate choice might be that value of Z0 which minimizes the R-M-S value of phase error. Generally a few possible choices of Z0 are selected, and CHECK3D3 is used to evaluate the phase error for each of these cases. The best case (i.e., the case minimizing the RMS value of phase error) is then used to evaluate system performance, along with the on-axis data generated by programs CHECK3D1 and CHECK3D2.

4.3 Expected Output

The program TRANS3D generates plots and/or listings as output. The phase data listings are not particularly useful without comparison to phase data generated by the feed system (e.g. the two-stack Rotman lens system modelled in the CHECK3D programs). The plots are used to analyze the focusing and beam shaping capabilities of the dome and feed array. Dome and feed array parameters are modified as necessary to yield desired scan results, especially at the maximum scan angle.

Once a dome and feed array system with acceptable scan capabilities has been chosen, the Rotman lens design to be used in the two-stack feed is chosen using ROLED3D or ROLED3D2. In either of these programs plots of lens shapes are used to determine an appropriate lens. When an appropriate lens is chosen, a table of lens parameters, including array port coordinates and cable length can be generated. If beamport locations are optimized, a table of these locations can also be generated.

Once the entire system has been designed, each of the CHECK3D programs generates phase data for each feed array element. These programs generate no plots, but each program generates a file containing phase delay data suitable for easy reading, as well as a brief description of the run. The file also contains the RMS value of the phase error.

4.4 Diagnostics/Messages/Fixups

The program TRANS3D has internal checks for some of the more obvious errors in input data. For example, radii must be positive and the outer radius of the dome must be larger than the inner radius.

Once a reasonable set of input dome and feed array parameters has been selected, there are still potential problem areas. In the process of finding the point on the inner surface of the dome through which a ray passes, an initial guess is given (in the program, not by the operator). If this guess is not sufficiently close to the proper point, the iterative process may not arrive at the proper point in the number of iterations allowed. Another possibility is that the accuracy of a solution cannot be found to the number of significant digits desired. If such problems occur within the subroutine ZXMIND, an error message is displayed at the terminal in the form

*** IMSL (UERTST) *** TERMINAL ZXMIN 2 (IER = ZZZ)

At the time of the run ZZZ is some number indicating the specific problem. For example ZZZ = 130 indicates some round-off error. This error message actually occurs frequently, but results appear to remain valid in most cases to a sufficient number of digits for later comparison in CHECK3D programs. The same set of error messages may be encountered when running ROLED3D, since this program also calls ZXMIND. Reference the IMSL subroutine library for the complete set of values possible for ZZZ.

Finally it is possible to find a result without generating error messages which is totally impossible physically. The easiest way to catch errors of this type, which are usually large in magnitude, is to plot the grid of projected points in the planar wave front, as well as the central ray paths.

V. QUALITY ASSURANCE

5.1 Testing Done

The programs in this document were modelled after previous programs which modelled a different dome style (See References 1,2, and 3.) Output from the two sets of programs were compared where possible to insure consistency and accuracy.

More than thirty different dome and feed array configurations were examined, and parameter studies indicated good agreement with parameter studies made with the previous dome style.

In addition results were checked against studies made by Sperry with the same dome concept and conclusions drawn by our investigations were corroborated by Sperry's results.

VI. MODIFICATIONS (NOV. 1981)

6.1 Purpose

The design and building of an antenna system with hemispherical coverage over a broad bandwidth is being investigated by Raytheon ESD.

The purpose of this document is to illustrate the different modifications and new programs that were generated during the summer and fall 1981. Different stages of design resulted in different program specifications.

This document will not provide conclusions as to the best design to choose.

6.2 Scope of Document

This document will describe the modifications and new programs related to the particular design stages. Input and output files are examined, as well as program interdependence.

All programs are written for use on the IBM 4341 and reside on the disk 92SWDEV1.

The initial software developed for the 3D DOME project is described in Memo No. 9283:668:KM:ds (July 11, 1980) written by Kim McInturff.

As of summer 1981, the following modifications were made in all of these programs:

1. Number of array ports is 23 instead of 17.
2. Beam pointing angles have been changed from:

   0° 15° 30° 45° 60° 75° 90°

   to

   0° 20.5° 42.0° 59.0° 71.2° 81.3° 90.2°

3. The user has the option to input data from a file or from the terminal.

This is a list of the existing programs with their appropriate execs:

1. TRANS3D FORTRAN with the following execs:
   a. TRANS3D EXEC
   b. TRANSQR EXEC

2. ROLED3D FORTRAN with the following execs:

   a. ROLED3D EXEC

   b. ROLED3M EXEC

3. ROLED3D2 FORTRAN with the following execs:

   a. ROLED3D2 EXEC

   b. ROLED3A EXEC

4. CHECK3D1 FORTRAN with CHECK3D1 EXEC

5. CHECK3D2 FORTRAN with CHECK3D2 EXEC

6. CHECK3D3 FORTRAN with CHECK3D3 EXEC

7. CHECKLE FORTRAN with CHECKLE EXEC

8. CHECKLE2 FORTRAN with CHECKLE2 EXEC

9. CHECKLE3 FORTRAN with CHECKLE3 EXEC

10. CHECSQR1 FORTRAN (modified version of CHECKLE) with CHECSQR1 EXEC

11. CHECSQR2 FORTRAN (modified version of CHECKLE2) with CHECSQR2 EXEC

12. CHECSQR3 FORTRAN (modified version of CHECKLE3) with CHECSQR3 EXEC

The following stages of design assume uniform lens stack design - using one slice (starting with 0 (zero) as the central slice)

1st Stage - Central Slice Design (Zero Slice)

Program ALPHAH FORTRAN A (with ALPHAH EXEC) was created to generate a table of amplitudes and phases, using the file UVWALP DATA C, generated by ROLED3D2 FORTRAN (with the appropriate EXEC).

*Note: the user has to input BPW (beam port widths) into the file UVWALP DATA C.

When ALPHAH is run file APFAR 81DATA C is generated.

APFAR 81DATA C consists of:

1. amplitude (volts)
2. phases with cables (radians)
3. phases (radians)

All of these are at different frequencies and beam pointing angles.

The program BREAK FORTRAN (with BREAK EXEC) was created to take the APFAR 81DATA C file and break it down into several files according to:

1. frequency (GHz)
2. beam pointing angle (degrees)

The program is invoked by typing BREAK followed by a list of beam pointing angles, i.e. BREAK 00 20 42 59 71 81 90.

The files generated are named as follows:

APFAR frequency DAT beam pointing angle DATA C consisting of: amplitude (volts), phase with cable (radians), phase (radians).

The user may choose to have the units converted to DB and degrees by answering YES to "PERFORM CONVERSIONS?"

This option generates the CAPFAR files, which contain the same data as the APFAR files.

CAPFAR files consist of: amplitude (DB), phase with cables (degrees), phase (degrees). These files are used to plot the far field patterns.

BREAK2 FORTRAN (with BREAK2 EXEC) was created to take each of the CAPFAR files and break them down as follows:

1. one file AMPH DATA C consisting of number of array ports and amplitude (DB).
2. another file PHAS DATA C consisting of number of array ports and phases (degrees).

These files get overwritten every time the program is invoked. They are used to plot amplitudes and phases.

Similar modifications resulted in the creation of TRANSQR EXEC.

The following three new programs have been created also in this stage of design:

1. CHECSQR1 FORTRAN with CHECSQR1 EXEC
2. CHECSQR2 FORTRAN with CHECSQR2 EXEC
3. CHECSQR3 FORTRAN with CHECSQR3 EXEC

These programs are modified versions of CHECKLE FORTRAN, CHECKLE2 FORTRAN and CHECKLE3 FORTRAN respectively.

The new CHECSQR series of programs are run with data that can be input from a file of the XYR DATA C Format, they also allow for several-slice lens stack design. They are run in conjunction with TRANSQR EXEC which runs TRANS3D.

Typically the input files for the CHECSQR series consist of the following:

1. XYR DATA C
2. TØTangle DATA C
   T1Tangle DATA C
   .
   .
   .
   TNTangle DATA C

   These files are outputs from the TRANS3D program and

3. RLD3DØ DATA C
   RLD3D1 DATA C
   .
   .
   .
   RLD3DN DATA C

   These files are outputs from the ROLED3D program. Since 3 slices were used to design the Rotman lens stack, this design was carried through in the set up of the RLD3D files.

LISTINGS FOLLOW

2nd Stage - Redesign Lens Using Various Slices (one at a time) Example 3rd slice, 5th slice, 7th slice away from the central (0) slice.

Program TRANS3D FORTRAN (with TRANS3D EXEC) was modified so it can accept data from a file XYR DATA C or any other file in the same format.

The file XYR DATA C consists of:

1. NX, NY, DELTX, DELTY, XREAD, YREAD, RRØ.

To invoke the program, the user must type TRANS3D beam pointing angle C (or D) and XYR, e.g., TRANS3D 0 C XYR.

ROLED3D2 EXEC was modified to create ROLED3DA which allows for the different beam pointing angles as stated previously.

ROLED3DM EXEC is a modified version of ROLED3D EXEC which also allows for the new beam pointing angles.

The same modifications have been implemented in the CHECK3D1, CHECK3D2, CHECK3D3 FORTRAN programs with their EXEC's respectively.

In the next stage the lens design assumed that the Rotman lens stacks were designed using several slices. In this case, three slices were used:

1. central slice (0) for the first 4 lenses away from the center.
2. slice 5 for the next 5 lenses.
3. slice 10 for the next 3 lenses.

Several modifications resulted as a consequence of this design stage.

ROLEDSQR EXEC is a modified version of ROLED3D EXEC - it distinguishes the input files that are used in this stage by naming them

TØT2Ø		TRØT2Ø
TØT42		TRØT42
.	rather than	.
.		.
.		.
TØT9Ø		TRØT9Ø

as they were named in the ROLED3D EXEC.

DISTRIBUTION LIST

Addressee	DODAAD Code	No. of Copies
Scientific Officer	N00014	1
Administrative Contracting Officer	S0519A	1
Director, Naval Research Laboratory, Attn: Code 2627 Washington, D.C. 20375	N00173	6
Defense Documentation Center Bldg. 5, Cameron Station Alexandria, Virginia 22314	S47031	12
Office of Naval Research Branon Office - Pasadena 1030 E. Green Street Pasadena, California 91106	M62887	1

END

FILMED

2-85

DTIC